**Microwave Sensing,**
**Signals and Systems**
Mekelweg 4,
2628 CD Delft
The Netherlands
http://radar.tudelft.nl//

**MS3-2022-5251559**

# M.Sc. Thesis

# Improvement of weak targets detectability in strong clutter using the polarization contrast enhancement

**Yiyang Song**

Faculty of Electrical Engineering, Mathematics and Computer Science
Delft University of Technology

# Improvement of weak targets detectability in strong clutter using the polarization contrast enhancement

Thesis

submitted in partial fulfillment of the
requirements for the degree of

Master of Science

in

Electrical Engineering

by

Yiyang Song

This work was performed in:

Microwave Sensing, Signals and Systems Group
Department of Microelectronics
Faculty of Electrical Engineering, Mathematics and Computer Science
Delft University of Technology

Delft University of Technology
Department of
Microelectronics

The undersigned hereby certify that they have read and recommend to the Faculty of Electrical Engineering, Mathematics and Computer Science for acceptance a thesis entitled **"Improvement of weak targets detectability in strong clutter using the polarization contrast enhancement"** by **Yiyang Song** in partial fulfillment of the requirements for the degree of **Master of Science**.

Dated: 31 October 2022

Chairman: ______________________________
prof.dr.Alexander Yarovoy

Advisor: ______________________________
dr.Oleg Krasnov

Committee Members: ______________________________
dr.ir. Gerard Janssen

______________________________

# Abstract

Ground clutter signal is a kind of unwanted echoes in target detection radar system, which are normally reflected by ground surface, ground-based objects, and obstacles. It can be collected and characterized in polar coordinates in terms of range and azimuth. By using polarimetric based algorithms, including the single channel detector, the span detector, the power maximization synthesis (PMS) detector, the identity-likelihood-ratio-test (ILRT), the polarimetric whitening filter (PWF), and the optimal polarimetric detector (OPD), the target detection radar system can distinguish the characteristics and diversity of multiple targets.

In this thesis, a polarimetric radar simulator to generate multi-channel polarimetric signals with specific statistical characteristics has been developed and validated in the simulation. In the measurement, a new noise-based equalization for all polarimetric radar channels has been proposed and tested, which improves the reliability and accuracy of the polarimetric information. After noised-based calibration and model-based decomposition of the polarization covariance matrix, with regenerated measurement slow-time data, a variety of targets in heavy clutter with signal power comparable to the target are detected by polarimetric algorithms in the environment of strong clutters. Starting from numerical simulation and comparison of different detector algorithms, this work has validated the feasibility and accuracy of each detector in realistic scenario. The measurement result agrees with the simulation result that with the use of radar polarimetric information as *a priori* knowledge, target detection can be improved by polarimetric detectors.

# Acknowledgements

It is a great fortune to have the opportunity to take my Master's degree in TU Delft as my dream university. I love living and studying in The Netherlands, which is a friendly, inclusive, and elegant country. During these two years, I have gained so much kindness from my supervisor, groupmates, housemates, and friends.

First of all, I would like to express my great appreciation to my daily supervisor, dr.Oleg Krasnov. I was used to regarding the radar domain as a black box full of challenges and difficulties. I came out with an interest in exploring this domain by taking his lectures, and I found my interests in radar signal processing. This is the first gift I received from my daily supervisor and TU Delft. It must be mentioned that my supervisor kept a weekly syncup on my master thesis progress, shared professional experience with me, and provided me with many valuable suggestions. By knocking on his office door every time I was struggling and confused, I learned a lot of professional knowledge by spending time discussing and looking for solutions with my supervisor.

Thanks for Prof.dr.Alexander Yarovoy encouraging me when he noticed that I was overstressed on the midterm presentation. During that experience I thought about sharing my work with my group members with what kind of expression. I should always warmly welcome the comments and questions of others.

Finally, I want to thank my friends and family. I also have so many smart suggestions from the discussions with all my friends from the MS3 group. They showed me how excellent and professional we should be as master students. It was a pleasant experience to study and work with them. I am also lucky to get so much support from my family throughout the process.

Yiyang Song
Delft, The Netherlands
31 October 2022

# Contents

# List of Abbreviations

**OPD** Optimal Polarimetric Detector

**ILRT** Identity Likelihood Ratio Test

**PWF** Polarimetric Whitening Filter

**PMS** Power Maximum Synthesis

**GLRT** generalized likelihood ratio test

**ROC** Receiver Operating Characteristic

**PSM** polarization scattering matrix

**LFM** Linear Frequency Modulation

**pdf** Probability Density Function

**CFAR** constant false alarm rate

**STAP** space-time adaptive processing

**CUT** cell under test

**SAR** synthetic aperture radar

**PRI** pulse repetition interval

**PPI** plan position indicator

# 1 Introduction

## 1.1 Motivation and goals

Clutter is an ineluctable factor with non-negligible interference in radar detection. Ground clutter signals are usually reflected by the ground surface, ground-based objects, and obstacles, while sea clutter signals are usually reflected by the sea surface. For radar applications in air surveillance and ship navigation, the detection of target signals in a sea and ground clutter environment may be problematic tasks. In the case of a stationary target in a heavy ground clutter environment where surrounding objects scatter comparable to the target amount of sensing signal energy, Doppler information is not usable for classifying the target signal from clutter. In the case of a small floating target in the ocean, it has the same low fluctuating speed as the ocean. The target Doppler also cannot be effectively separated from the sea clutter Doppler. As a result, the method to extract the target Doppler information based on the time-frequency distribution, such as the extraction of micro-Doppler characteristics [1], cannot show impressive performance in the target detection cases mentioned above.

One of the promising technologies in target detection is the use of polarimetric estimation of the target and clutter polarimetric parameters. In recent decades, such detection algorithms were proposed which utilize not only the usual energy feature of single polarization or multipolarization channels but also single- and joint statistical polarization characteristics as *a priori* knowledge depending on the physical characteristics and geometry structures [2] [3] [4]. However, the limitation of those previous studies is that the detection algorithms were mostly developed and tested for the case where the clutter is assumed to be spatially homogeneous within the measured range.

In remote sensing of maritime and terrain, one of the main challenges is radar target detection in heavy clutter, when surrounding objects scatter comparable to the target amount of sounding signal energy, the desired precise target detection cannot be achieved. Another challenge in terrain remote sensing is that the spatial homogeneity of clutter within reasonable intervals of radar ranges and azimuths cannot be observed. There are many types of surface-based objects, terrain types, and features in real-world scenarios. In this research, in order to suppress clutter and then detect the target from a specific area with a low false alarm rate and high detection accuracy, we are interested in the analysis of the performance of various detection schemes. To perform the detection process, the three channels of polarimetric data must be reduced to a single decision criterion. This transformation should be performed in such a way that the target is more easily discriminated from the clutters [5].

The ultimate objective of this study is to estimate the potential for the use of polarimetric information for target detection in the cases of inhomogeneous clutter. During this process, the following sub-goals are required:

1. Implement polarimetric detectors with polarimetric model data obtained by polarimetric signal modeling and feature vectors generation for both target and clutter;
2. To evaluate the efficiency of polarimetric detectors with polarimetric measurement model data in simulation;
3. To analyse the spatial statistical characteristics of real ground clutter and observed object with measurement data of realistic scenario;
4. To evaluate the experimental validation of polarimetric detectors with measurement data, and evaluate the detectability and sensitivity to the difference in terms of polarization characteristics of the target and clutter.

## 1.2 Research problem definition

In recent years, most radar systems have the ability to transmit and receive electromagnetic waves at orthogonal polarization (i.e. horizontal and vertical). Polarization information has become an important tool to improve target detection performance in the background of clutters and jammers [6]. Detection of ground-based stationary targets such as vehicles and substations by space radar, and detection of low-velocity sea surface targets such as sailing boats and driftwoods by marine radar are considered as challenging subjects in both military and civil fields. In such cases, the real targets may be omitted among strong clutters or the strong clutters may be miscalculated as targets, resulting in a decrease in detection probability. To address this problem, polarization energy features and polarimetric characteristics can be considered as additional information to enhance the polarization contrast between clutter and target signals so as to improve detectability.

This thesis will present an compatitive analysis of the performances of various polarimetric target detection algorithms: the Optimal Polarimetric Detector (OPD) [2], the Identity Likelihood Ratio Test (ILRT) [5], the Polarimetric Whitening Filter (PWF) [3], the single-polarimetric channel detector [5], the span detector [5], and the Power Maximum Synthesis (PMS) detector [5], which are proposed in previous research. To study the efficiency of these algorithms in the condition of homogeneous clutter, a polarimetric radar simulator is realized for generating feature vectors and applying these polarimetric detection algorithms. In simulation, with polarimetric models of clutter and targets that were proposed in previous literature [5] [2], the performance of all six detection algorithms will be compared for multi-scatterer targets and deterministic targets, which performs the validation of the polarimetric radar simulator used in this research. The analysis of performances shown in the simulator will give the basic understand of these polarimetric detection algorithms for further analysis in non-homogeneous cases. Considering the effect of target mismatch in the ILRT method is not well understood, this thesis will mainly focus on implementations of other five detection algorithms with measurement data. The empirical Receiver Operating Characteristic (ROC) that enables one to plot the probability of detection versus the probability of false alarm calculated from the dataset will present the detection performance of these algorithms in simulation. Experimental validations and performances of these detectors with measurement data will be presented by comparing the detection result maps with a real global map as a reference.

The results of simulation of model data with known clutter and target covariance matrices will be presented for both random and deterministic targets in the presence of complex Gaussian clutter. Then the same detection algorithms will be tested on the measurement data for target detection in the large-scale realistic scenario which contains a variety of clutters. The aim of this research is to detect the power line mast (in Figure. 1.1) in the terrain environment with grasslands, forests, and other ground-based objects as various types of clutters with homogeneous and inhomogeneous polarimetric characteristics.

Figure 1.1: Power line mast

The realistic scenario is given in Figure. 1.2. This is a rural/recreation area in Delft city surroundings. The measured area is within the scope between two red paths beginning from the PARSAX radar, and the direction of the main beam of the antenna is denoted by the blue line in the center. As the placemarks on the map, power line masts are located in a line which are labeled EP1 - EP6. Forests and grasslands marked on the map in terms of target detection are supposed to be recognized and suppressed by applying different target detection algorithms. Using various detection algorithms, the polarization contrast between power line masts and ground-based clutters will be strengthened, and heavy clutters will be distinguished and filtered, leading to more precise target detection.

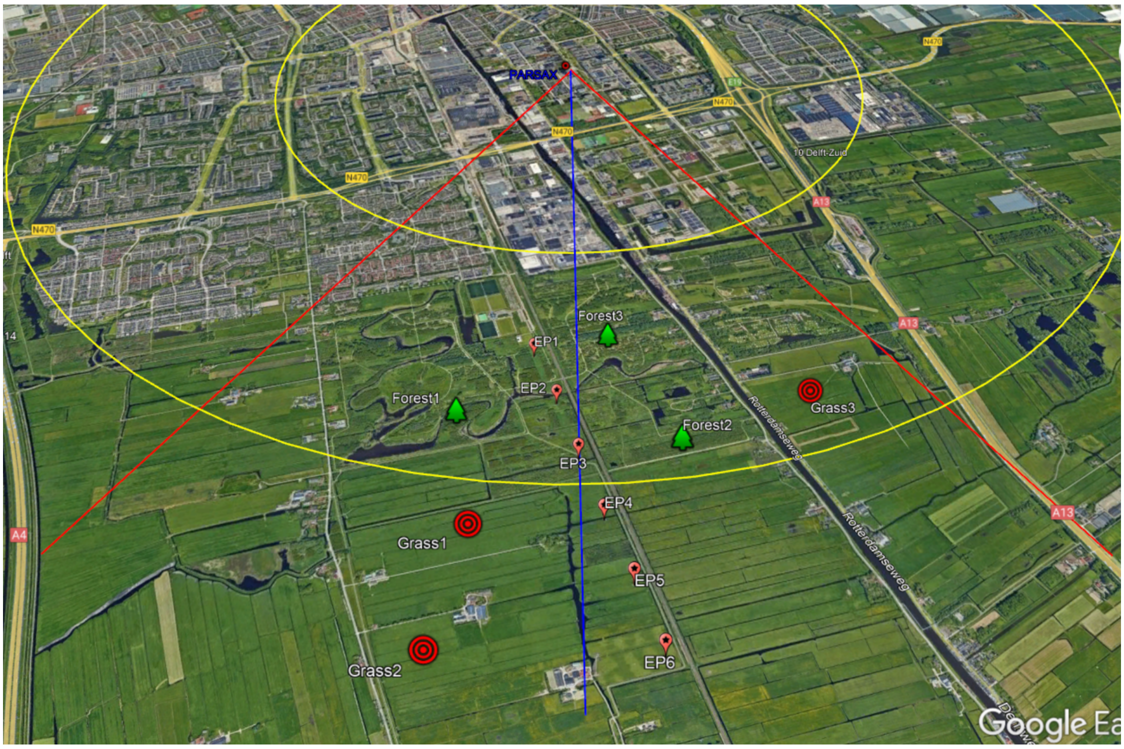


Figure 1.2: Realistic scenario of measurement data

## 1.3 Overview of the state-of-the-art

As one of the most significant techniques in modern battlefield reconnaissance, meteorological observation, resource exploration, and environmental monitoring, radar plays a pivotal role in military and civil fields. Based on fully mining the information contained in space electromagnetic waves, in addition to obtaining the target's distance, speed, and orientation, radar can also analyze and distinguish the target's type, characteristics, and structure information.

Polarization is another important piece of information that radar can use, except for information in the time domain, frequency domain, and airspace domain. The effort to apply polarization diversity to improve radar performance dates back to the 1950s [6]. As an inherent property of an electromagnetic wave, polarization reflects the variation of the electric field vector endpoint in the time domain. According to the shape and handedness of the space trajectory formed by the polarization, it can be divided into linear, circular, and elliptic polarization, and left- and right-handedness polarization. The application of electromagnetic wave polarization in the radar field has excellent development potential, since the polarization state of the received electromagnetic wave is related not only to the polarization state of the electromagnetic wave transmitted from the transmitting antenna, but also affected by the shape, size, attitude, material composition, and other factors of the target [7].

The polarization radar system has generally experienced variable/double polarization to full polarization, a long development process. Full polarization measurement capabilities developed from multiple pulse intervals measuring to the single pulse interval measuring simultaneously. In addition, in terms of the target of interest, it extended from the simple stable target (ideal static point scattering target) to a complex non-stationary target (large complex target or high-speed maneuver target [8], etc.). The polarization radar system is widely applied and can adapt to a more complex electromagnetic environment such as wideband signal, partially polarized wave, all kinds of noise, clutter, interference, etc.

Polarization, as another dimension of information, in addition to amplitude, phase, and frequency, also plays an important role in the detection of radar targets. Generally speaking, target detection methods based on polarization information can be divided into two main classes: optimal reception detection and polarization statistical detection. The basic idea of the former is to make the target echo in the received signal stronger than noise or clutter by controlling the weighting of the polarization channel in the transmitter/receiver to achieve the target detection purpose [9] [10]. In summary, optimal reception detection focuses on the use of polarimetric scattering mechanisms to distinguish the target from clutters [11]. This class of detection method is represented by a variety of scattering power detectors, for example, the polarimetric span (total power) detector, the Polarimetric Whitening Filter (PWF), and the Power Maximization Synthesis (PMS) detector [5] [3] were developed to fuse multichannel polarimetric information to discriminate the target from clutter. The latter was supposed to establish a reliable polarization information model of the target, noise, or clutter, and to perform target detection based on statistical decision criteria, such as an adaptive polarization detector based on generalized likelihood ratio test (GLRT) on a Gaussian clutter background [12] and Constant False Alarm Rate (CFAR) detection [13]. In the second class of target detection methods, the widely used statistical models that characterize the statistical properties of the clutter contain K-distribution, Weibull, Gamma, etc. Liu and Lampropoulos used the multi-CFAR detector to detect the ship as the target [14]. In the literature, there were also many other ways to use scattering mechanisms to detect targets on the sea surface, e.g. polarimetric entropy (H) [15], the symmetry scattering characterization method [16], and the similarity of polarimetric scattering [17]. Wang and Liu [18] took into account the surrounding region of the ships, and superpixel technology was adopted to derive new polarimetric scattering features for ship detection.

Regarding optimal reception detection approaches, although these detectors could detect most of sea and ground targets with less prior knowledge required and were easier to implement, they may still lose the weak target whose backscattered intensity is weak [19]. Recent work in the field of polarization statistical detection has addressed the design of the optimal detector under the assumption of known target and clutter scattering parameters [2]. However, this assumption is non-trivial for many radar applications in practice. It may not be possible to measure the statistics of the target a priori when the target is covered among strong clutter. Similarly, clutter statistics are difficult to obtain a priori because they vary spatially with the type of terrain and temporally due to weather and seasonal changes. As a result, different detection algorithms that used training data were developed subsequently [12]. These data, also known as secondary data, consist of recorded echoes from range cells adjacent to the cell under

| Class | Detector | Main method | Requirement |
|---|---|---|---|
| **Optimal reception detection** | Single channel detector | Magnitude of single polarimetric channel | Simplest implementation |
| | Span detector | Total power of HH, HV, VV | Physical approach only |
| | Power maximization synthesis | Components of measurement vector | Physical approach only |
| **Polarization statistical detection** | Polarimetric whitening filter | Minimize the standard deviation of the backscattering intensity | *a priori* clutter information |
| | Optimal polarimetric detector | Likelihood ratio test | *a priori* clutter and target information |
| | Texture Free-Generalized Likelihood Ratio Test (TF-GLRT) detector (2001) | Texture Free-Generalized Likelihood Ratio Test (TF-GLRT) | known normalized covariance matrix |
| | Multi-CFAR detector (2007) | several single CFAR detectors | polarimetric decompositions and transformations + adaptive Principal Component Analysis (PCA) + multi-CFAR detection (only simulation) |
| | superpixel-level CFAR detection (2015) | superpixel segmentation | extreme homogeneity and compactness properties of superpixels (ship detection) |

Figure 1.3: Comparison of target detection techniques

test, assuming that those cells have the same clutter covariance structure and are free of targets. A comparison of several target detection techniques is shown in Fig. 1.3. A significant trade-off among these detection algorithms is the amount of statistical information required by the algorithms versus the performance of the algorithm.

## 1.4 Research contribution

The main contributions and novelties of this research are the following:

- Based on the S-band polarimetric-Doppler FMCW PARSAX radar high-resolution range measurements in azimuthal scanning mode
  a. the polarimetric detection algorithms' applicability to the real radar scene with highly inhomogeneous clutter has been validated;
  b. the spatial variability of polarimetric characteristics of the rural/recreation area in the Delft city surroundings has been studied for the first time;

- The novel usage of the Polarimetric Whitening Filter and the Optimal Polarimetric Detector for the classification of targets and clutter has been demonstrated, which can be implemented in parallel for different types of clutter within a simple real-time streaming signal processing algorithm.

## 1.5 Thesis structure

This thesis presents an analysis of the spatial statistical characteristics of real ground clutter and presents comparative analysis and experimental validation for the performance of five different types of target detection algorithms with measurement data. Chapter 1 proposes the motivation and goals of this research, the main focus problem, and the contribution of this research. Here, it also discusses the study of the relative literature. Chapter 2 first introduces the PARSAX polarimetric Doppler FMCW radar system and the noise-based calibration of a polarimetric radar system, and then discusses the polarimetric signal models of radar return for terrain clutter, and also discusses the polarimetric target models for multi-scatterer target and deterministic target depending on various resolution conditions. Chapter 3 gives a description of the algorithms considered in this research and presents algorithm performance comparisons corresponding to the ideal case in which target and clutter statistics are known exactly in the polarimetric radar simulator. Chapter 4 presents the analysis of the spatial statistical characteristics of the reference target and real spatially inhomogeneous ground-based clutters, and displays a covariance matrix map for the full area that is interested in. Chapter 5 presents algorithms performance comparisons and experimental validation for the performance of target detection algorithms with measurement data in the real ground clutter. At the end of this thesis, Chapter 6 sheds light on the conclusions of this research and discusses the limitations of this research and future work.

# 2 Polarimetric Radar System

This chapter mainly describes a new method of noise-based equalization of the polarimetric radar system's channels [20], which was for the first time implemented, tested, and applied within this study as a default tool for the internal calibration of the radar polarimetric measurements using the PARSAX radar. The theoretical polarimetric models [5] of clutter and different types of targets in various resolution conditions which were proposed by previous references are described for further application of polarimetric radar simulator.

## 2.1 The PARSAX Polarimetric Doppler FMCW Radar System

### 2.1.1 Model of the polarimetric radar measurements

The polarization scattering matrix (PSM) can adequately describe the instantaneous polarimetric properties of any observed object. It illuminates the relation between the polarization state of the incident electromagnetic signal and the polarization state of the signal scattered in a specific direction [21] [22]:

$$\dot{\mathbf{E}}_{\mathbf{R}}(t) = \dot{\mathbf{S}} \cdot \dot{\mathbf{E}}_{\mathbf{T}}(t) = \begin{Vmatrix} S_{11}e^{j\psi_{11}} & S_{12}e^{j\psi_{12}} \\ S_{21}e^{j\psi_{21}} & S_{22}e^{j\psi_{22}} \end{Vmatrix} \cdot \dot{\mathbf{E}}_{\mathbf{T}}(t) \tag{2.1}$$

where $\dot{\mathbf{S}}$ denotes the PSM of an observed object, $\dot{\mathbf{E}}_{\mathbf{T}}(t) = \left\| \dot{E}_{1T}(t), \dot{E}_{2T}(t) \right\|^T$ denotes the polarization vector of the transmitted radar signal, and $\dot{\mathbf{E}}_{\mathbf{R}}(t)$ denotes complex polarization vector of the received radar signal. Polarization vectors and PSM are expressed on the same polarization basis (PB) $\{1, 2\}$. The symbol $\langle \cdot \rangle$ above the letters in this thesis means complex values of related variables. As mentioned above, Eq. 2.1 with normalized vectors $\dot{\mathbf{E}}$ is able to describe the polarization state of the transmitted and received signals. In addition, this expression can fully describe signal propagation within radar channels with information about the amplitudes (power) and phases of the signal and noise.

In reality, the expression of the polarization state of the received radar signal is considered to be more complicated than that of Eq. 2.1 in the ideal propagation radar system. To be more specific, several factors need to be included:

- non-ideality and non-equality of transmission channel chains for transimitted signals with both orthogonal polarizations, non-equality of the transmit antenna gains on these polarizations, and non-zero cross-polarization coupling which is possible to present;

- possible signal depolarization in the propagation to the target and back to the radar, for example, in the case of propagation in the ionosphere or in rain;
- the presence of clutter signals;
- interactions between scattered signal (clutter included) and non-ideal receive antenna and non-equal receiver channels chains;
- thermal noise in measurement channels as independent white Gaussian random signals.

Therefore, at the output ports of the received antenna, the measured signals with orthogonal polarizations can be given as follows:

$$\dot{\mathbf{E}}_{\mathbf{R}}(t) = \frac{A}{r^2}e^{-2jkr} \cdot \dot{\mathbf{R}} \cdot \dot{\mathbf{R}}_{\mathbf{A}} \cdot \dot{\mathbf{P}}_{-} \cdot \left(\dot{\mathbf{S}}_{\mathbf{0}}+\dot{\mathbf{C}}\right) \cdot \dot{\mathbf{P}}_{+} \cdot \dot{\mathbf{T}}_{\mathbf{A}} \cdot \dot{\mathbf{T}} \cdot \dot{\mathbf{E}}_{\mathbf{T}}+\dot{\mathbf{N}} \tag{2.2}$$

with

$$A = \left(\frac{2\eta_0 P_t G_t G_r \lambda^2}{(4\pi)^2}\right)^{1/2} \tag{2.3}$$

where $\dot{\mathbf{S}}_{\mathbf{0}}$ denotes the exact PSM of the observed object in the radar, $\dot{\mathbf{C}}$ denotes the PSM of clutter, $\dot{\mathbf{T}}_{\mathbf{A}}$ denotes the distortion matrix of the dual-polarized transmit antenna, $\dot{\mathbf{T}}$ denotes the diagonal distortion matrix of the transmitter, $\dot{\mathbf{R}}_{\mathbf{A}}$ denotes the distortion matrix of the dual-polarized receiving antenna, $\dot{\mathbf{R}}$ denotes the diagonal distortion matrix of the output ports of the receiving antenna and input circuits of the receiver. $\dot{\mathbf{P}}_{+}$ and $\dot{\mathbf{P}}_{-}$ denote the distortion matrices of the propagation channel in the propagations to the target and back to the radar, respectively. $\dot{\mathbf{E}}_{\mathbf{T}}$ denotes the polarization state of the transmitted signal without non-ideality, $\dot{\mathbf{E}}_{\mathbf{R}}$ denotes the polarization state of the received signal.

In addition, the received signal amplitude $A$ and phase are dependent with the range $r$ between radar and the target as shown in Eq. 2.2. In Eq. 2.3, the constant $A$ denotes the amplitude of the initial transmitted signal, $\dot{\mathbf{N}}$ denotes the thermal noise in every measurement channel. $P_t$ is transmit power of the transmitted antenna, $G_t$, $G_r$ are the gains of the transmitted and received antennas, respectively. $\lambda$ is known as the radar wavelength, $\eta_0$ is the intrinsic impedance of free space, and $k$ denotes the modulus of the propagation vector.

In the relation (2.2) there are the scalar relations between the total amplitudes, powers, and phases of the transmitted and received signals, and also the vector/matrix relations that describe the dependencies between their polarization components. The normalization of every matrix and vector within Eq. 2.2 for one selected element (e.g. with indexes 1,1) can be used to separate these scalar and the vector/matrix relations. Such a separation gives a possibility to process and to analyze the total amplitude (radar cross section) and Doppler velocity of the target separately from its polarization characteristics.

For the measurements of all elements of the PSM (in Eq. 2.1), the polarization-orthogonal waveforms have to be transmitted with the reception of the scattered signal in polarization-orthogonal receiver channels. To benefit from an independent and precise estimation of the waveforms in terms of amplitudes and phases, transmitting on orthogonal polarizations is a reasonable option. The polarimetric radar is capable of measuring the PSM of the object using sensing signals with dual orthogonality in polarization and in waveform spaces [23] [24], [25]. Sensing signals with dual orthogonality can be represented as the sum of two orthogonal polarization components. The polarization basis of the radar measurements is formed by these two orthogonal polarization components. Then the sensing signals are modulated with some kind of orthogonal waveforms that can be separated during reception with some type of matched processing.

For received signal processing, the time-multiplexed polarimetric waveform is the simplest technique in terms of implementation. This means that the transmission and reception of the orthogonally polarized components are separated in time. However, using time-multiplexed polarimetric waveform causes non-simultaneous measurement of the columns of the PSM; this may lead to a decrease of accuracy of the measurements for fast moving and fast changing targets. Furthermore, the full PSM is measured with two times reduction of the operational pulse/sweep/waveform repetition frequency, this can lead to a critical drawback in Doppler velocity estimation of two times reduction of the ambiguity.

Transmitting polarization components simultaneously is considered as an alternative [23]. Polarization components are modulated with orthogonal waveforms. These waveforms satisfy the condition for the polarization components of the transmitted signal :

$$U_T = \int \dot{E}_{iT}(t) \cdot \dot{E}^*_{jT}(t) \cdot dt \equiv 0,\ i, j = 1, 2,\ i \neq j, \tag{2.4}$$

To be able for the efficient matching processing of the received signals, a similar condition has to be satisfied between the polarization-orthogonal components of the received and transmitted signals. As soon as, in general, the received signal is a copy of the transmitted signal, which is delayed for the time $\tau$ and shifted in frequency with a Doppler shift $\omega_d$, this condition can be written in a form:

$$U_{ij}(\tau, \omega_d) = \int \dot{E}_{iT}(t) \cdot \dot{E}^*_{jR}(t - \tau, \omega_d) \cdot dt \cong 0,\ i, j = 1, 2,\ i \neq j, \tag{2.5}$$

where $\dot{E}_{iT}(t)$ and $\dot{E}_{jR}(t - \tau, \omega_d)$ are polarization orthogonal components of the transmitted and received signals.

By means of joint matching processing, all elements of the PSM are able to be measured simultaneously. In the research of [23] [24], [25], [26], various types of Linear Frequency Modulation (LFM)-based polarimetric signals for FMCW radars have been proposed. The block diagram shown in Figure.2.1 illustrates the implementation of transmitting simultaneously polarization components that are modulated with orthogonal waveforms. Eq. 2.2 defines the output signals on the four polarimetric receiver channels on the polarimetric FMCW radar.

### 2.1.2 Noise-Based Polarimetric Channels Equalization

For further analysis it will be suitable to represent the measured $2 \times 2$ PSM at the output of polarimetric radar receiver in a $4 \times 1$ vector form, which better reflects the

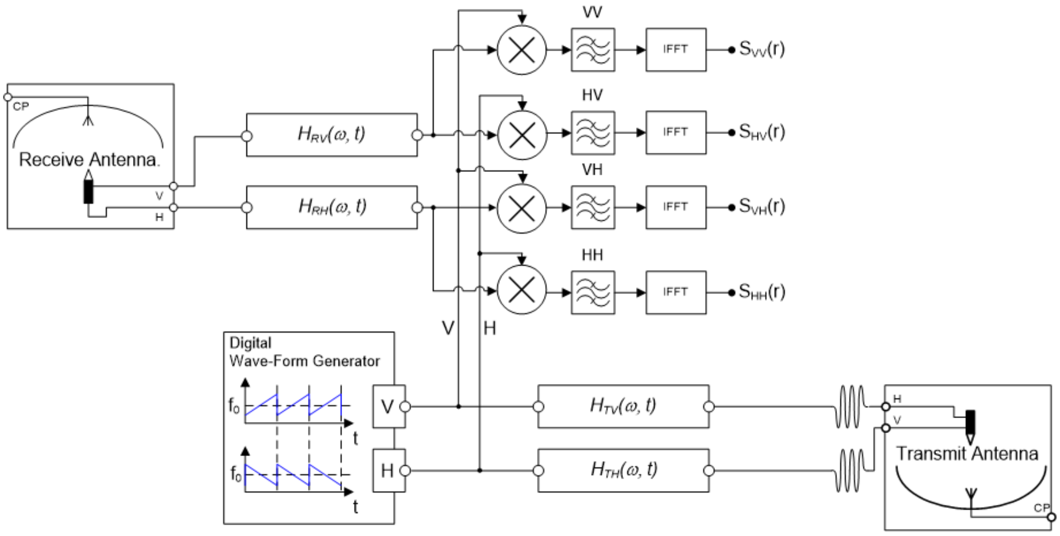


Figure 2.1: Bloc-diagram of the polarimetric FMCW radar with dual-orthogonal sensing signals

measurement procedure:

$$\dot{\mathbf{X}} = \begin{bmatrix} S_{11i} + j \cdot S_{11q} \\ S_{12i} + j \cdot S_{12q} \\ S_{22i} + j \cdot S_{22q} \end{bmatrix} + \begin{bmatrix} n_{11i} + j \cdot n_{11q} \\ n_{12i} + j \cdot n_{12q} \\ n_{22i} + j \cdot n_{22q} \end{bmatrix} = \begin{bmatrix} \dot{S}_{11} \\ \dot{S}_{12} \\ \dot{S}_{22} \end{bmatrix} + \begin{bmatrix} \dot{n}_{11} \\ \dot{n}_{12} \\ \dot{n}_{22} \end{bmatrix} \tag{2.6}$$

where $S_{k,l_i}$ and $S_{k,l_q}$, $k, l = 1, 2$ are the in-phase and quadrature components of the polarization scattering matrix element $k, l$ polarimetric channel, respectively. Similarly, $n_{k,l_i}$ and $n_{k,l_q}$ are the quadrature components of the thermal white Gaussian noise in the polarimetric channel $k, l$.

All elements of the PSM can be obtained by the polarimetric FMCW radar. Therefore, in every polarimetric channel the range- and the time-dependent received signal can be defined as a sum of the backscattered from the observed object signal and the thermal noise:

$$x_{i,j}(r, t) = \dot{S}_{i,j}(r, t) + \dot{n}_{i,j}(r, t), \tag{2.7}$$

where the indices $i, j = 1, 2$, $i \neq j$, refer to the transmitted horizontal and vertical polarization channels and the received horizontal and vertical polarization channels, respectively. $r$ stands for the range coordinate after compression of the beat signal range, $t = n \times SRI$ denotes the discrete slow time, which is the integer number of the sweep repetition intervals ($SRI$). At the output of four polarimetric receiver channels, shown in this equation, $\dot{S}_{i,j}$ are the actual complex scattered signals, which are presented by the slow-time-dependent range profile. $\dot{n}_{i,j}$ is the complex white Gaussian thermal noise with zero mean and variance $\sigma^2_{i,j}$. As for the relation between Eq. 2.7 and Eq. 2.2, $\dot{S}_{i,j}$ is the received signal $\dot{\mathbf{E}}_{\mathbf{R}}$ without taking into account the thermal noise $\dot{n}_{i,j}(r, t)$ (in Eq. 2.7) or $\dot{\mathbf{N}}$ (in Eq. 2.2).

Non-ideality and non-equality exist at the received channels due to the independence of electronic devices. As a result, the actual measured signals at the output of four polarimetric receiver channels are rewritten by

$$V_{i,j}(r,t) = a_{i,j}(r) \cdot x_{i,j}(r,t) + b_{i,j}(r), \tag{2.8}$$

where $a$ denotes the amplification in each channel and $b$ denotes the bias of the output signal in each channel. Normally, the amplification and bias of the output signal are related to the range and are assumed to be without short-term temporal dependency.

Ideally, the noise signals in all channels are supposed to be the same, since the radar channels with the same electronic design and the same system temperature are in the same physical environment. Measurement of noise signals in each polarimetric channel can be accomplished by blanking the transmitter power amplifier. The noise signals obtained at the output of four polarimetric receiver channels can be represented as

$$N_{i,j}(r) = a_{i,j}(r) \cdot n + b_{i,j}(r), \tag{2.9}$$

where $n$ is the actual white Gaussian noise with zero mean and variance $\sigma_0^2$. Noise is supposed to be independent in terms of range, time, and channel. And $N_{i,j}(r)$ is the noise measured at the output of the receive channel $(i,j)$. Based on these assumptions, the measured noise signals can be estimated and analyzed by the mean value and variance, which are defined by

$$\begin{aligned} &mean(N_{i,j}(r)) = b_{i,j}(r) \quad , \\ &var(N_{i,j}(r)) = [a_{i,j}(r)]^2 \cdot \sigma_0^2 \quad . \end{aligned} \tag{2.10}$$

One of the calibrations in the polarimetric radar system is equalization for all channel signals, which is defined by

$$\begin{aligned} z_{i,j}(r,t) \quad &= V_{i,j}(r,t) - mean(N_{i,j}(r))/\sqrt{var(N_{i,j}(r))} \\ &= S'_{i,j}(r,t) + n'_{i,j}(r,t). \end{aligned} \tag{2.11}$$

By this equalization, the amplitude of $S'_{i,j}(r,t)$ is actually the square root of the signal-to-noise ratio ($\sqrt{SNR}$) in each channel, and $n'_{i,j}(r,t)$ as the variance of the equalized noise is 1.

### 2.1.3 The PARSAX radar data and their noise-based equalization

The polarimetric data that are used in this study have been measured using the PARSAX S-band polarimetric-Doppler FMCW radar. This radar measures the polarization scattering matrix of objects in the linearly-polarized polarization basis $H, V$. For this reason in all further chapters, we will use the equivalence of the general indexes $i, j,\ i, j = 1, 2$ with the standard notation of the $\{H, V\}$ polarization basis: $S_{HH} = S_{11}, S_{HV} = S_{12}$ and $S_{VV} = S_{22}$. For covariance matrix indexing in this report, we used the following notation: index 1 is used for $HH$, index 2 - for $HV$, index 3 - for $VV$.

It is also necessary to mention that the PARSAX radar measures the PSM elements $HV$ and $VH$ independently, but as soon as we used in this study the covariance matices with the size $3 \times 3$, for all further analysis we used the averaging of the measured cross-polarized channels $S^m_{HV}$ and $S^m_{VH}$: $S_{HV} = (S^m_{HV} + S^m_{VH})/2$.

In this research, the mean values of noise signals in full polarimetric channels measured in 15 bursts are analyzed at each range index. Through this analysis of the measured noise signals, the non-equality characteristic is found between the polarimetric channels instead of the identical noise signals in all channels. As seen in Figure 2.2, with total range indices of 1200, the mean value of the noise power of the $HH$ polarization is approximately 97 dB, while the mean value of the noise power of the $HV$ polarization is 6dB higher than $HH$, and the $VV$ polarization is 7dB higher than $HH$.

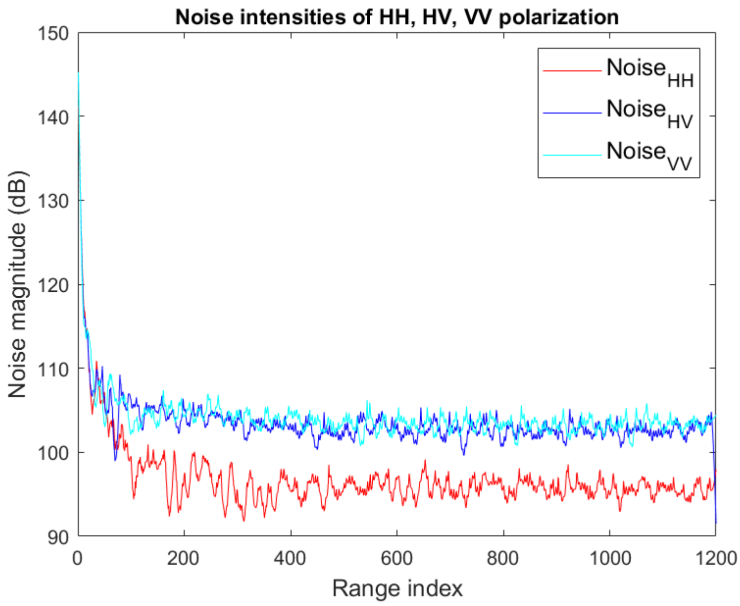


Figure 2.2: Noise Power of HH, HV, and VV polarization before system calibration

To solve the non-equality of measured noise signals in the $HH$, $HV$, and $VV$ channels, and minimize the thermal noise influence on the further estimation of the polarization parameters, calibration is carried out with the idea of equalization on the mean value of noise powers. In the measurement of this research, since the observed objects are static, long ($\approx 0.5$ s) Doppler coherent integration of measured signals is used with the following filtration of stationary signals with zero Doppler velocity. First, after the Fourier transform for the slow-time measured received signals $s(r, t)$ and the measured noise signals $n(r, t)$ in polarimetric channels, the zero Doppler data $S(R)$ and $N(R)$ are collected. Then the amplitude of zero Doppler data corresponding to the received signals is replaced by $\sqrt{SNR}$:

$$SNR = \frac{|S(R)|^2}{|N(R)|^2} \tag{2.12}$$

and the phase of zero Doppler data $\varphi_s(R)$ corresponding to the received signals is preserved. Note that the SNR in Eq. 2.12 in terms of the same range index, which means that the zero Doppler data of the signals are divided by the zero Doppler data of the noise measured at the same range index as the received signal. As a result, the regenerated zero Doppler data can be represented by:

$$S^{'}(R) = \sqrt{SNR} \cdot e^{j\varphi_s(R)} \tag{2.13}$$

Assume that the distortions due to this non-equality of noise powers are similar for both target signal and clutter signals; the noise-based equalization as the internal calibration for all channel signals is accomplished on zero Doppler after Fourier transforms on the measurement slow-time data. The experimental efficiency of such calibration will be tested and discussed in the performance of detection algorithms used in the real radar scene (in Chapter 5).

## 2.2 Model of the Polarimetric Radar Signals

The polarization scattering matrix described above characterizes the instant polarimetric characteristics of the target and is not suitable in case when these characteristics are changing in time, especially when they are random. At the same time, the random variability of the PSM in space is the standard behavior of this characteristic in real-world scenarios. To study the statistical characteristics of real radar objects, the covariance matrix is essential in this research.

The covariance matrix as a common way to estimate second-order statistics exploits the scattering vector [22], its standard expression which is estimated starting from the Lexicographic basis scattering vector is shown below on H-V polarization basis, where the random variables have zero mean.

$$\mathbf{C_{4L}} = \begin{bmatrix} \langle |S_{HH}|^2 \rangle & \langle S_{HH}S_{HV}^* \rangle & \langle S_{HH}S_{VH}^* \rangle & \langle S_{HH}S_{VV}^* \rangle \\ \langle S_{HV}S_{HH}^* \rangle & \langle |S_{HV}|^2 \rangle & \langle S_{HV}S_{VH}^* \rangle & \langle S_{HV}S_{VV}^* \rangle \\ \langle S_{VH}S_{HH}^* \rangle & \langle S_{VH}S_{HV}^* \rangle & \langle |S_{VH}|^2 \rangle & \langle S_{VH}S_{VV}^* \rangle \\ \langle S_{VV}S_{HH}^* \rangle & \langle S_{VV}S_{HV}^* \rangle & \langle S_{VV}S_{VH}^* \rangle & \langle |S_{VV}|^2 \rangle \end{bmatrix} \tag{2.14}$$

For a monostatic sensing system, the Sinclair scattering matrix is symmetrical, which means $S_{VH} = S_{HV}$. Then the polarimetric covariance matrix can be expressed as:

$$\mathbf{C_{3L}} = \begin{bmatrix} \langle |S_{HH}|^2 \rangle & \langle S_{HH}S_{HV}^* \rangle & \langle S_{HH}S_{VV}^* \rangle \\ \langle S_{HV}S_{HH}^* \rangle & \langle |S_{HV}|^2 \rangle & \langle S_{HV}S_{VV}^* \rangle \\ \langle S_{VV}S_{HH}^* \rangle & \langle S_{VV}S_{HV}^* \rangle & \langle |S_{VV}|^2 \rangle \end{bmatrix} \tag{2.15}$$

Normally, the scattered polarization signal from an object is received with noise. In this case, the polarimetric covariance matrix of the received signals is the sum of the polarimetric covariance matrix of an object and the polarimetric covariance matrix of noise, which can be expressed by

$$\mathbf{C} = \mathbf{C_{ob}} + \mathbf{C_n} = \mathbf{C_{ob}} + \sigma_\mathbf{n}{}^\mathbf{2}\mathbf{I} \tag{2.16}$$

where $\mathbf{C}$ denotes the covariance matrix of received polarization signals, $\mathbf{C_{ob}}$ denotes the covariance matrix of an object, $\mathbf{C_n}$ denotes the covariance matrix of noise. When the noise is assumed to be white Gaussian noise with zero mean and variance ${\sigma_n}^2$, its covariance matrix is a diagonal matrix with ${\sigma_n}^2$ on the main diagonal. When the total power of the full polarization channels of an object is much larger than the total power of full polarization channels of noise, the covariance matrix of noise can be considered negligible.

The aim of this chapter is to provide the polarimetric clutter model of radar return for terrain environment, and the polarimetric target models for multi-scatterer target and deterministic target depending on various resolution conditions. These signal models will then be used in the process of deriving the OPD, ILRT, and PWF detectors.

### 2.2.1 Polarimetric Clutter Model

This subsection presents a basic explanation of the polarimetric clutter model that is learned from previously published literature [2] and used further in our study.

The main assumption of this model is that in case of measurements with a coherent fully polarimetric radar the terrain clutter return can be modeled as a complex Gaussian random vector (2.6) with zero mean values of all components. The Probability Density Function (pdf) of this measured vector can be written as

$$f(\mathbf{X}) = \frac{\mathbf{1}}{\pi^{\mathbf{3}}\left|\mathbf{C}\right|} \exp\{-\mathbf{X}^{\dagger}\mathbf{C}^{-\mathbf{1}}\mathbf{X}\} \tag{2.17}$$

where † denotes the complex conjugate transpose and

$$\mathbf{C} = \mathbf{E}\left\{\mathbf{X}\mathbf{X}^{\dagger}\right\} \tag{2.18}$$

is the covariance matrix of the complex polarimetric vector $X$, and again, the clutter data is assumed to have zero mean values of the observation vector $E\left\{\overline{X}\right\} = 0$.

The complete statistical characteristics of the jointly Gaussian radar returns HH, HV, and VV are presented by the covariance matrix. Discussed for the cases where the electromagnetic wave scattering in the reflection-symmetric medium [22] where the cross-polarization scattering will not be correlated with the co-polarization, and based on the Born approximation [27], four of the elements in the covariance matrix reducing to zero theoretically. On a linear polarization basis (H-V), the corresponding covariance matrix for complex Gaussian clutter is supposed to be expressed as

$$\mathbf{C} = \sigma \begin{bmatrix} 1 & 0 & \rho\sqrt{\gamma} \\ 0 & \epsilon & 0 \\ \rho^{*}\sqrt{\gamma} & 0 & \gamma \end{bmatrix} \tag{2.19}$$

where $\sigma$ denotes the backscattering cross section per unit area of the HH polarimetric channel,

$$\sigma = E\left\{\left|S_{HH}\right|^{2}\right\}; \tag{2.20}$$

and $\epsilon$ denotes the intensity ratio of $HV$ and $HH$ returns,

$$\epsilon = \frac{E\left\{\left|S_{HV}\right|^{2}\right\}}{E\left\{\left|S_{HH}\right|^{2}\right\}}; \tag{2.21}$$

while $\gamma$ denotes the intensity ratio of the returns of $VV$ and $HH$,

$$\gamma = \frac{E\left\{|S_{VV}|^2\right\}}{E\left\{|S_{HH}|^2\right\}}; \tag{2.22}$$

and $\rho$ denotes the correlation coefficient between the returns of $HH$ and $VV$.

$$\rho = \frac{E\left\{S_{HH}S_{VV}^*\right\}}{E\left\{|S_{HH}|^2\right\}E\left\{|S_{VV}|^2\right\}} \tag{2.23}$$

This is the "normalized" form of the covariance matrix where the elements of the matrix are normalized by $C_{11}$ as the HH intensity showing as the weight factor in front of the matrix.

In other words, the clutter covariance is specified by four parameters $(\sigma_c, \epsilon_c, \gamma_c, \rho_c)$. The reason of the four zero elements of the covariance matrix is that the random medium model employed is azimuthally isotropic, which straightforwardly indicates that there is no correlation between the co-polarization ($VV$ and the $HH$) and cross-polarization returns ($HV$). Therefore, all elements of the covariance matrix can be obtained from the theoretical model for various terrain covers.

The fully polarimetric Gaussian clutter model that characterizes homogeneous clutter regions is used to derive and analyze the theoretical performance of various polarimetric target detection algorithms including the span algorithm, the polarimetric whitening filter (PWF), the optimal polarimetric detector (OPD) algorithm, and the identity likelihood ratio test which uses polarimetric information.

### 2.2.2 Polarimetric Target Models

This subsection describes the theoretical model of the polarimetric characteristics of a ground-based clutter that are learned from previously published literature [5].

The radar targets can be thought of as consisting of a spatially distributed set of multiple simple polarized scatterers. For example, dihedral and trihedral reflectors. Due to the polarimetric radar resolution and the size of the target, these elementary scattering points may be captured and collected in two different target models. In case of the measurements with the high-resolution polarimetric radar, these scattering elements can be captured individually - such a case is called the "deterministic target". The counterparts of deterministic targets are the multi-scatterer targets model in the case of a medium- or low-resolution polarimetric radar system, where the scattering points are combined into one scatterer coherently [28], [29]. In this section, both models are taken into account. To be more specific, the descriptions of the target models for these two cases are as follows.

#### 2.2.2.1 Multi-scatterer Target

In the case of medium- or low-resolution polarimetric radar systems, the target yields a multi-scatterer return, which cannot be represented by a single sample acquisition since any implementation may be different from each other for stochastic processes.

The multi-scatterer target is assumed to have a jointly complex-Gaussian PDF, which is independent of the clutter return. It is also called a random target or a partial target.

Basically, the random target-plus-clutter return is expressed as

$$\mathbf{X_{t+c}} = \mathbf{X_t} + \mathbf{X_c} \tag{2.24}$$

This implies that the measured target-plus-clutter return is a zero-mean complex Gaussian with covariance.

$$\mathbf{C_{t+c}} = \mathbf{C_t} + \mathbf{C_c}. \tag{2.25}$$

In summary, for the multi-scatterer target, the covariance matrix is assumed to have the same general structure as the covariance of the polarimetric clutter model and is also specified by the four parameters $(\sigma_t, \epsilon_t, \gamma_t, \rho_t)$. To be specific, $\sigma_t$ denotes the backscattering cross section per unit area of the $HH$ polarimetric channel of target, $\epsilon_t$ denotes the target's intensity ratio of $HV$ and $HH$ returns, $\gamma_t$ denotes the target's intensity ratio of the returns of $VV$ and $HH$, and $\rho_t$ denotes the correlation coefficient of target between the returns of $HH$ and $VV$ polarization.

#### 2.2.2.2 Deterministic Target

Each scattering element is captured individually in the case of the high-resolution polarimetric radar system [30], as a result, the target is modeled as a deterministic individual resolved scatterer. Algebraically, the scattering matrix, as a transformation from an incident to a scattered wave, is essential and qualified for the polarimetric characteristic of deterministic target if and only if the target polarimetric behavior is polarimetric stationary in time/space. For some typologies of single targets, the hypothesis of polarized illumination can be relaxed, since the scattered wave is always completely polarized.

The return reflected from a deterministic target is given below.

$$\mathbf{X} = \alpha \begin{bmatrix} \cos x \\ e^{jy}\sin x \\ -e^{j2y}\cos x \end{bmatrix} \tag{2.26}$$

In the scattering return expression Eq. 2.26, parameter $\alpha$ specifies the amplitude of the return, $x$ and $y$ are based on the general structure of the scattering matrix of the deterministic target.

Simple polarized deterministic scatterers that are mostly discussed and widely used are the trihedral [31] and the dihedral [32] [33] shown in Fig. 2.3 [34] and Fig. 2.4 [34].

For the trihedral reflector, $x = 0$ and $y = \pi/2$ based on the general structure of the scattering matrix of the trihedral corner reflector as in Eq. 2.27

$$[S]_{trihedral} = \alpha \begin{pmatrix} 1 & 0 \\ 0 & 1 \end{pmatrix} \tag{2.27}$$

where $\alpha$ implies the scale of backscattering intensity of the polarization channels. For dihedral, $x = 2\theta$, where $\theta$ specifies the orientation of the dihedral corner reflector, and

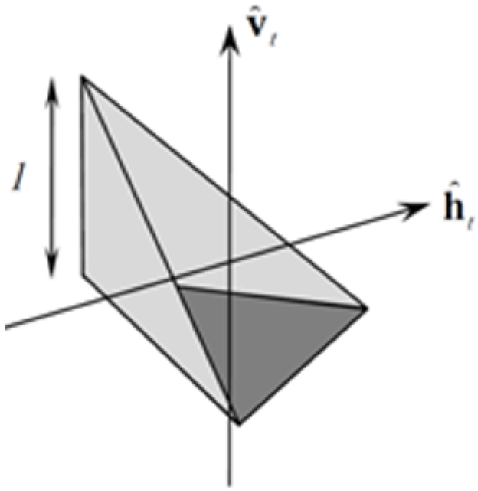


Figure 2.3: trihedral corner reflector

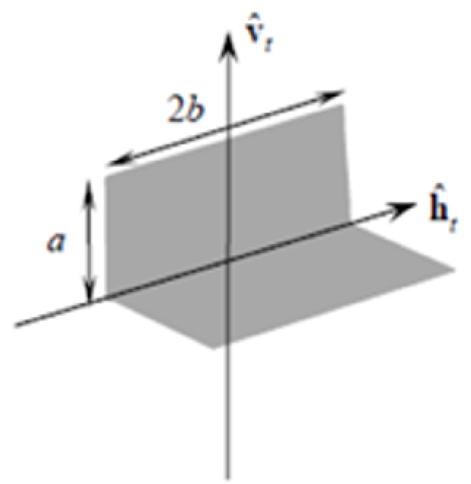


Figure 2.4: dihedral corner reflector

$y = 0$ based on the general structure of the scattering matrix of the dihedral corner reflector as in Eq. 2.28

$$[S]_{dihedral} = \alpha \begin{pmatrix} \cos 2\theta & \sin 2\theta \\ \sin 2\theta & -\cos 2\theta \end{pmatrix} \tag{2.28}$$

## 2.3 Conclusions

This chapter first introduces the PARSAX polarimetric Doppler FMCW radar system, including the descriptions of polarimetric sensing waveforms and processing algorithms, measurement setup, and a noise-based calibration method that is proposed in this research for the measured polarimetric data. Assuming that the distortions for target and clutter are similar, this internal calibration compensates for the distortion at the receiver in the radar system that was not calibrated well. Internal calibration improves to determine accurate measurements of the returned signals scattered by the objects in the realistic scenario. One of the important advantages of noise-based calibration is that the amplitude of calibrated signals in every channel becomes equal to the square root of the signal-to-noise ratio. It opens the way for the absolute noise-based calibration of radar signals.

This chapter also describes the polarimetric signal model of clutter with complex Gaussian probability density function, which will be used to characterize homogeneous terrain, and the polarimetric signal models of targets, which are classified as multi-scatterer targets or as deterministic targets. Based on these theoretical models, polarimetric detection algorithms based on statistical approaches are able to realize in a polarimetric radar simulator, and experimental data of the observed targets and ground-based clutter can be successfully interpreted.

# Target Detection using Polarimetric Information 3

In this thesis, the target detection algorithms taken into account can be categorized as polarimetric detectors based on statistical approaches (OPD, ILRT, and PWF detectors) and polarimetric detectors based on physical approaches (single channel, span, PMS detectors). This chapter provides an overview of six different target detection algorithms which are operated with the polarimetric clutter and targets models as the ideal case in which target and clutter statistics are known exactly. Then the performance comparison analysis, which includes target detectability and polarization contrast enhancement, is presented for the two target-in-clutter scenarios: multi-scatterer target (an armored target and truck) in the meadow clutter and deterministic target (dihedral and trihedral reflector) in the meadow clutter with changing the target-to-clutter ratio. By comparing the ROC curves results by using the polarimetric radar simulator in this research with the results of the previous reference using the same type of theoretical models, the developed polarimetric radar simulator is tested and validated. With the comparative analysis in terms of the gain of detectability compared with the simplest single-channel detection method, the improvement of using polarization information is presented.

## 3.1 Polarimetric Detection Algorithms

The polarimetric detection algorithms discussed and tested in this research were proposed in the previous studies [5] [35] [3] [3], their performance analysis is to prove the validation of the proposed, developed, and implemented polarimetric radar simulator, which can generate feature vectors of radar observations according to the specific covariance matrix of object in this research. So that the polarimetric detection algorithms and the feature vectors generation method will be able to apply to the polarimetric data based on real radar measurements of the environment with non-homogeneous clutter.

Before introducing the polarimetric detectors based on statistical approaches with requirements of *a priori* knowledge, the three polarimetric detectors only based on physical approaches are interpreted, which are single channel detector, span detector, and PMS detector, respectively.

### 3.1.1 Single Channel Detector

The single polarimetric channel is the simplest scattering signal processor. A classical single-channel detector is supposed to require only the magnitude information of a single polarimetric channel. For example, the single channel detector $HH$ simply compares the intensity of the $HH$ polarization of the signal under test with the detection threshold

$T$. The single channel detector's expression is shown below.

$$|S_{HH}|^2 > T \tag{3.1}$$

$$|S_{VV}|^2 > T \tag{3.2}$$

$$|S_{HV}|^2 > T \tag{3.3}$$

A single-channel detector can work impressively with a simple calculation when the target of interest has a significant cross-section, leading to a magnitude higher than that of the surrounding clutter. It can be widely used for artificial targets mainly made up of corner reflectors and mirrors with consequent strong backscattering. One type of single-channel detector is linear co-polarization, including horizontal or vertical magnitude information as Eq. 3.1 and Eq. 3.2 [35]. It is the best choice for odd-bounces and horizontal even-bounces detection if the *a priori* knowledge is not available and only one polarization is available. In the cases where the clutter shows particularly high intensity at linear co-polarization, a single channel $HH$ or $VV$ detector may not be the ideal choice. With dual-polarimetric scattering data, cross-polarization may address detection in such a situation. The cross-polarization detector HV can be expressed as Eq 3.3 [35]. In the case of the detection of ships on a rough sea surface, bright backscattering occurs in $HH$ and $VV$ but not in $HV$.

The single channel detector performs target detection with relatively low implementation complexity of the acquisition system [35]. However, performance may be poor due to false alarms and missed detections. As we mentioned before, for the target with relatively low intensity at the only available polarimetric channel, the target may be missed during such simple detection. Missed detection also appears when the target under test shows poor linear co-polarization backscattering, and only co-polarization information is accessible in the current radar acquisition system, such as in the case of detecting an aloft horizontal wire with a single $VV$ channel detector. The false alarm occurs when the surrounding area includes many clutters with strong backscattering at a single polarimetric channel.

The single channel detector can be adopted as a pretest for filtering the clutter with significant differences from the target on the single polarimetric channel. To improve the performance of this simple detector, *a priori* information can be used in the subsequent statistical step.

### 3.1.2 Span Detector

Considering the total power of fully polarimetric channels in the scattering matrix can be a possible solution to reduce the rate of missed detection, in the case where the target cannot provide significant backscattering at the selected polarization, causing missed detection by using a single channel detector. The span of the scattering matrix $[S]$ can provide the total power information by calculating a weighted non-coherent summation of the three polarimetric channels $HH$, $HV$, and $VV$ [36]. The span detector is used to compare the span of the signal under test with the detection threshold $T$, which can be expressed as Eq. 3.4 [5].

$$span = |S_{HH}|^2 + 2|S_{HV}|^2 + |S_{VV}|^2 > T \tag{3.4}$$

The span detector is supposed to display better target detection performance, since it considers physical knowledge of all three polarimetric channels compared with a single channel detector, even though it cannot avoid problems with false alarms from natural targets and missed detection of weak targets.

This detection algorithm is also relatively simple in terms of implementation because it is not necessary to introduce statistical information as *a priori*. The same as the single channel detector mentioned above, the span detector is a useful pre-test filter followed by a subsequent statistical step to improve detection performance.

### 3.1.3 Power Maximization Synthesis

The Power Maximization Synthesis (PMS) detector has been proposed as an improvement to the span detector. It is specified as Eq. 3.5 [5], which is a function of the components of the measurement vector and does not contain *a priori* statistical knowledge of the target or clutter [5] [35].

$$0.5\left[|S_{HH}|^2 + 2|S_{HV}|^2 + |S_{VV}|^2 + \sqrt{\left(|S_{HH}|^2 - |S_{VV}|^2\right)^2 + 4|S_{HH}^* S_{HV} + S_{VV} S_{HV}^*|^2}\right] > T \tag{3.5}$$

Then we pay particular attention to the polarimetric detector algorithms with the use of polarimetric characteristics as *a priori* knowledge for developing target detection with statistical approaches, which are the polarimetric whitening filter (PWF), optimal polarimetric detector (OPD), and identity likelihood ration test (ILRT), respectively.

### 3.1.4 Polarimetric Whitening Filter

The Polarimetric Whitening Filter is a widely used technique based on statistical signal processing of quad-polarimetric data that employs *a priori* clutter information [37]. It has been shown to be a processing strategy capable of optimally reducing the speckle of image target detection of synthetic aperture radar (SAR) [3].

The PWF derivation is given by considering the scattered signal from the object with three complex measurements, HH, HV, and VV. The Polarimetric Whitening Filter is represented by the quadratic expression as Eq. 3.6 [3]

$$\mathbf{X}^\dagger \mathbf{C_c}^{-1} \mathbf{X} > T \tag{3.6}$$

where $\mathbf{C_c}$ denotes the clutter covariance matrix, the subscript $c$ represents clutter. The mainly theoretical idea of the Polarimetric Whitening Filter can be divided into two steps:

1. passing the polarimetric measurement vector $X$ through a whitening filter to obtain $\mathbf{Y} = \mathbf{C_c^{-1/2}} \mathbf{X}$, which will have unit covariance if the covariance matrix of

$\mathbf{X}$ satisfies $\mathbf{C_c}$. This is the reason for the name "Whitening Filter" since this processing makes clutter look like a "white", non-correlated noise. Especially for the homogeneous clutter region, each pixel of clutter in the scene has the same averaged polarimetric power and the same covariance between the polarimetric returns;

2. summing the powers contained in the elements of $\mathbf{Y}$ by $\mathbf{y} = \mathbf{Y}^{\dagger} \cdot \mathbf{Y}$.

In theory, this filter is supposed to realize the target detection in the homogeneous clutter environment where the clutters statistical characteristics are the same spatially.

### 3.1.5 Optimal Polarimetric Detector

The polarimetric whitening filter (PWF) we discussed above only takes into account the reduction in speckle (or the standard deviation to mean ratio of the clutter background). If the resolution cell is large enough, targets as well as the ground clutter can be treated as multi-scatterers. In that case, they can be described by means of a multi-dimensional complex Gaussian pdf:

$$f(\mathbf{X}) = \frac{1}{\pi^3 |\mathbf{C}|} \exp\left\{-\mathbf{X}^{\dagger}\mathbf{C}^{-1}\mathbf{X}\right\} \tag{3.7}$$

In the ideal case, the pdf of clutter and target (plus clutter) is known from previous experience. In the expression of hypothesis, the subscript $C$ represents the null hypothesis of clutter only, and the subscript $T + C$ represents the alternative hypothesis of target plus clutter. Then both hypotheses are shown in Eq. 3.9 - $H_1$: target plus clutter and $H_0$: clutter only - can be separated by means of a simple likelihood ratio test that considers complete knowledge of the clutter and target statistics. This corresponds to a quadratic detector for the presence of a target as Eq. 3.10.

$$H_1 : H_{T+C}; \tag{3.8}$$

$$H_0 : H_C \tag{3.9}$$

$$\frac{f(\mathbf{X}|\mathbf{H_{T+C}})}{f(\mathbf{X}|\mathbf{H_C})} > T \tag{3.10}$$

The detection threshold is $T$. The solution to this likelihood ratio is easily shown to be a quadratic detector of the form [2]

$$\mathbf{X}^{\dagger}\left(\mathbf{C_c^{-1}} - \mathbf{C_{t+c}^{-1}}\right)\mathbf{X} + \ln\frac{|\mathbf{C_c}|}{|\mathbf{C_{t+c}}|} > \ln T. \tag{3.11}$$

where $|\mathbf{C_c}|$ denotes the determinant of the clutter covariance matrix and $|\mathbf{C_{t+c}}|$ denotes the determinant of the total return covariance matrix with the target plus clutter.

Note that the detector requires *a priori* information on the covariance matrices of the target and the clutter. These must be adjusted to the different scenarios before any detection; therefore, this method is difficult in terms of implementation. The optimal polarimetric detector gives the best performance in most environments, especially in the low probability of false alarm cases.

### 3.1.6 Identity-Likelihood-Ratio-Test

Identity-Likelihood-Ratio-Test (ILRT), as an alternative to OPD, replaces the target covariance matrix with a scaled identity matrix [5]. Therefore, the ILRT detection algorithm is shown as Eq. 3.12 [5]

$$\mathbf{X}^{\dagger}\left[\mathbf{C_c^{-1}}-\left(\frac{1}{4}E\left[span(\mathbf{X_t})\right]\cdot\mathbf{I}+\mathbf{C_c}\right)^{-1}\right]\mathbf{X}>T \tag{3.12}$$

where $\mathbf{I}$ is the 3-by-3 identity matrix, and $E\left\{span(\mathbf{X_t})\right\}$ is the target's mean value of the total power in the full polarization channels, which is also defined as the expected span of the target return.

The algorithm still requires a priori knowledge of the clutter covariance matrix plus the target-to-clutter ratio, which is contained in the calculation of the expected span of the target return. The strength of this detector is that the target mean and target covariance are not necessary.

## 3.2 Simulation Results on Detection Performance Comparison

This section presents the performance comparison of the detection algorithms introduced above. The results are summarized for both the multi-scatterer (random) target-in-clutter and the deterministic (dihedral and trihedral) target-in-clutter with changing target-to-clutter ratio.

### 3.2.1 Target-to-clutter Ratio Definition

The target-to-clutter ratio is defined as Eq. 3.13 [5] where $E\left\{span\left(\mathbf{X}_t\right)\right\}$ is the expected span of the target return, $E\left\{span\left(\mathbf{X}_c\right)\right\}$ is the expected span of the clutter return, and the target-to-clutter ratio $T/C$, which means the total power ratio of target and clutter, is defined by the ratio of these two expected span values.

$$T/C=\frac{E\left\{span\left(\mathbf{X}_t\right)\right\}}{E\left\{span\left(\mathbf{X_c}\right)\right\}} \tag{3.13}$$

### 3.2.2 Feature Vectors Generating With Model-based Decomposition

In this research, the main development of the polarimetric radar simulator is that the feature vectors $\mathbf{X_t}$ of the target and $\mathbf{X_c}$ of the clutter are generated according to the polarimetric covariance matrix models of the meadow clutter, different types of multi-scatterer targets and deterministic targets, this method is known as the name of model-based decomposition [38]. Firstly, random signals are generated with 10000 complex samples at a slow time with normally distributed real and imaginary parts. The random signal covariance matrix in all polarization channels ($HH$, $HV$, and $VV$) is known as a 3-by-3 identity matrix with ones on the main diagonal and zeros elsewhere.

Then calculate the Cholesky decomposition $\mathbf{C_{upper}}$ of the covariance matrix $\mathbf{C}$ using the diagonal and upper triangle of $\mathbf{C}$, so that $\mathbf{C}=\mathbf{C_{upper}}'\cdot\mathbf{C_{upper}}$. It is worth

| | $\varepsilon$ | $\gamma$ | $\rho\sqrt{\gamma}$ |
|---|---|---|---|
| Armored target | 0.19 | 1.0 | 0.28 |
| Truck target | 0.02 | 1.1 | 0.83 |
| Meadow clutter | 0.18 | 1.1 | 0.63 |

Table 3.1: Polarimetric Parameters of Targets and Clutter

mentioning that the polarimetric covariance matrix can satisfy the requirement to be positive definite for the Cholesky decomposition [39] [40].

The radar feature vector $X$ consisting of three complex elements, $S_{HH}$, $S_{HV}$, and $S_{VV}$ with the typical polarimetric covariance matrix model is then created by multiplying random vectors $\mathbf{X_{randn}}$ with the Cholesky decomposition $\mathbf{C_{upper}}$ of the covariance matrix $\mathbf{C}$. The expression of this feature vector generation can be shown by $\mathbf{X} = \mathbf{X_{randn}} \cdot \mathbf{C_{upper}}$.

### 3.2.3 Algorithms Performance Comparison with Polarimetric Radar Simulator

#### 3.2.3.1 ROC curves

One of the challenges in interpreting the results of diagnostic tests for target detection that produce continuous measures is the selection of the threshold to distinguish a 'positive' test (radar return with target) from a 'negative' test (radar return without target). The role of the ROC curve is to choose the threshold cut-off points for target detection. To produce a ROC curve, the sensitivity and specificity of different values of a continuous test measure are first tabulated [41]. This essentially results in a list of various test values and the corresponding sensitivity and specificity of the test at that value. Then the graphical ROC curve is produced by plotting the sensitivity (true positive rate), which is shown as the probability of detection on the $y$ axis against 1–specificity (false positive rate) which is shown as the probability of false alarm on the $x$ axis for the various values tabulated.

First, the performance results for the detection of random targets are presented in Figure. 3.1, 3.2, 3.3, 3.4. For random target-in-clutter scenarios, it is worth mentioning that the radar returns from the terrain-clutter environment are simulated according to the polarimetric parameters of the covariance statistics of clutter and various types of target, which are also employed as a known a priori knowledge of clutter and target for target detection. The values of the covariance matrix for an armored target (Target 1), truck (Target 2), and meadow clutter are given in Table. 3.1 [5]. Polarization covariance parameters were obtained empirically.

Figure. 3.1 and Figure. 3.2 display the detection performance for an armored target in a meadow clutter with a target-to-clutter ratio of 6dB and 10dB, respectively. For this type of target, the ROC curves of six detectors can be split into three groups. The OPD, the PWF, and the ILRT which are all based on statistical approaches are clustered as the first group with impressive performance. The span and PMS detectors

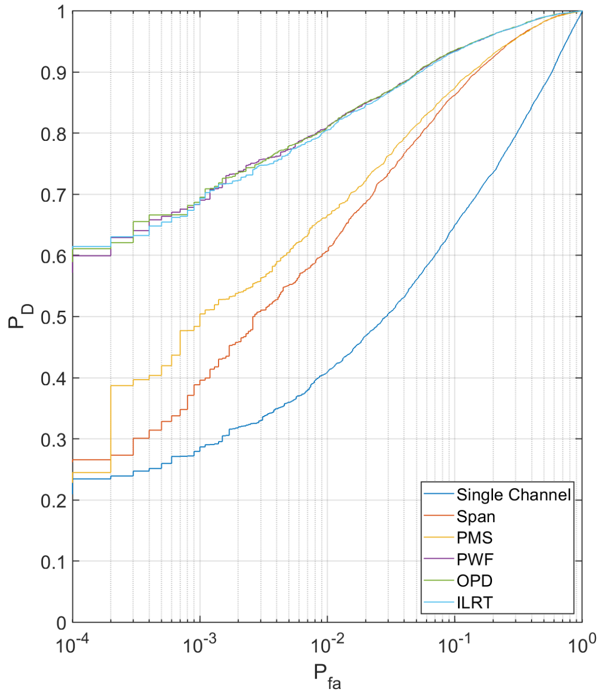


Figure 3.1: Detection performance for armored target with 6 dB T/C ratio

have degraded performance compared to the first group. Both are based on a physical approach; it seems that, with a relatively lower probability of false alarms, the PMS will detect the armored target better than the span detector. However, it is difficult for the single polarimetric channel detector $HH$ to detect such a target.

In the case of the truck in the meadow, it is similar when the target-to-clutter ratio is 10dB as seen in Figure 3.4. However, it shows an exception for the $T/C$ ratio dropping to 6 dB, as seen in Figure 3.3 where the ILRT detector gives a worse performance than OPD and PWF.

Furthermore, it is obvious that the probability of detection can improve as the target-to-clutter ratio increases to some extent.

Then the performance results are presented in Figures 3.5, 3.6, 3.7, 3.8 for the deterministic target-in-clutter case, which employ the detection algorithms for a dihedral scatterer oriented at 0°, 22.5° and 45°, respectively, and a trihedral scatterer. The $T/C$ ratio for each case is 3 dB.

Figures 3.5, 3.6 and 3.7 compare the detectability of the polarimetric detectors for the dihedral reflector with different dihedral orientation angles. The PWF and ILRT yield similar detection performances, which is preceded only by the OPD detector, which achieves the most accurate result in terms of detecting dihedral scatterers. It is interesting to note that both the PMS and the span detector show performance degradation from the optimal, but it is not significantly influenced by the difference in the target-oriented angle because of the specific physical structure of the dihedral reflector. The single-polarimetric-channel HH detector is not effective in detecting dihedral targets. For the dihedral with 45° orientation angle, the probability of detection of the $HH$ detector is significantly minimized for a constant probability of false alarm.

This happens because there is no target return in the HH channel, so the probability of detection always equals the probability of a false alarm.

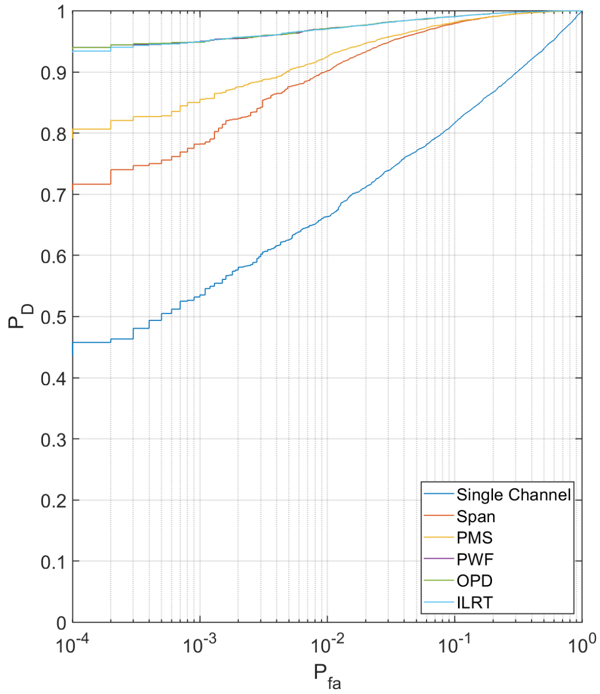


Figure 3.2: Detection performance for armored target with 10 dB T/C ratio

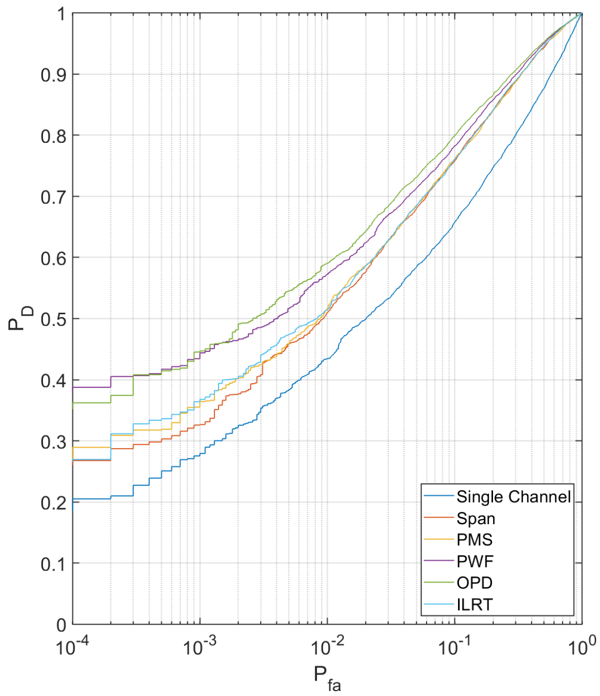


Figure 3.3: Detection performance for truck target with 6 dB T/C ratio

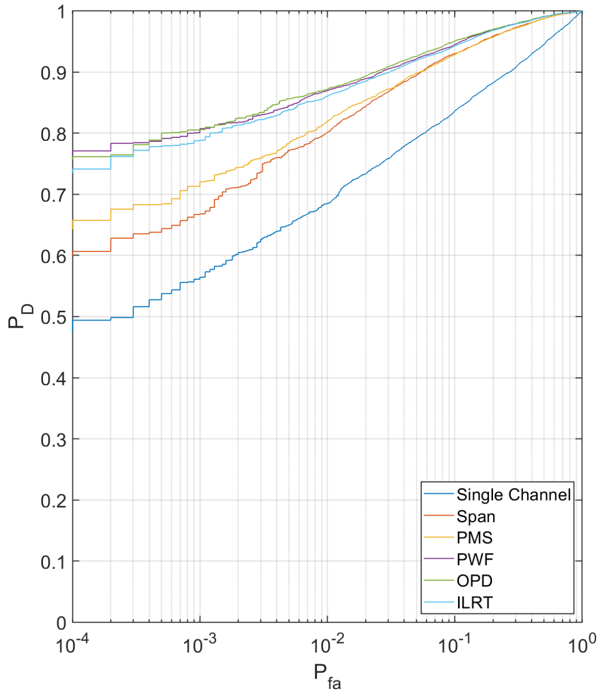


Figure 3.4: Detection performance for truck target with 10 dB T/C ratio

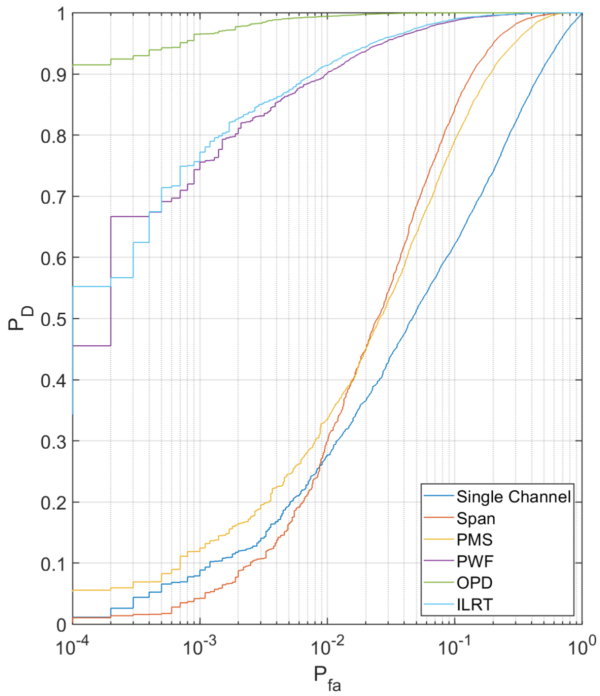


Figure 3.5: Detection performance for dihedral reflector oriented at 0° with 3 dB T/C ratio

Figure 3.8 illustrates the detection performance for the trihedral case. When comparing the ROC curve of the OPD in Figure 3.8 with Figures 3.5, 3.6 and 3.7, it shows that the optimal detection of a trihedral scatterer is much more challenging than the op-

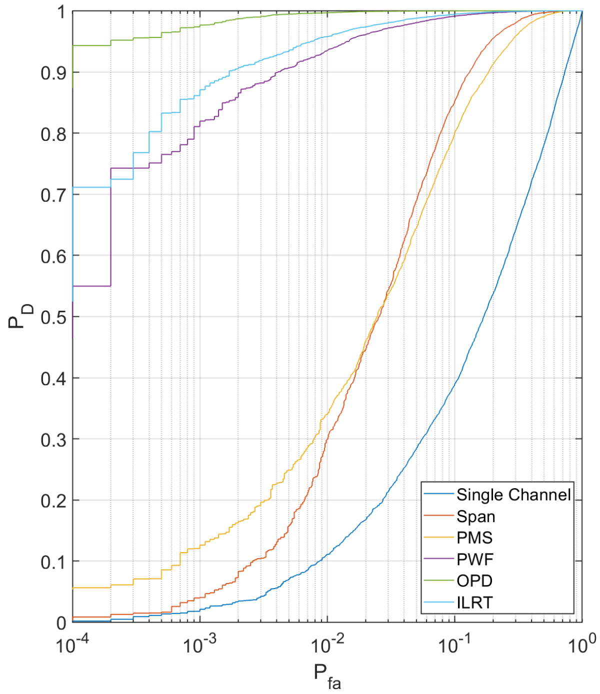


Figure 3.6: Detection performance for dihedral reflector oriented at 22.5° with 3 dB T/C ratio

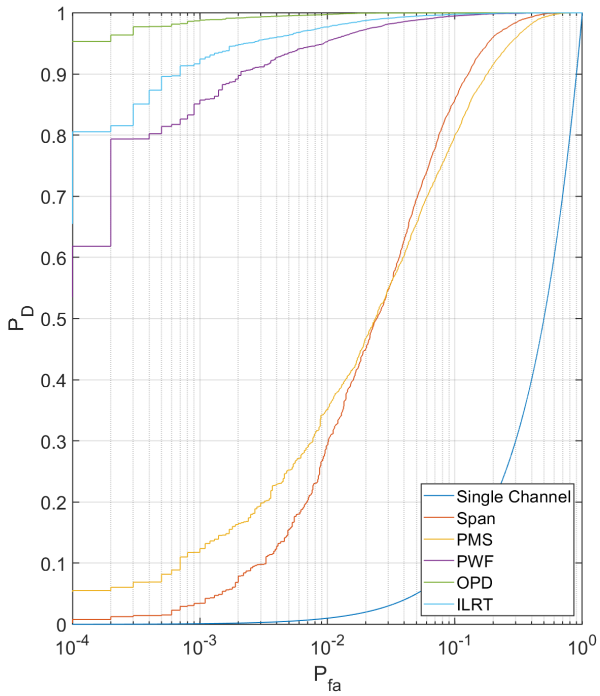


Figure 3.7: Detection performance for dihedral reflector oriented at 45° with 3 dB T/C ratio

timal detection of a dihedral scatterer. This result illustrates the physical fact that the clutter is statistically more similar to the trihedral than dihedral reflector. The same difficulty occurs for the PWF and ILRT, since these detectors aim to discriminate the

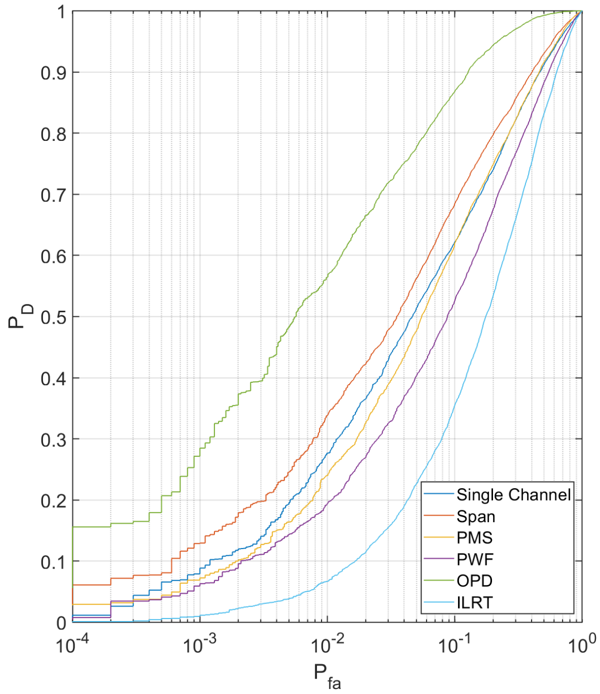


Figure 3.8: Detection performance for trihedral reflector with 3 dB T/C ratio

trihedral target from the clutter based on the statistical characteristics. However, the detection algorithms based on only physical information of the radar return, such as the span detector and the PMS, display more similar performances against dihedral and trihedral.

#### 3.2.3.2 Gain of Detectability

The gain in targets detectability in this thesis is defined by the gain in the probability of detection, which is equal to the ratio of $P_d$ for the detectors that use the polarization information to the probability of detection for the single channel detector (for the fixed value of false alarm rate). This definition is expressed as

$$Gain = \frac{P_D(\text{span, or PMS, or PWF,or OPD, or ILRT})}{P_D(HH)} \tag{3.14}$$

With such a definition, when the gain values are positive (when the gain in target detectability is converted to decibels), it means that compared with the single-channel detector, the polarimetric detectors can improve the detectability to different extents.

To analyze the results in terms of the gain in targets detectability, for example, from Fig. 3.9 to 3.12, this gain for multi-scatterer targets detection by OPD and PWF have impressive detection improvement compared with classical single-channel detector. For the detection algorithms based on physical approaches (span and PMS detector), with full polarization channels feature vectors known, the target detection can be improved. Seen from the gain of detectability analysis for the dihedral target at different orientation angles in Fig. 3.13 - 3.15, these detectors are effective to increase the probability of detection. The reason why the span detector does not help in the case of 0-degree orientation of the dihedral reflector can be that the HH polarization channel is dominant for this specific type of target. For the trihedral target, only the OPD has a great improvement in terms of the gain of detectability. In addition, the ILRT cannot guarantee to be helpful for all types of targets.

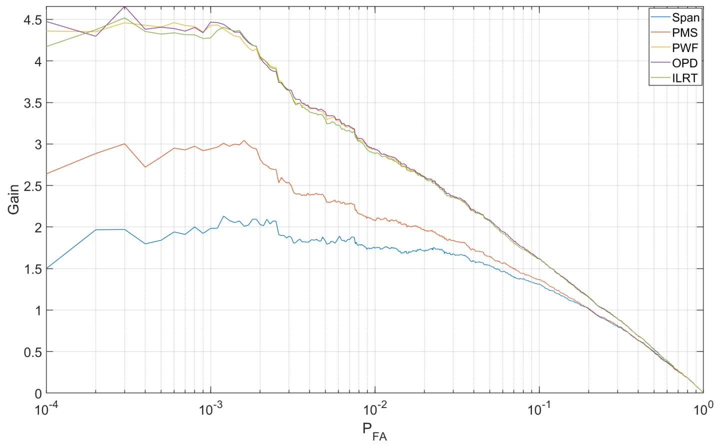


Figure 3.9: Gain of detectability for armored target with 6 dB T/C ratio

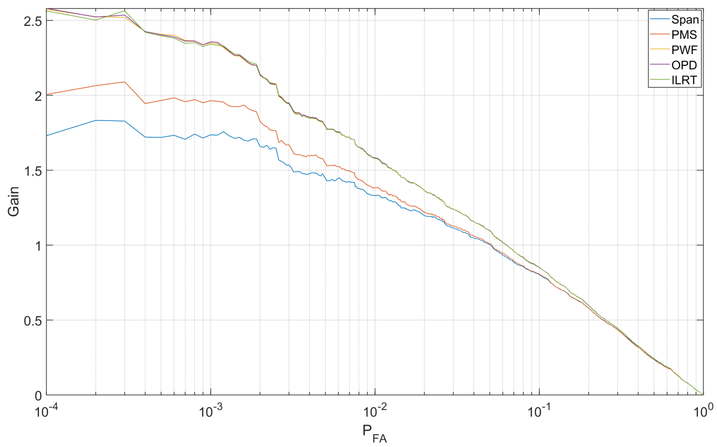


Figure 3.10: Gain of detectability for armored target with 10 dB T/C ratio

These simulation results correspond to the ideal situation where the target radar return vector, target statistical characteristic, and clutter statistical characteristic are exactly known. However, this essential information about the desired target may not be easy to measure in practice. The same is also correct for the clutter surrounding the target to obtain *a priori* since clutter can vary spatially within the type of terrain and temporally within the changing of weather and seasonal conditions. Fortunately, clutter statistics may be estimated at processing time with a considerable computational cost, such as the adaptive polarimetric whitening filter method.

The results discussed above indicate that a significant improvement in detection performance can be achieved by using clutter statistics. The target statistic as ad-

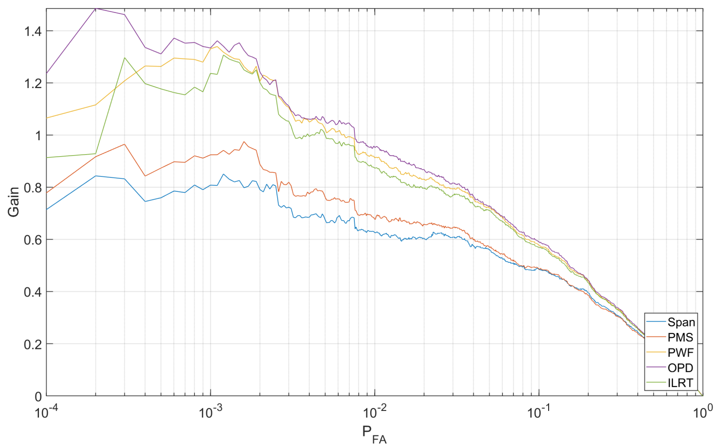


Figure 3.11: Gain of detectability for truck target with 6 dB T/C ratio

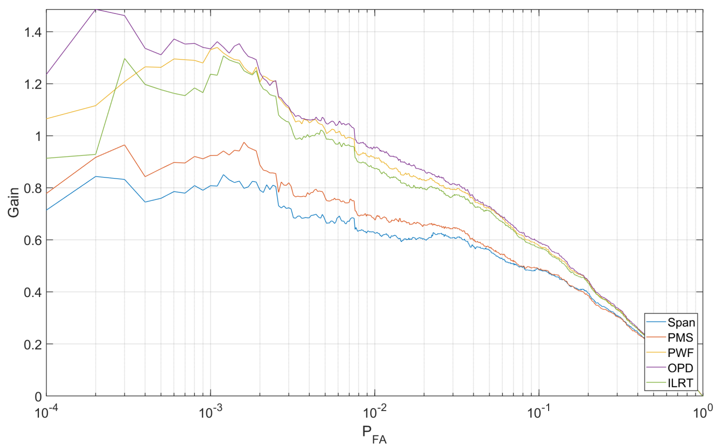


Figure 3.12: Gain of detectability for truck target with 10 dB T/C ratio

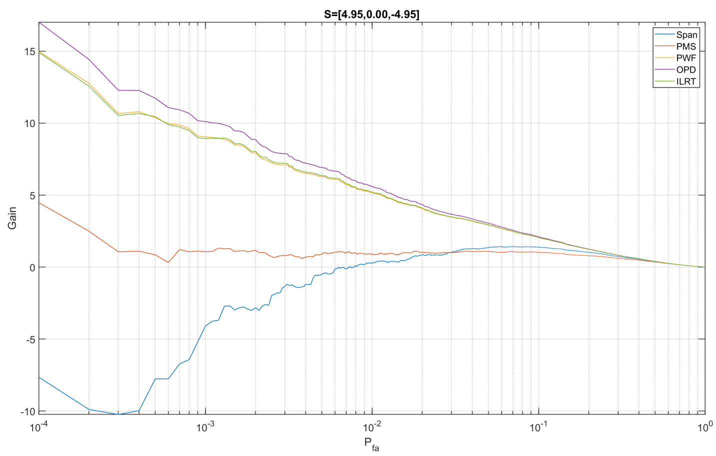


Figure 3.13: Gain of detectability for dihedral oriented at 0° with 3 dB T/C ratio

ditional knowledge shows a modest improvement in terms of detectability seen from the performance of ILRT compared with that of PWF, and even worse than that of

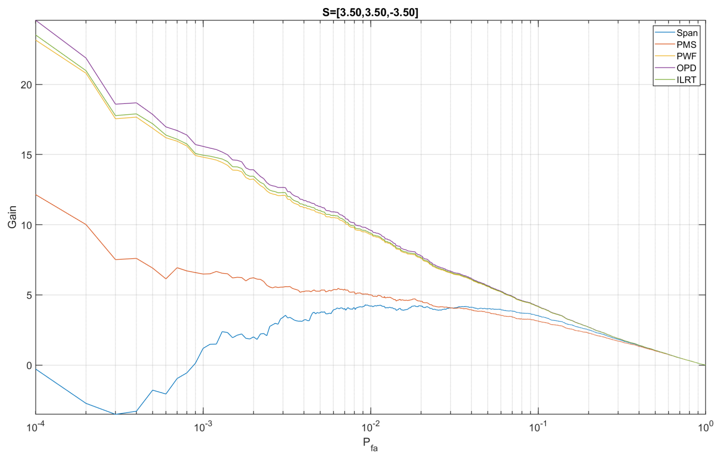


Figure 3.14: Gain of detectability for dihedral oriented at 22.5° with 3 dB T/C ratio

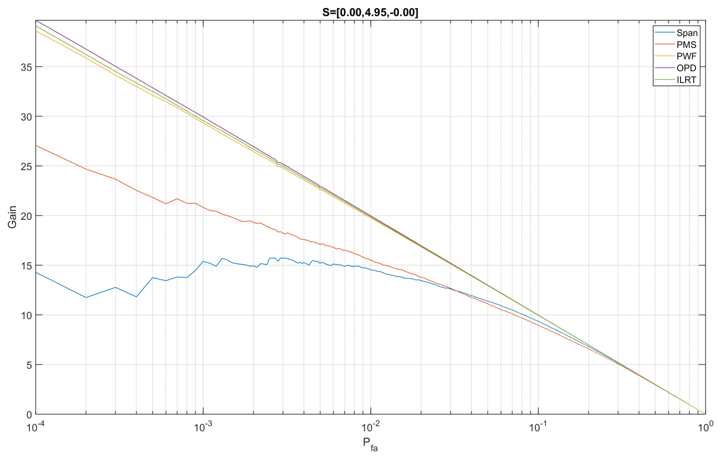


Figure 3.15: Gain of detectability for dihedral oriented at 45° with 3 dB T/C ratio

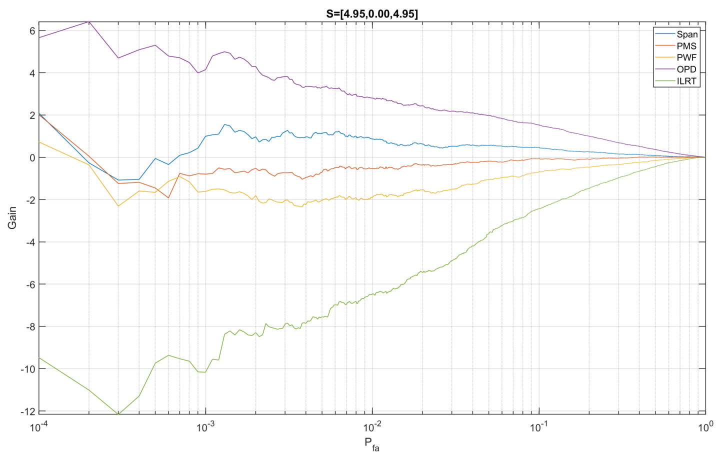


Figure 3.16: Gain of detectability for trihedral with 3 dB T/C ratio

the PWF in some cases. Optimal performance can typically be obtained by the PWF detector, which requires the clutter covariance only. For most cases, detectors based on only physical approaches to maximize the energy of the target's signal instead of taking into account the target and clutter statistics, yield to poorer effectiveness than the PWF. As a reasonable prediction, considering the trade-off between the amount of statistical knowledge required and the detection performance, the polarimetric whitening filter may become the best choice in practical measurement for the homogeneous clutter case [5].

## 3.3 Conclusions

This chapter provides brief derivations and descriptions of polarimetric detection algorithms. These algorithms are classified into two main classes. The first set includes the detectors based on physical approaches (single-channel, span, PMS detectors) by maximizing the received from the scattered target signal. The second class includes detectors based on statistical approaches (OPD, ILRT, and PWF detectors), which use a priori information about targets' and/or clutter's polarization characteristics to maximize the signal-to-clutter ratio.

The way to generate feature vectors according to the covariance matrix with the values of typical elements has been introduced in this chapter (**3.2.2**). By applying the feature vector generation in the polarimetric radar simulator, these algorithms are tested for various multi-scatterer and deterministic targets in the homogeneous meadow clutter environment with different target-to-clutter ratio conditions. The performances of the algorithms are displayed and compared by ROC curve results in simulation. in this research, the roc curve results show reproduction of previous study in the literature [5] by using the polarimetric radar simulator, which illustrates the method in the simulator has been tested and validated successfully. To present the performances of the detections with full polarization channels' information in terms of the improvement of detectability compared with the simplest single channel detector, the definition of gain of detectability is introduced as a criteria for this analysis.

The analysis of presented results shows that detectors, which are based on physical approaches only, without the information about expected target and clutter polarimetric characteristics, have less effect than statistical approaches for most cases. The performance of the identity likelihood ratio test method is quite irregular due to the different types of target. Since the effect of target mismatch (substituting information of target span for target covariance matrix) is not well understood, this method will not be further discussed in application to real measurements. For targets in a homogeneous clutter environment, the Polarimetric Whitening Filter may become the best choice since this method requires only knowledge of the clutter covariance matrix and can achieve reliable performance in terms of target detection. In practical measurement, it can be challenging to obtain a priori the polarimetric characteristics of the target, but the Optimal Polarimetric Detector that requires *a priori* knowledge of both the target and the clutter reaches the best performance for all types of targets that were analyzed within the simulation.

# Statistical Characteristics of Real Ground Clutter and Reference Targets

# 4

Modern radar systems have implemented adaptive processing techniques such as constant false alarm rate (CFAR) detectors, adaptive arrays, and space-time adaptive processing (STAP) to mitigate the harmful effects of clutter and jamming [42]. Typically, in adaptive radars, the disturbance covariance matrix is estimated using training data collected from the cells surrounding cell under test (CUT). All these estimators are based on the assumption that the training data vectors do not contain interference or targets and share the same covariance matrix as the primary data. These techniques are quite restrictive, as they are based on a stationary and homogeneous environment during adaptation [43]. Stationarity and homogeneity requirements are rarely met in practice. In fact, training data vectors are often contaminated by interfering targets, discrete large clutter, spiky clutter, and other outliers of different types rendering them non-homogeneous. Another type of non-homogeneity is caused by the non-stationary nature of the clutter, which also significantly degrades radar performances. Moving averaging window for the estimation of the polarimetric covariance matrix of the radar returns is one of the recommended approaches to achieve simplicity and ease of implementation.

## 4.1 Moving Spatial Averaging Window in Covariance Matrix Estimation

In the monostatic radar system, the polarimetric covariance matrix is defined as the outer product of the feature vector with its conjugate transpose as

$$\mathbf{C} = \begin{bmatrix} \left\langle |S_{HH}|^2 \right\rangle & \langle S_{HH} S_{HV}{}^* \rangle & \langle S_{HH} S_{VV}{}^* \rangle \\ \langle S_{HV} S_{HH}{}^* \rangle & \left\langle |S_{HV}|^2 \right\rangle & \langle S_{VV} S_{HH}{}^* \rangle \\ \langle S_{VV} S_{HH}{}^* \rangle & \langle S_{VV} S_{HV}{}^* \rangle & \left\langle |S_{VV}|^2 \right\rangle \end{bmatrix} \tag{4.1}$$

where $\langle ... \rangle$ indicates the averaging of the temporal or spatial ensemble. The covariance matrix, consisting of three real powers and three complex covariance elements, contains complete information on the amplitude and phase variance and correlation for all complex elements of [$\mathbf{S}$]. The covariance matrix is a Hermitian positive semi-definite matrix, which implies that these possess real non-negative eigenvalues and orthogonal eigenvectors.

### 4.1.1 Covariance Matrix Calculation With Moving Spatial Averaging Window

Covariance estimation is widely used for signal processing and even cryptanalysis [44]. The use of an estimated covariance matrix originated in the area of speech processing [45]. The moving averaging window method is a prominent auto-correlation and covariance estimator for smoothing measured data by replacing a data point with the average (or a weighted form of it) of its neighbors. The moving averaging window for covariance calculation is a biased estimator, and its output is a Hermitian, positive semi-definite matrix, so it is guaranteed to be non-singular. This is unlike the output of other methods, such as auto-correlation, and often causes the moving averaging window method to be preferred. It is an important computational building block to smooth spatial clutter by averaging over given transposed data or performing a 2D spectral analysis.

Computation of the estimated covariance matrix essentially entails the averaging of inner products within a moving window over the input matrix: for each window position, a vector is formed by column-stacking the column of the window and is then multiplied by its conjugate transpose. Averaging those results over all possible positions of the window within the input matrix yields the estimated covariance matrix.

The single-dimension averaging window is moved over the data, shifting it by one time step after each calculation. Such a moving-window averaged covariance matrix, which is also called a sample covariance matrix, can be denoted in a more general form by

$$\mathbf{C} = \frac{1}{K}\sum_{i=1}^{K}\mathbf{X}_i\mathbf{X}_i^H \tag{4.2}$$

where $K$ denotes the number of data samples of the chosen window size.

In the case of our measurement, to obtain smoothed polarimetric characteristics of target and clutter, instead of calculating the mean value of observations in the slow-time domain, the moving averaging window will be applied in the 2D spectral analysis. As mentioned in Chapter 2, for minimization of the thermal noise influence on the polarization parameters estimation, the long (0.5 sec) Doppler coherent integration of measured signals has been used with the following filtration of the stationary signals with zero Doppler velocity. These signals are used to estimate the polarimetric covariance matrix using the moving spatial averaging window method.

The input zero Doppler matrix (range-by-azimuth) in the entire area is denoted by $\mathbf{A}$. To estimate the spatial characteristics of objects and clutter, the covariance matrix is smoothly obtained by employing the moving window in space, including range index and azimuth index. $W^{n_R,n_A}$ denotes the moving $n_R \times n_A$ window, which is a block within $\mathbf{A}$, where the $(n_R, n_A)$ superscripts denote the position of its lower right corner. Figure 4.1 is shown as an example of a moving averaging window with window size $n_R \times n_A (n_R = 5, n_A = 7)$, which is also the window size chosen applied to the real measurement. The moving window is also known as a sub-aperture.

In the measurement of this research, the range index has a high range resolution of around 3.3 meters (each range index represents approximately 3.3 meters in practice), and the azimuth index has an azimuth resolution of 0.1 degrees (azimuth varying 0.1 degrees from one azimuth index to the next azimuth index). The width of the moving averaging window is a small portion of the range index, which is indicated by $n_R$, and the length of the moving averaging window is a small portion of the azimuth index, which is indicated by $n_A$.

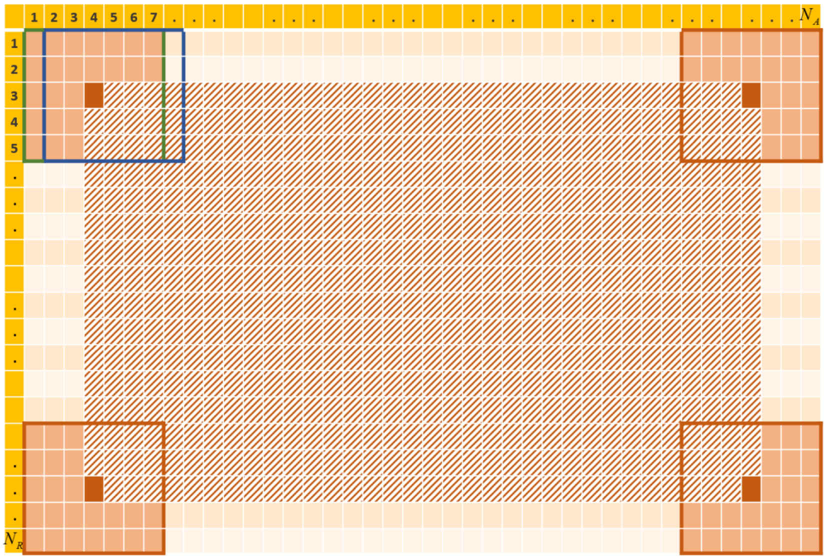


Figure 4.1: Moving spatial averaging window (window size 5x7)

The position of the center point of the window is represented as $(i, j)$ and will move slightly as the window moves with $i$ changing from $(1 + \frac{n_R-1}{2})$ to $(N_R - \frac{n_R-1}{2})$ and $j$ changing from $(1 + \frac{n_A-1}{2})$ to $(N_A - \frac{n_A-1}{2})$, $i \in N_R$, $j \in N_A$.

Each calculation of the covariance matrix by the moving window can be expressed as

$$\begin{aligned}\mathbf{C}(i,j) &= E\left\{\mathbf{X}\cdot\mathbf{X}^{\dagger}\right\} = \\ &= \frac{1}{n_R \cdot n_A}\sum_{i_w=-n_R/2}^{n_R/2}\sum_{j_w=-n_A/2}^{n_A/2}\mathbf{X}(i+i_w, j+j_w)\cdot\mathbf{X}^{\dagger}(i+i_w, j+j_w)\end{aligned} \tag{4.3}$$

Note that $\mathbf{C}$ is a symmetric positive definite matrix, so only the diagonal and upper triangle or lower triangle portion of this matrix needs to be computed.

### 4.1.2 Effect of Window Size in Moving Average

Estimation of the covariance matrix using the moving averaging window aims to improve the similarity of pixels related to the specific type of object and to demonstrate the differences among different types of object or terrain features. The variabilities of each covariance component changing with range and azimuth are smoother than in the original data. Based on this improvement in every component of the covariance matrix, we can more easily recognize the specific features of the ground. The order of the moving average (or, in other words, the window size) determines the smoothness of the covariance components in space. In terms of the number of observations included in the moving window, an even-numbered window size with both even-numbered width and length is preferred, since the estimated covariance matrix will be concluded as the center-point's covariance matrix.

The size of the window is supposed to be optimized based on the trade-off between the minimal degradation in the spatial resolution and the similarity of the pixels related to the same specific type of observed objects.

In theory, the covariance matrix of the moving averaging window is the mean value of all samples in the window. In the case that the window is not wide enough, the contrary appears in the range and azimuth indexes. To smooth the contrary in range index and azimuth index between two variables, a wider window with more observations is required. However, in the case of over-smoothed when the window is too wide, serious degradation in the spatial resolution can lead to the failure to classify two different objects in terms of polarimetric characteristics.

In this subsection, the results of the elements of the covariance matrix $C_{11}$, $C_{12}$, $C_{13}$, $C_{22}$, $C_{23}$, and $C_{33}$ obtained by applying different window sizes are shown as comparison. The expressions of these six elements are as follows:

$$C_{11} = E\left\{|S_{HH}|^2\right\} \tag{4.4}$$

$$C_{22} = \frac{E\left\{|S_{HV}|^2\right\}}{E\left\{|S_{HH}|^2\right\}} \tag{4.5}$$

$$C_{33} = \frac{E\left\{|S_{VV}|^2\right\}}{E\left\{|S_{HH}|^2\right\}} \tag{4.6}$$

$$C_{12} = \frac{E\left\{S_{HH} \cdot S_{HV}^*\right\}}{E\left\{|S_{HH}|^2\right\}} \tag{4.7}$$

$$C_{13} = \frac{E\left\{S_{HH} \cdot S_{VV}^*\right\}}{E\left\{|S_{HH}|^2\right\}} \tag{4.8}$$

$$C_{23} = \frac{E\left\{S_{HV} \cdot S_{VV}^*\right\}}{E\left\{|S_{HH}|^2\right\}} \tag{4.9}$$

where $C_{11}$ represents the backscattering cross section per unit area for the HH polarization. $C_{22}$ is the intensity ratio of the polarization of $HV$ and $HH$, and $C_{33}$ is the intensity ratio of the polarization of $VV$ and $HH$. $C_{12}$, $C_{13}$, and $C_{23}$ illustrate the correlation between the returns $HH$ and $HV$, the returns $HH$ and $VV$, and the returns $HV$ and $VV$, respectively, which are normalized by the intensity of the $HH$ polarization ($C_{11}$). The elements of the covariance matrix $C_{11}$, $C_{12}$, $C_{13}$, $C_{22}$, $C_{23}$, and

$C_{33}$ contain all the information in the covariance matrix, as the covariance matrix is symmetric.

We compared each element of the covariance matrix calculated by moving the average window with the window size of $3 \times 3$, $5 \times 7$, and $5 \times 15$, which can be found in Appendix A. When selecting the specific range of 3.42 km (with range index = 1026), the variables among the azimuth index for each element of the covariance matrix can be clearly seen. Small window size causes more fluctuations, while the curves of window size $5 \times 7$ captures the features more smoothly. This phenomenon is obviously shown in terms of $C_{11}$ , $C_{22}$, $C_{33}$, $C_{13}$. Figure 4.2b versus Figure 4.2a are presented below as an example of this phenomenon.

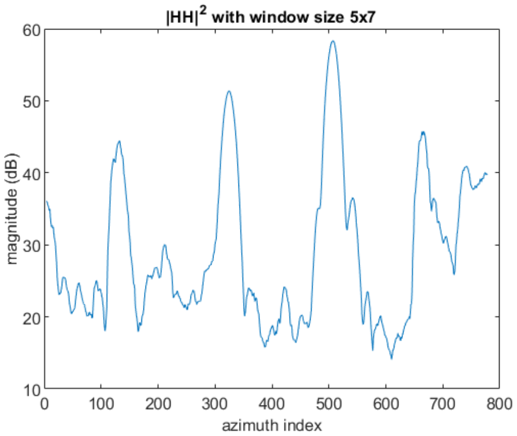


(a) $C_{11}$ (window size 5x7)

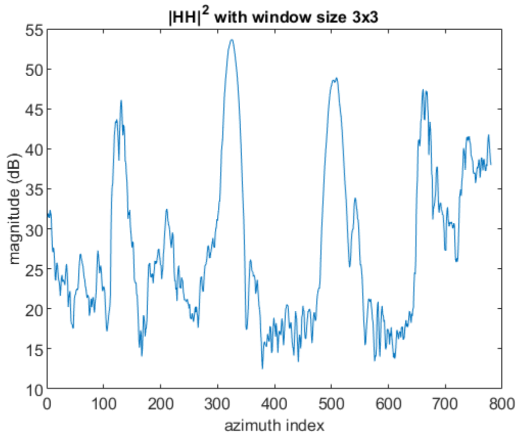


(b) $C_{11}$ (window size 3x3)

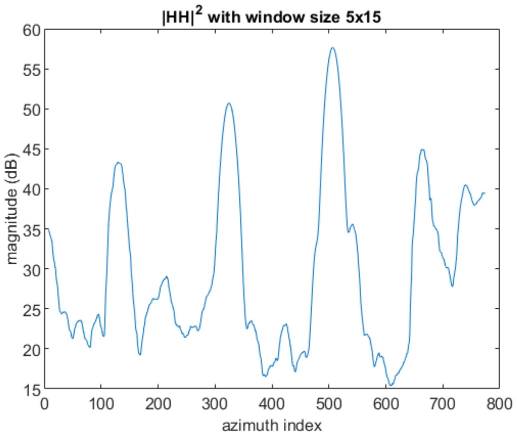


(c) $C_{11}$ (window size 5x15)

Figure 4.2: Amplitude of the element $C_{11}$ along the azimuth index for the various sizes of moving averaging window

A moving averaging window with a window size $5 \times 15$ averages the polarimetric characteristics more smoothly. However, this size of window removes most of the fluctuations and peaks within every 20 azimuth indices and only preserves outstanding peaks, such as in the comparison of Figure. 4.3c versus Figure. 4.3a. In this case, some variations of each covariance element may be overlooked, which may lead to the risk of emitting the information of polarimetric characteristics by the oversmoothed. As a result, the curves of window size $5 \times 7$ seem suitable to capture the impressive variables among the azimuth index.

Based on the test results with various sizes of moving averaging windows, it can be concluded that the window size $5 \times 7$ is the optimal window size.

It should be mentioned that the larger the window size, the more gaps we will have towards the edges of the dataset, since at the edge there will not be enough data points to make the estimate (with a window size $5 \times 7$ there will be no estimates for the first and the last two data points in the range and the first and last three data points at the azimuth in the dataset).

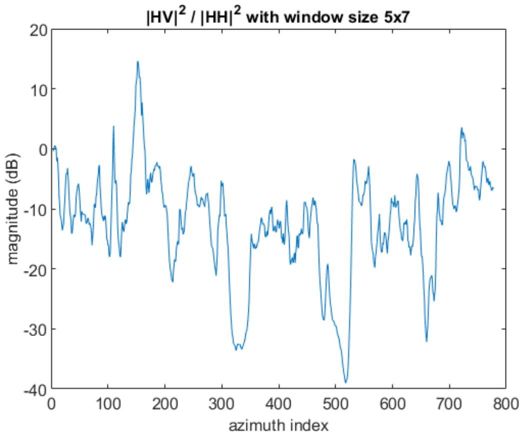


(a) $C_{22}$ window size 5x7

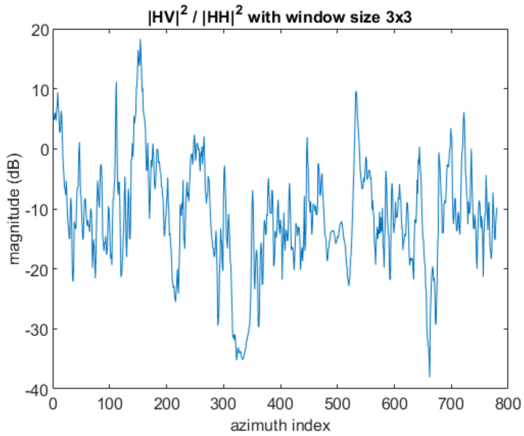


(b) $C_{22}$ window size 3x3

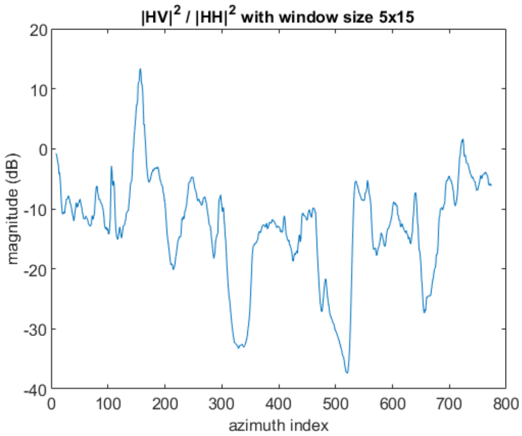


(c) $C_{22}$ window size 5x15

Figure 4.3: Amplitude of the element $C_{22}$ along the azimuth index for the various sizes of moving average window

## 4.2 Estimation of Covariance Matrix Elements With Moving Spatial Averaging Window

### 4.2.1 Maps of the Covariance Matrix Elements

After assigning the result of the covariance matrix of moving the average window to the center point of the window, each pixel on the map has its own covariance matrix representing the polarimetric characteristics of every pixel. To extract the covariance matrix of the reference target and clutter as knowledge of *a priori*, the element maps of the covariance matrix, which can be found in Appendix B, will be applied as a library of polarimetric characteristics.

First, three elements of the covariance matrix related to the intensities of $HH$, $HV$, $VV$ polarization are discussed together to interpret the power information of different polarization channels of the backscatterers in the entire scenario.

Figure. 4.4 is the result of the covariance matrix element $C_{11}$ denoting the intensities of the $HH$ polarization for the entire area on the map. By overlaying the $C_{11}$ map result on the Google Earth satellite map in Figure. 4.5, the measured scenario can be easily recognized that the blue areas correspond to grasslands with a relatively low intensity of $HH$ of less than 30 dB, while the forest areas and constructions on the map correspond to the yellow and red regions with a high intensity of $HH$ greater than 40 dB. It is worth mentioning that the power line masts with strong $HH$ intensities, which are approximately larger than 45 dB, range in line on the map shown as the red placemarks named TS1 - TS6 in Figure. 4.5.

The results of the intensity ratio of the $HV$ polarization and the $HH$ polarization for the entire area show that the grass clutter has a low intensity on the HV polarization. However, the forest clutter does not show a regional similarity in terms of the intensity of $HV$. Also, this covariance matrix element does not help to recognize 6 power line masts in a line significantly.

In terms of the covariance matrix $C_{33}$, grasslands have a typical low intensity of $VV$ polarization. Forests and constructions have higher intensities in $VV$ polarization than grasses, and in some pixels the intensities of $VV$ are even higher than those of $HH$. For power line masts as targets, unfortunately, there is no apparent similarity in terms of the intensity ratio of the $VV$ and $HH$ polarization.

Furthermore, to interpret the correlation characteristics between different polarization channels of the backscatterers in the entire scenario, the other three elements of the covariance matrix related to the correlation between $HH$ and $HV$, $HH$ and $VV$, and $HV$ and $VV$ are discussed together.

In most pixels on the map that illustrates the correlation between $HH$ and $HV$ polarization, the element $C_{12}$ normalized by the intensity of the HH polarization is less than 0.4, which means that the correlation between $HH$ and $HV$ polarization is weak. Similar results are obtained for the element of the covariance matrix $C_{23}$ normalized by the intensity of the $HH$ polarization,

In Figure. 4.6, the covariance matrix element $C_{13}$ normalized by the intensity of $HH$ polarization of the grass clutter region is obviously lower than that of other regions,

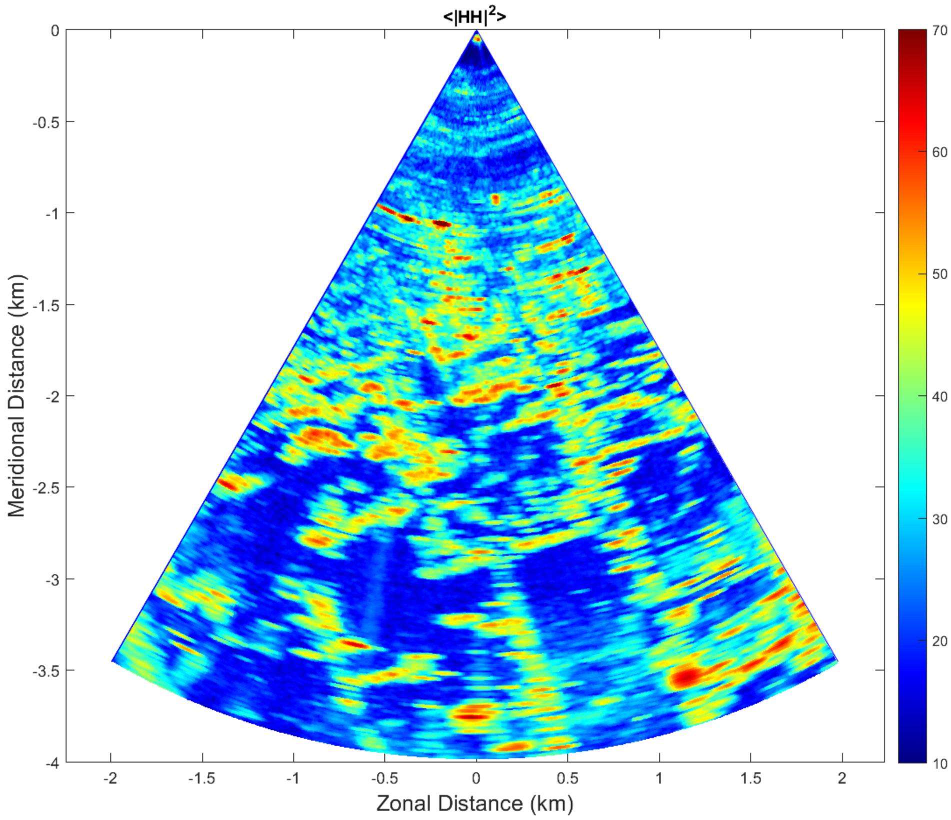


Figure 4.4: The map of the estimation of the amplitudes of the covariance matrix element $C_{11}$ by moving averaging window

which can help recognize grass clutter from other ground-based clutter in terms of polarimetric characteristics.

As a result, the covariance matrix can be effective in helping to recognize different ground-based features in terms of polarimetric characteristics by combining the intensity information on each polarization channel and the correlation between the co- and cross-polarizations.

### 4.2.2 Covariance Matrices of Target And Clutter

The covariance matrix elements of the target, two different types of clutter forest and grass are shown in the Figure. 4.7a to Figure. 4.7f. The red curves represent elements of the covariance matrix of our target, which is a power line mast located on grasslands. The blue curves represent elements of the forest clutter covariance matrix, and the orange curves represent elements of the grass clutter covariance matrix.

First, the geo-referenced plan position indicator (PPI) representation of the radar data is compared with Google Earth satellite images and maps. Based on this interpretation, the reference target (the set of power line masts) and two types of ground-based clutter - the "forest" and the "grassland" are selected. First, the range is set as constant. Then the azimuth cut is set as + / - 45 azimuth indices to the center point of the target location, forest and grasslands.

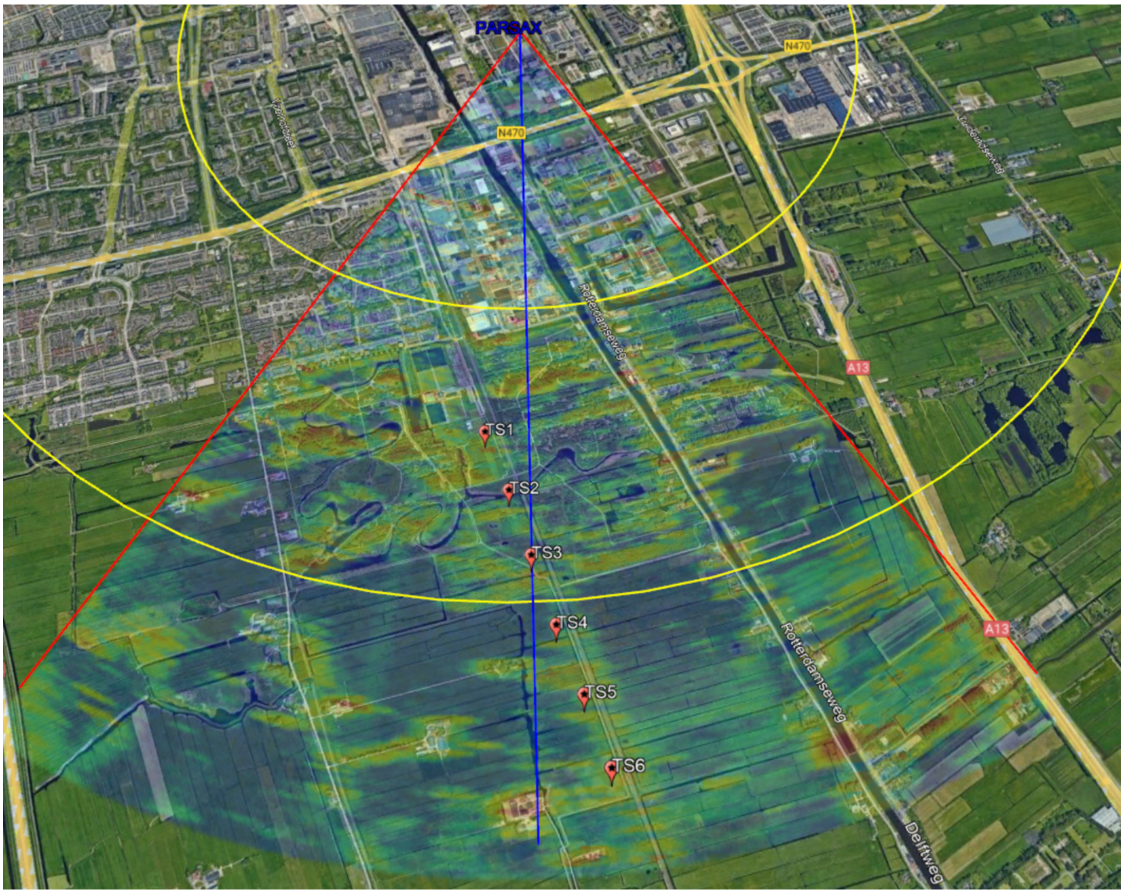


Figure 4.5: Intensity of the $HH$ polarization channel on the geographic map with the set of geo-located targets

As seen in Figure 4.7a, it is interesting to find the specific covariance patterns of the target, grasslands, and forests that are achieved by convolution with the antenna pattern, with a relatively clear transition boundary. Apparently, the transition boundaries of forest and grass are wider than the target's, and the forest's polarimetric characteristics vary within the boundary. According to the specific covariance pattern of the target and the transition boundary, clearly shown by the red curve in the Figure. 4.7a, it is reasonable to conclude that the target occupies about 30 azimuth indices in the middle of this chosen azimuth indices scale, and samples beyond this azimuth scale can be considered to be approaching the clutter, which is the grassland illustrated by the real global map as a reference. As a result, the result analysis for the target will focus only on these 30 azimuth indices in the middle (from azimuth index 36 to 66).

In Figure 4.7a the intensity of the $HH$ polarization (covariance matrix element $C_{11}$) of the target is approximately 50 dB, and the intensity of the HH polarization of the forest zone is also competitive, but with more fluctuations between the chosen azimuth index scale. The intensity of the $HH$ polarization of the grass is about 23 dB, which is obviously less than those of the target and the forest.

In Figure 4.7b the intensities of $HV$ polarization of the target and grassland are

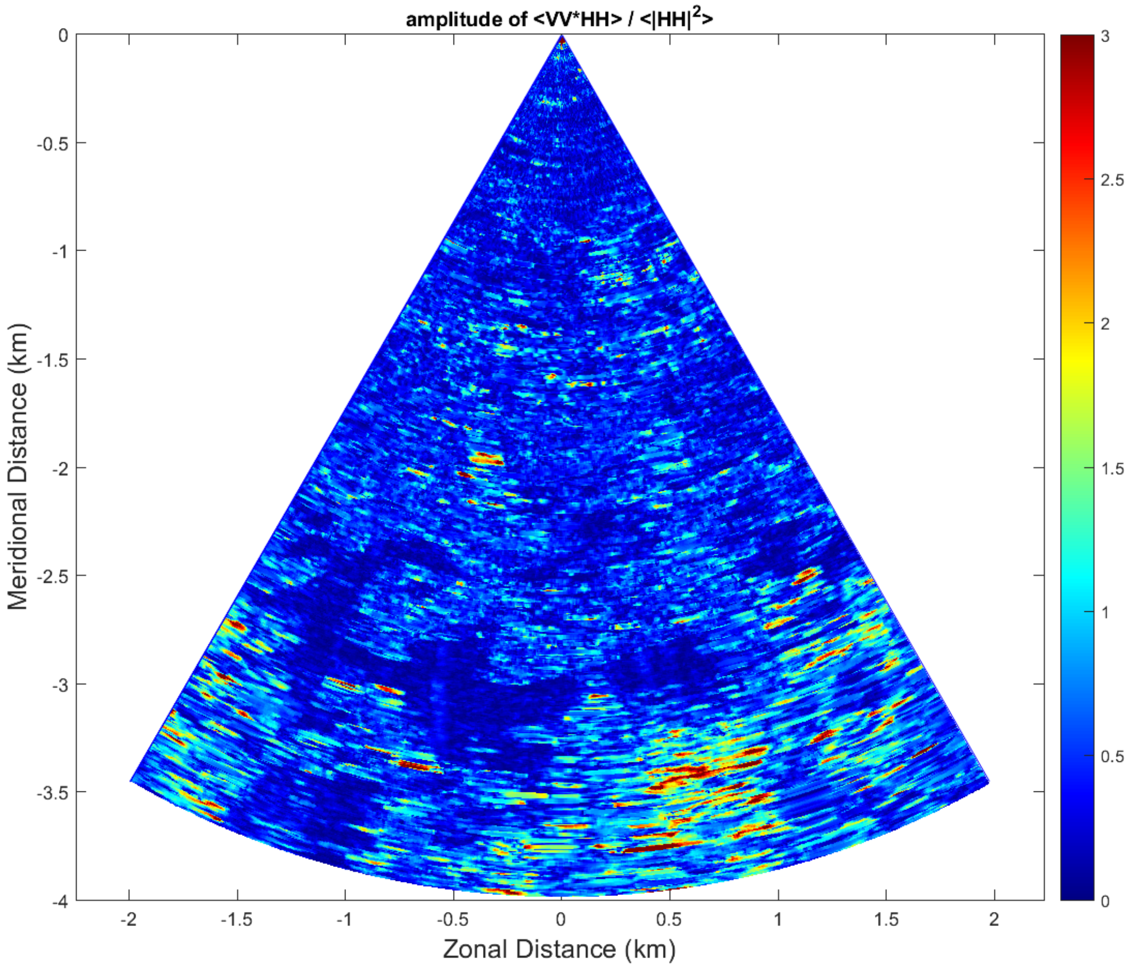


Figure 4.6: The map of the estimation of the amplitudes of the covariance matrix element $C_{13}$ by moving averaging window

quite low. Since the variability of the forest is large (within -20 dB to 5 dB), this forest element is difficult to predict.

In Figure 4.7c the intensity ratio of $VV$ polarization and $HH$ polarization (covariance matrix element $C_{33}$) is about 0 dB, which means that the co-polarization ($HH$ and $VV$) of this target are almost the same intensity. The grass clutter ratio fluctuates around -10 dB, while the variability of the forest ratio is still large within -7 to 15 dB.

In Figure. 4.7d the correlation between the polarization $HH$ and $HV$ is demonstrated by the element of the covariance matrix $C_{12}$. The amplitudes of this element of the target and grass are about 0.1 and 0.3, respectively, which can be considered a weak correlation. However, this element of the forest changes within the azimuth index; in this case, it can be challenging to predict the correlation between $HH$ and $HV$ for forest clutter.

In Figure. 4.7e the correlation between $HH$ and $VV$ is demonstrated by the covariance matrix $C_{13}$. For this target, $VV$ and $HV$ are supposed to be highly correlated. In general, the forest also has a strong correlation between $HH$ and $VV$ polarization, while the grass has a weak correlation between $HH$ and $VV$ polarization.

In Figure. 4.7f the correlation between $HV$ and $VV$ is demonstrated by the covariance matrix element $C_{23}$. It is difficult to draw a conclusion about the correlation between $HV$ and $VV$ for the forest zone in this case. The correlation between $HV$ and $VV$ for the target is weak, and the same is true for grass clutter.

In conclusion, the power line mast (located in the range = 3.42 km, azimuth = 176.25°) has strong intensities of co-polarization, and a weak intensity of cross-polarization that can be negligible compared to the intensity of co-polarization. It has a weak correlation between cross-polarization ($HV$) and co-polarization ($HH$ and $VV$), but it has a strong correlation between $HH$ and $VV$. The forest clutter shows a competitive HH polarization intensity compared to that of the target. However, the polarimetric characteristics of the forest obtained from other elements of the covariance matrix have strong variability. In this case, it may be challenging to summarize a polarimetric covariance matrix model for the forest, so it is reasonable to regard forest clutter as non-homogeneous clutter. The polarization power of the grass clutter is much weaker than that of the forest and target. For grass clutter, the correlations between $HH$ and $VV$, $HV$ and $HH$, $HV$ and $VV$ are weak. Furthermore, the polarimetric characteristics of grass clutter are much more stable than those of forests. As a result, polarimetric characteristics can be effective information in terms of recognition and suppression of clutter and detection of the target.

### 4.2.3 Covariance Matrix of Reference Target And ground clutter

The covariance matrix of the power line mast, grass, and forest can be easily extracted from the polarimetric characteristic library and used later in the calculation of the target detection algorithms.

As seen from the covariance matrix element maps, as mentioned above, grass clutter has similarity in terms of each covariance matrix element. Unfortunately, although the power line masts seem quite similar on the global map, they have strong variability in terms of polarimetric characteristics with each other, which brings challenges to summarize a theoretic covariance matrix model for such a type of object. In addition, forest clutter will be considered as non-homogeneous clutter in our case, since its covariance matrix elements also fluctuate intensively.

In this thesis, a list of covariance matrices for each power line mast, grass clutter, and forest clutter is provided. This information will later be used in the calculation of detection algorithms as *a priori* knowledge of the target and clutter. The covariance matrix list is as follow:

power line mast 1

$$C = 59.57\ dB \cdot \begin{bmatrix} 1.00 & 0.25 \cdot e^{j20.68} & 0.81 \cdot e^{j-27.75} \\ 0.25 \cdot e^{j-20.68} & 0.07 & 0.21 \cdot e^{j-50.01} \\ 0.81 \cdot e^{j27.75} & 0.21 \cdot e^{j50.01} & 0.69 \end{bmatrix}$$

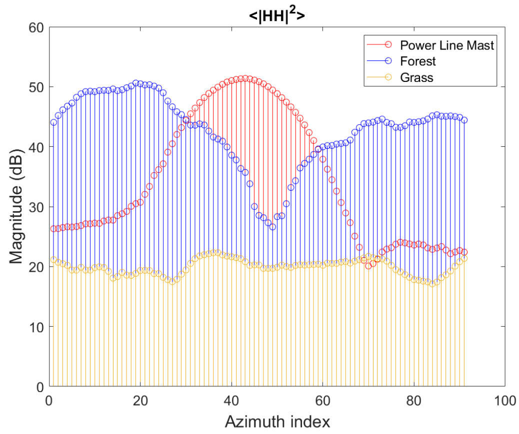


(a) Covariance matrix element $C_{11}$

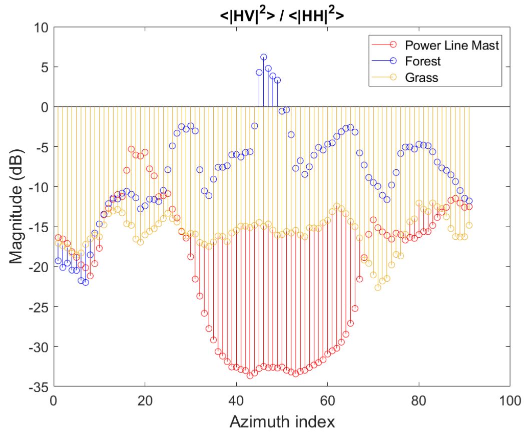


(b) Covariance matrix element $C_{22}$

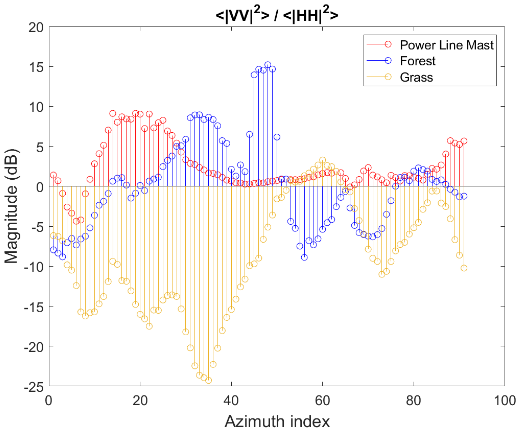


(c) Covariance matrix element $C_{33}$

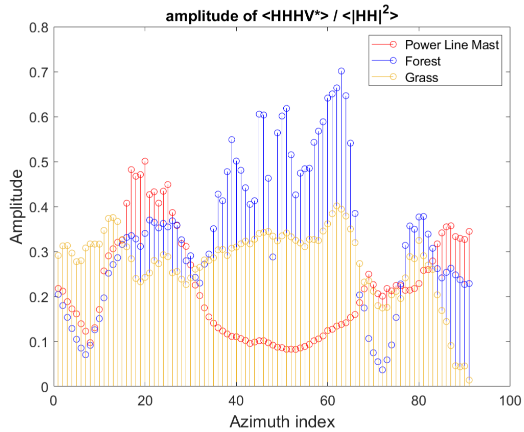


(d) Covariance matrix element $C_{12}$

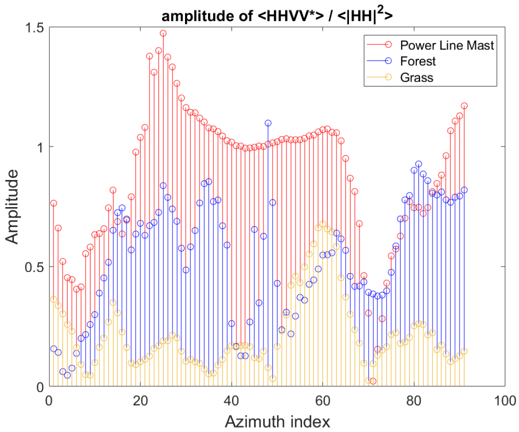


(e) Covariance matrix element $C_{13}$

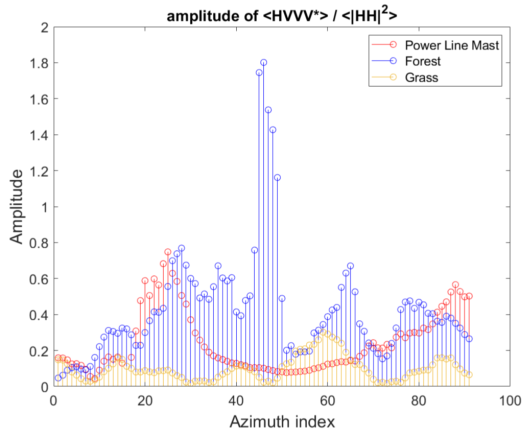


(f) Covariance matrix element $C_{23}$

Figure 4.7: Covariance matrix elements of target, forest clutter, and grass clutter

power line mast 2

$$C = 51.47\ dB \cdot \begin{bmatrix} 1.00 & 0.65 \cdot e^{j18.30} & 0.33 \cdot e^{j127.15} \\ 0.65 \cdot e^{j-18.30} & 0.50 & 0.26 \cdot e^{j111.66} \\ 0.33 \cdot e^{j-127.15} & 0.26 \cdot e^{j-111.66} & 0.35 \end{bmatrix}$$

power line mast 3

$$C = 55.78\ dB \cdot \begin{bmatrix} 1.00 & 0.19 \cdot e^{j-2.19} & 0.39 \cdot e^{j10.93} \\ 0.19 \cdot e^{j2.19} & 0.09 & 0.11 \cdot e^{j55.53} \\ 0.39 \cdot e^{j-10.93} & 0.11 \cdot e^{j-55.53} & 0.29 \end{bmatrix}$$

power line mast 4

$$C = 49.24\ dB \cdot \begin{bmatrix} 1.00 & 0.64 \cdot e^{j-30.02} & 0.69 \cdot e^{j-112.45} \\ 0.64 \cdot e^{j30.02} & 0.44 & 0.45 \cdot e^{j-86.95} \\ 0.69 \cdot e^{j112.45} & 0.45 \cdot e^{j86.95} & 0.61 \end{bmatrix}$$

power line mast 5

$$C = 51.21\ dB \cdot \begin{bmatrix} 1.00 & 0.11 \cdot e^{j0.32} & 1.00 \cdot e^{j-38.46} \\ 0.11 \cdot e^{j-0.32} & 0.02 & 0.12 \cdot e^{j-31.61} \\ 1.00 \cdot e^{j38.46} & 0.12 \cdot e^{j31.61} & 1.05 \end{bmatrix}$$

power line mast 6

$$C = 50.72\ dB \cdot \begin{bmatrix} 1.00 & 0.09 \cdot e^{j-1.02} & 0.73 \cdot e^{j-22.56} \\ 0.09 \cdot e^{j1.02} & 0.03 & 0.10 \cdot e^{j-29.53} \\ 0.73 \cdot e^{j22.56} & 0.10 \cdot e^{j29.53} & 0.74 \end{bmatrix}$$

Forest

$$C = 50.29\ dB \cdot \begin{bmatrix} 1.00 & 0.37 \cdot e^{j-84.50} & 0.63 \cdot e^{j-42.76} \\ 0.37 \cdot e^{j84.50} & 0.26 & 0.37 \cdot e^{j45.94} \\ 0.63 \cdot e^{j42.76} & 0.37 \cdot e^{j-45.94} & 0.94 \end{bmatrix}$$

Grass

$$C = 39.42\ dB \cdot \begin{bmatrix} 1.00 & 0.13 \cdot e^{j77.32} & 0.57 \cdot e^{j-76.12} \\ 0.13 \cdot e^{j-77.32} & 0.07 & 0.06 \cdot e^{j-147.83} \\ 0.57 \cdot e^{j76.12} & 0.06 \cdot e^{j147.83} & 0.38 \end{bmatrix}$$

To check the precision of measurement result in terms of the covariance matrix, the grass covariance matrix obtained by the measurement data is compared with the theoretical polarimetric clutter model with elements values of meadow clutter given in Chapter 2 Table. 3.1. Except that the intensity of $VV$ polarization of the result of the grass measurement is slightly lower than its theoretical value, the grass clutter in the measurement is strongly similar to its theoretical model with a low intensity of $HV$ polarization and a weak correlation between $HV$ and $HH$, $HV$, and $VV$.

## 4.3 Conclusions

This chapter mainly discusses the estimation of the polarimetric covariance matrix with the moving spatial averaging window method. The size of such a window has been optimized based on the trade-off between the minimal degradation in the spatial resolution and the similarity of the pixels related to the same specific type of observed objects. Then the covariance matrix element maps demonstrate the result of the covariance matrix estimation that applies the moving spatial averaging window method with the chosen window size for the entire measured scenario.

The covariance matrix element maps show that the moving spatial averaging window method improves the smoothness of the covariance matrix components in space, so that the similarity of the pixels related to the same specific type of ground-based feature has been improved, and the differences among various objects and terrain features have been demonstrated. These maps also demonstrate that, in general, the analyzed radar scene has a high variability of polarization characteristics and can be defined as a case of heavy inhomogeneous clutter.

A library of polarimetric characteristics of the measured scenario consists of the covariance matrix estimation results shown in the maps, which can be used as a reference source to extract the covariance matrices of the reference target and clutter as knowledge *a priori*. For such interpretation of radar data, the geo-referenced plan position indicator (PPI) representation of the radar data is compared with Google Earth satellite images and maps. Based on this interpretation, the reference target (the set of power-line mast constructions) and two types of ground-based clutter - the "forest" and the "grassland" were selected.

The covariance matrix estimation result of the power line mast, grass, and forest clutter shows that the forest and grass clutter are distributed much more widely than the power line mast as the observed object. Although the power line masts ranging in line seem similar in their appearances, they are different from each other in terms of polarimetric characteristics denoted by covariance matrix elements. The elements of the covariance matrix of forest clutter display larger variabilities compared to those of grass clutter. As a result, we can draw a conclusion that grass can be regarded as homogeneous clutter with relatively stable polarimetric characteristics, while forest should be categorized as non-homogeneous clutter with polarimetric characteristic variations in our measurement case.

At the end of this chapter, we provide a list of covariance matrices for each power line mast, grass clutter, and forest clutter. The accuracy of the estimation of the covariance matrix is proved by comparing the grass covariance matrix obtained by the measurement data with the theoretical covariance matrix of the meadow clutter.

# Experimental Validation of Polarimetric Algorithms for Targets Detection in Heavy Inhomogeneous Clutter

# 5

In Chapter 3, the derivations of a variety of polarimetric detection algorithms are given and then their performances are compared in simulation, focusing on the trade-off between the amount of statistical knowledge *priori* required by an algorithm and the corresponding performance of the algorithm. In Chapter 4, analysis of the spatial statistical characteristics of the reference target and different types of ground-based clutter in terms of polarization covariance matrices is provided.

In this chapter, with *a priori* knowledge of clutters and the reference target provided in Chapter 4, the set of polarimetric detection algorithms is implemented based on the S-band polarimetric-Doppler FMCW PARSAX radar high-resolution range measurements (3.3 m) in azimuthal scanning mode.

## 5.1 Experimental Validation of the Detection Algorithms

To prove the measurement validation of the polarimetric target detection algorithms mentioned earlier, this section tests the algorithms using real target and clutter data collected by the PARSAX polarimetric Doppler FMCW radar system. Full polarimetric measurements ($HH$, $HV$, and $VV$) are generated based on the covariance matrix, which is obtained by zero Doppler measurement data. The performances are displayed by the detection output maps.

### 5.1.1 Measurement Setup

The PARSAX radar is mounted at the top of the EEMCS (Faculty of Electrical Engineering, Mathematics and Computer Science) building. It is the S-band polarimetric Doppler FMCW radar system used to collect the measurements. PARSAX is full polarimetric with two independent highly linear polarimetric RF channels in both the transmitter and receiver. The radar operates on the S-band with carrier frequency $f_c = 3.315GHz$ and bandwidth $B = 50MHz$. The pulse repetition interval (PRI) is 240 $\mu$s.

More specifically, the realistic scenario measurement in this research is set as follows. The polarization angle of 21.56 degrees occurs due to the inclination axis of the PARSAX radar, when the radar antennas pointed towards the measured scenario at elevation angle of -0.85 degrees during the measurement. Measurement of polarization scattering matrix (PSM) of each point in the realistic scenario has been carried out with actual rotation angles ranging from 150 to 210 degrees. PARSAX radar data are measured with high range resolution (approximately 3.3 meters) in the azimuthal scanning mode with azimuth resolution of 0.1 degrees per burst. The beam width of the antenna system in the azimuth direction is 2.8 degrees. The measurement setup parameters are shown in the list in Fig. 5.1.

| parameters | values |
|---|---|
| Carrier frequency | 3.315 GHz (S-band) |
| Bandwidth | 50 MHz |
| Pulse Repetition Interval | 240 $\mu s$ |
| Beam width | 2.8 degrees |
| Range resolution | 3.3 m |
| Azimuth resolution | 0.1 degrees |
| Elevation angle | -0.85 degrees |
| Polarization angle | 21.56 degrees |
| Rotation angles | 150 – 210 degrees |

Figure 5.1: PARSAX polarimetric Doppler FMCW radar system parameters

It is necessary to mention that the noise-based equalization is applied as an internal calibration on zero Doppler data in the measurement of this research, which has been mentioned in Chapter 2.

### 5.1.2 Generating Feature Vectors As Measurements For Detection Algorithms

Assuming that there are similar distortions for the target and clutter, noise-based calibration of the radar system is addressed as an internal calibration for the measured polarimetric data. After noise-based calibration, the zero Doppler data of each pixel are then utilized to perform spatial averaging in the moving average window for the calculation of the covariance matrix. In order to operate the target detection algorithms that are introduced in Chapter 3 for the polarimetric radar data, the measured target and clutter returns on the slow-time scale need to be generated as measurements. The method of generating feature vectors with random signals and Cholesky decomposition of covariance matrix introduced in Chapter 3 for the polarimetric radar simulator can be used to generate multichannel polarimetric signals in real measurements as well. The measurements of the full polarimetric channels are obtained according to the estimated covariance matrix obtained by the moving averaging spatial window of each pixel (from the polarimetric characteristics library) in the entire measured scenario.

### 5.1.3 Target-to-clutter Ratio of the measurement data

The target-to-clutter ratio can be obtained by the ratio of the target span and clutter span. We define the ranges of reference targets that are the radii from PARSAX to the power line masts. At the ranges of the reference targets, the powers of clutters are obtained by the averaged value of the clutters, which are five clutter positions with relatively strong powers. Figure. 5.2 demonstrates the situation of weak target in heavy clutter environment in terms of the target-to-clutter ratio. The maximum TC ratio in these six ranges is 10.35 dB, while the minimum TC ratio is -5.73 dB, which means that the power of clutter is 5.73 dB stronger than the reference target's power.

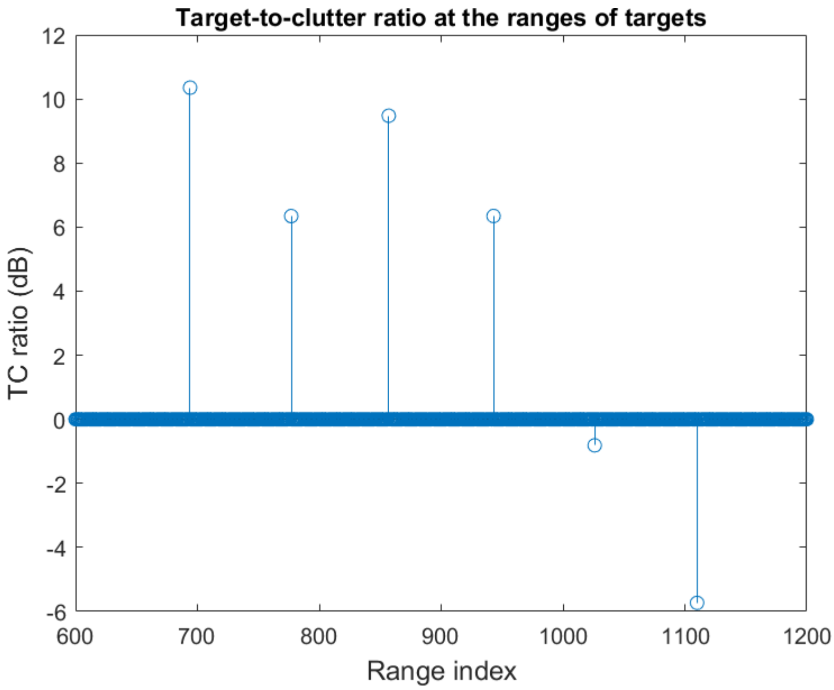


Figure 5.2: Target-to-clutter ratio at the ranges of targets

### 5.1.4 Results of Target Detection Algorithms Using Physical Method With Measurement Data

It is necessary to clarify that in this research, the detection performance of different polarimetric detection algorithms using polarization information is evaluated by comparing the map of geo-reference plan position indicator (PPI) result of the detectors' output to the Google Earth satellite map.

First, methods that use only physical information are addressed without the requirement of polarimetric characteristics such as *a priori* knowledge. The performances of these detectors are shown below.

#### 5.1.4.1 Single Channel HH Detector

The single-channel HH detector, which considers only the intensity of $HH$ polarization, is the simplest method in terms of implementation. Seen in Figure. 5.3 the reference targets have relatively strong HH intensities. However, after applying a single-channel HH detector, these targets are still hidden among ground-based clutter whose powers of $HH$ polarization are within or even beyond the level of HH intensities of reference targets. For complex realistic scenarios, single-channel HH detectors cannot effectively detect targets.

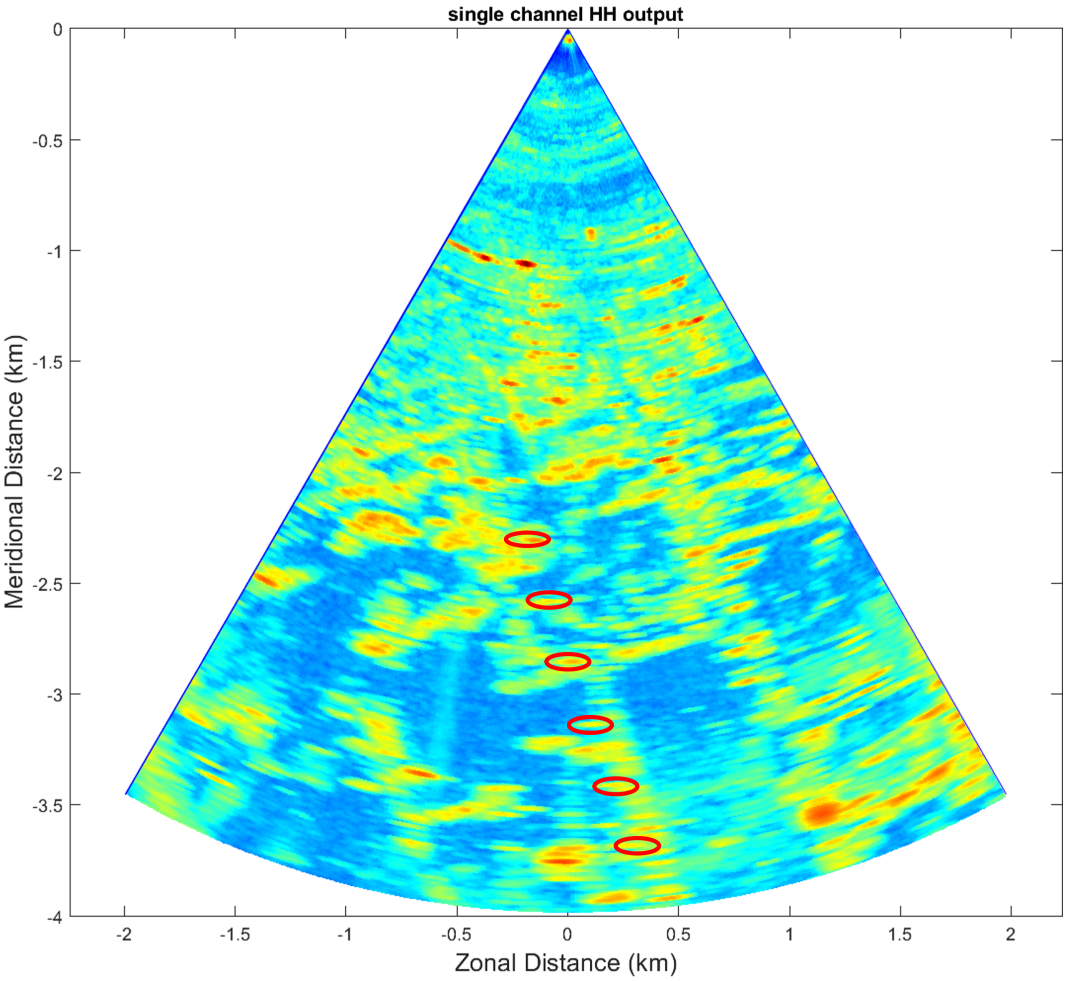


Figure 5.3: Target detection by single channel HH detector

#### 5.1.4.2 Span Detector

The span detector considers the weighted non-coherent sum of all three polarimetric channels $HH$, $HV$, and $VV$. Considering that the measured scenario covers a large range scale, one of the drawbacks of the span detector could be that objects closer to the radar receiver may have stronger total received power, because the radar received power is proportional to $\frac{1}{R^2}$ known in the radar range equation Eq. 5.1, where R is the range from the transmit antenna to the object, $P_s$ is the transmitted power, $P_r$ is the reflected power, $G$ is the antenna gain, and $\sigma$ in the radar range equation is the radar cross section.

In Figure. 5.4, span detector can suppress clutter with relatively low total power, such as the grass zone. However, the power line mast cannot yet be classified from forest clutter or other constructions.

$$P_r = \frac{P_s}{4\pi R^2} G \cdot \sigma \tag{5.1}$$

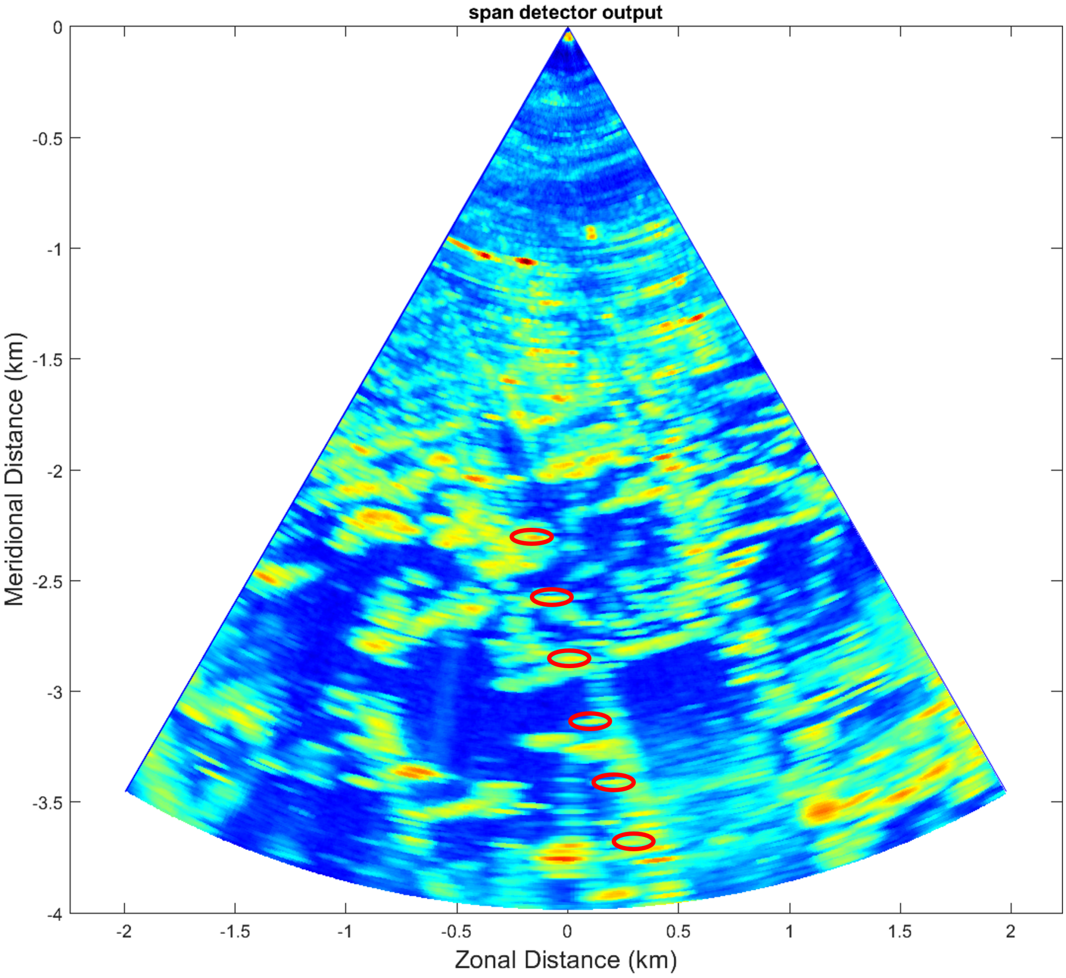


Figure 5.4: Target detection by span detector

#### 5.1.4.3 Power Maximum Synthesis (PMS) Detector

As an improvement of the span detector, the power maximum synthesis detector is a function of the components of the measurement vectors. It makes no use of a priori target or clutter statistics. Compare Figure. 5.5 with Figure. 5.4, there are no obvious differences between the performance of the PMS detector and the span detector. Therefore, the PMS detector also cannot detect reference targets from the ground-based clutter environment.

Based on the performance described above, for our complex realistic scenario, detectors with physical approaches cannot effectively detect targets. The results of a single-channel, span, and PMS detector with measurement data agree with the performance of these detection algorithms in simulation.

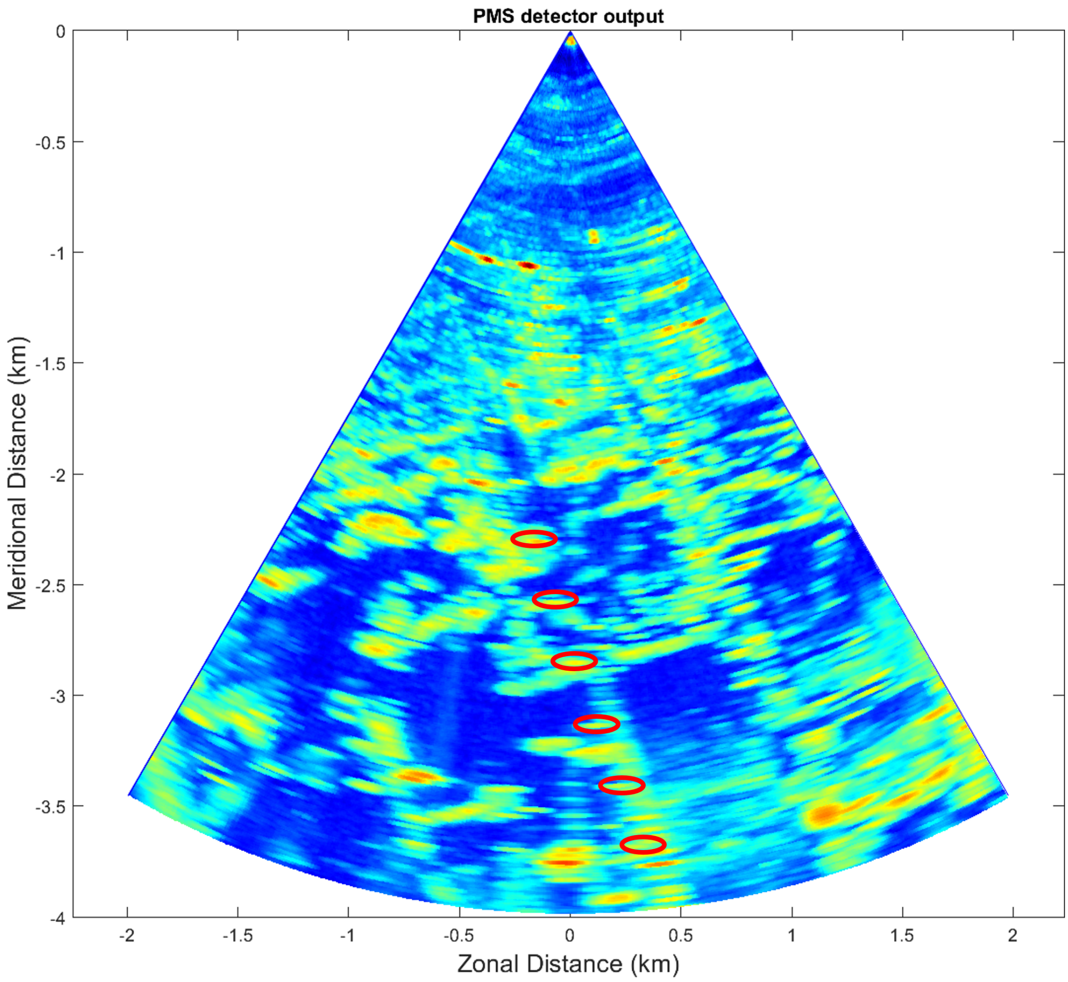


Figure 5.5: Target detection by power maximization synthesis (PMS) detector

In addition, in Appendix C the span detector used without noise-based calibration is shown as an example of tests on the efficiency of noise-based calibration on the improvement of polarization information's accuracy and reliability. It is necessary to mention that for detection algorithms based on physical approaches, the accuracy of the total powers of scattered signals is shown with slight improvement with noise-based calibration.

### 5.1.5 Results of Target Detection Algorithms Using Statistical Method With Measurement Data

After the discussion on experimental results of detectors based on physical approaches, in this part, the methods are tested with the requirement of polarimetric characteristics such as *a priori* knowledge with measured data. The performance of these detectors is shown below.

#### 5.1.5.1 Optimal Polarimetric Detector (OPD)

The optimal polarimetric detector utilized in our measurement operates as the expression in Eq. 3.11. Note that in the measurement, $\Sigma_{t+c}$ is replaced by the covariance matrix on the pixel of the reference target, since we consider all the positions that are not the reference target as clutter with $\Sigma_c$, and the reference target corresponds to the covariance matrix $\Sigma_t$. In other words, with an optimal polarimetric detector, every pixel on the map is supposed to be categorized into two classes: clutter as class 1, and target as class 2. The expression of OPD in the measurement can be shown in Eq. 5.2.

$$\mathbf{X}^{\dagger}\left(\mathbf{C_c^{-1}} - \mathbf{C_t^{-1}}\right)\mathbf{X} + \ln\frac{|\mathbf{C_c}|}{|\mathbf{C_t}|} > \ln\mathbf{T}. \tag{5.2}$$

In this research, OPD uses the polarimetric covariance matrix of the reference target and uses the spatial moving window to estimate the clutter's covariance matrix for every location. The maximum detector response will be in the location of objects with polarimetric characteristics that are similar to the "reference" target.

In order to increase the difference between the output results of the target and clutter after the optimal polarimetric detector, the output results are addressed by scaling in a reasonable way. $s$ represents the original OPD output result, and the final OPD output result is represented by $s^{'}$ after scaling as in Eq. 5.3.

$$s^{'} = 10\log_{10}\left(10^{s}\right) \tag{5.3}$$

Since power line masts have a large variability in terms of polarimetric characteristics, once OPD is used, it can only be achieved to detect the power line mast at one specific position from the ground-based clutter. With *priori* knowledge of the reference targets at six positions, it is possible to detect all reference targets from grass and forest clutter. The scaling processing for six targets detection is given as Eq. 5.4, where $s_i$ is the output result of each power line mast after OPD.

$$s^{'} = 10\log_{10}\left(\sum_{i=1}^{6} 10^{s_i}\right) \tag{5.4}$$

Setting a reasonable threshold $T = -10$, the performance of the OPD method output for the detection of the reference target is shown in Figure. 5.6. By modifying the detector threshold, the number of false alarms and missed detections can be reduced. When the threshold is set to $T = -15$, several false alarms appear with a value lower than the reference targets but can lead to incorrect detection (Figure 5.7). As in the performance shown in Figure. 5.6 by set threshold $T = -10$, it successfully detects reference targets from all ground-based clutter throughout the scenario without false alarms and without missed detection on the detection map.

As in the conclusion given in Chapter 4, the grass can be regarded as homogeneous clutter with relatively stable polarimetric characteristics, while the forest's polarimetric characteristics have strong variabilities implied by the covariance matrix. To test the sensitivity of the OPD method, this detection algorithm is also used for the detection of the grass zone and the detection of the forest zone. In this processing, $\Sigma_t$ is assigned by the reference covariance matrices of grass and forest.

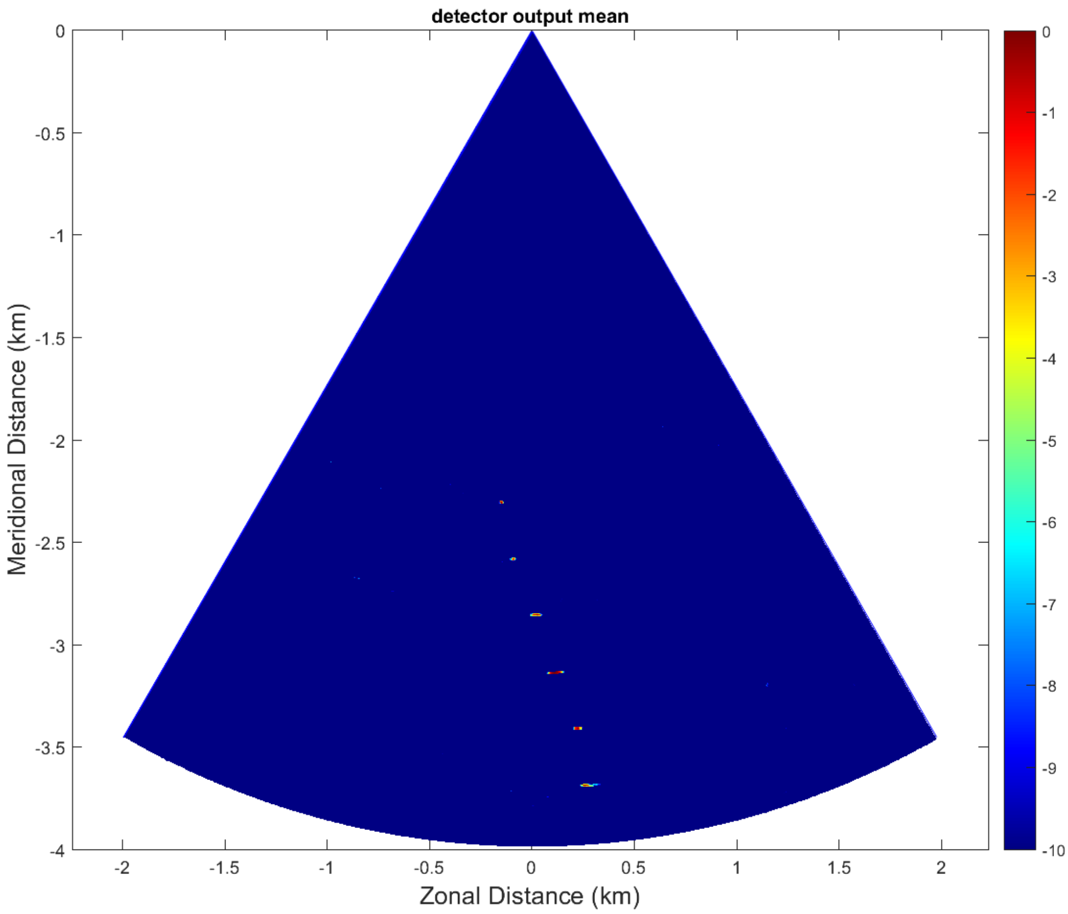


Figure 5.6: Reference targets detection by optimal polarimetric detector

The grass areas among the realistic scenario are distributed on different azimuth and range scales. Seen in Figure. 5.8, OPD method for the detection of grasslands is quite effective, and the grasslands show a scale similar to the detector output with significantly stronger level than other objects.

The forest areas among the realistic scenario are also distributed on different azimuth and range scales, and some forests are surrounding constructions. Seen in the Figure. 5.9, OPD method for forest area detection is also effective. Because the polarimetric characteristics of the forest are not homogeneous, the results of OPD detection have values on different scales, indicating that OPD is sensitivity with the target covariance matrix as reference. It is interesting to notice that the forest surrounding constructions can be recognized quite well, which are displayed as ellipses on the map.

As a result, the OPD method is a promising detection algorithm for target detection and polarimetric contrast enhancement.

In addition, the efficiency of noise-based calibration in improving polarization information's accuracy and reliability are also tested for the OPD method. Note that the performance of detection algorithms based on statistical approaches, such as the OPD, does not perform obvious changes between with and without noise-based calibration. This is also reasonable because the order of magnitude of noise is at least 20 dB less

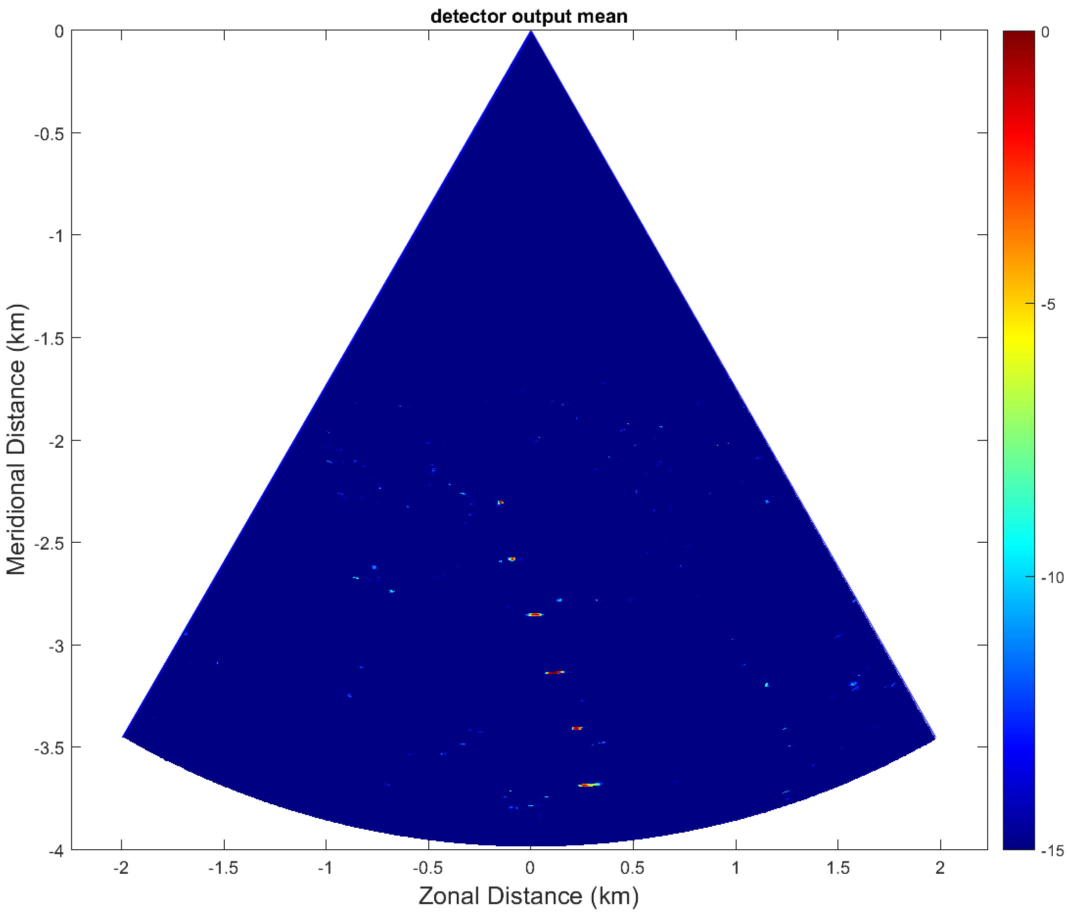


Figure 5.7: Reference targets detection by optimal polarimetric detector

than that of scattered signals from objects.

#### 5.1.5.2 Polarimetric Whitening Filter (PWF)

In theory, the PWF detector is supposed to convert the specified type of clutter return to white noise. From the result of the simulation of PWF, it is concluded that PWF is the best choice to suppress clutter and detect the target in a homogeneous clutter situation. For the complex scenario in the measurement, it is challenging to reduce all kinds of clutter by applying PWF at one time, especially for non-homogeneous clutter such as forest area. Therefore, the performance analysis focuses on the ability of the PWF detector to suppress the specific type of clutter.

Figure 5.10 represents the contrast between the power of HH polarization, the OPD detection result of the grass area to indicate the positions of the grass area, and the performance of the PWF method in terms of grass clutter suppression. Grass clutter can be significantly suppressed by PWF, although other objects such as power line masts, constructions, and forest zones cannot be easily classified in this way.

Figure 5.11 represents the contrast between the power of HH polarization, the result of OPD detection of the forest area to indicate the positions of the forest area, and the

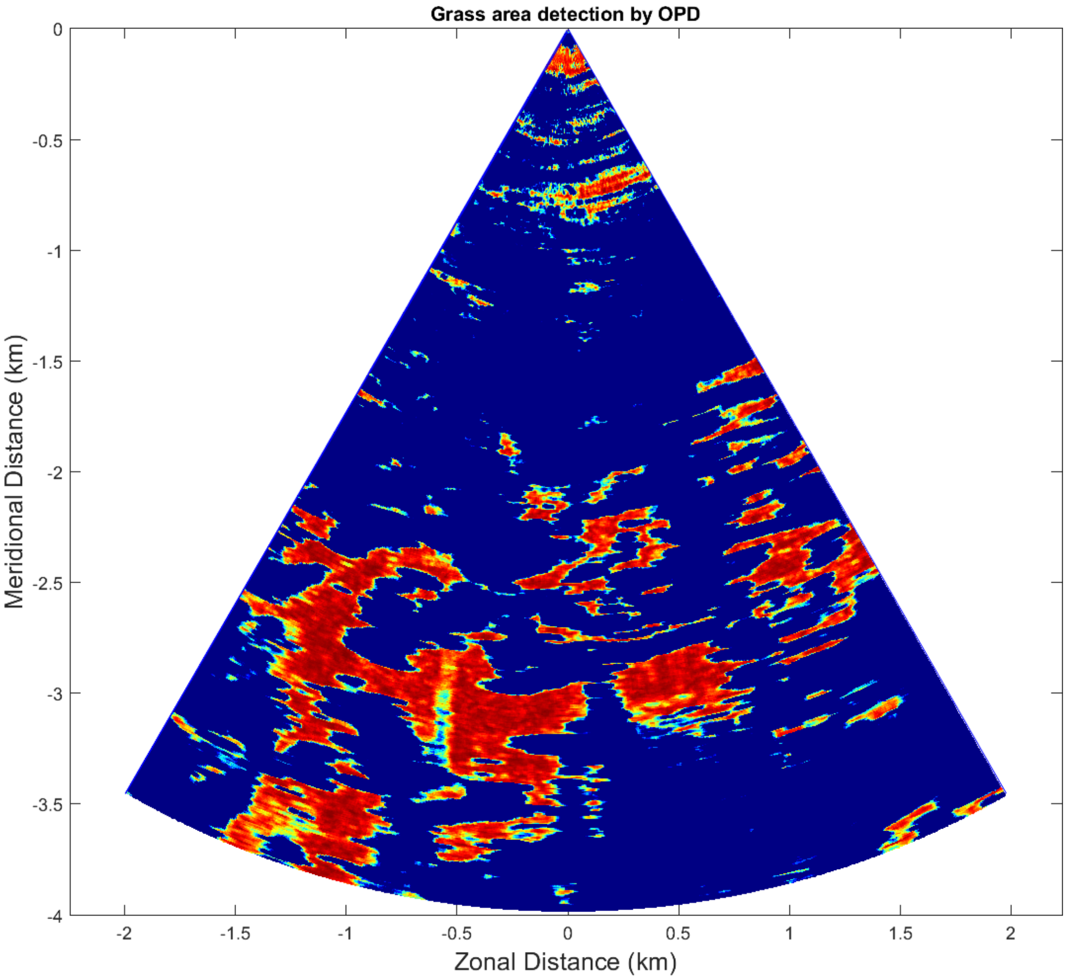


Figure 5.8: Grass area detection by optimal polarimetric detector

performance of the PWF method in terms of forest clutter suppression. It is exciting to notice that the forest clutter can be excellently filtered by PWF, with only the power line masts and the constructions surrounded by forest remaining on the map after processing by the polarimetric whitening filter.

From another point of view, PWF is an excellent processing for classifying whether the measured signal is the radar return of specific clutter or not. The specific type of clutter can be effectively suppressed by PWF; the performance of this clutter filter depends on the variability of the polarimetric characteristics of the clutter.

### 5.1.6 Recognition Map

To provide an explicit comparison of the detection of terrain features with a realistic scenario on the global map, it is necessary to create an image with a mixture of the detection results of the power line masts, the grass area, and the forest area as three components on the map. In this thesis, these three components detected by an optimal polarimetric detector are displayed on a recognition map, which is created by making

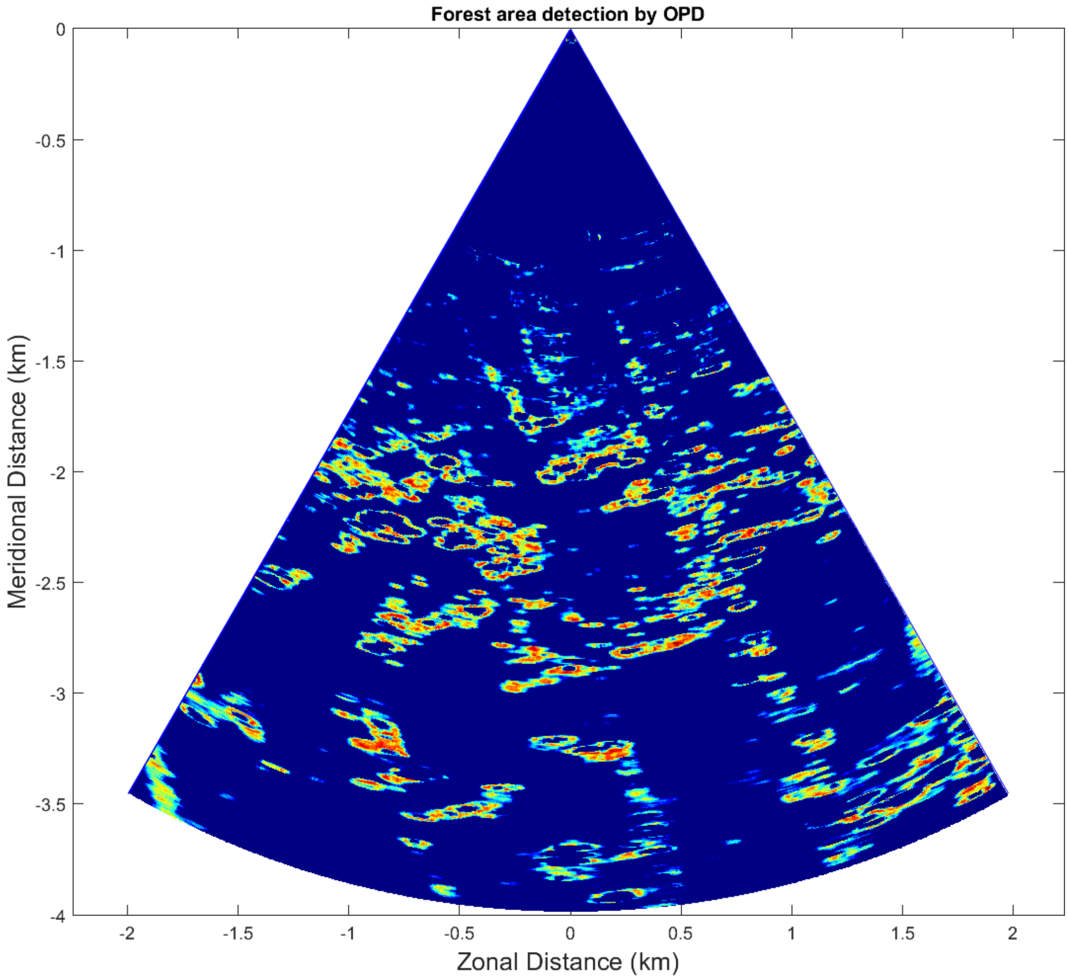


Figure 5.9: Forest area detection by optimal polarimetric detector

an image of the 2D mixture of OPD output using RGB pallets for every component.

The recognition map shown in Figure 5.12 is the combination of the output of the OPD algorithm, which is used to demonstrate the detection results of the reference targets, the grassland area and the forest area. All output values below the threshold as suppressed clutter are shown in white. Different targets detected by OPD with an output value above the threshold are considered as every component of the recognition map. Three components are shown in different colors: power line masts as reference targets are represented in red, the forest area is represented in green, and the grass area is yellow.

In view of the performance comparison of these detection algorithms, there is no doubt that with *a priori* knowledge of the reference target, the OPD algorithm exhibits the best performance in terms of target detection and polarimetric contrast enhancement.

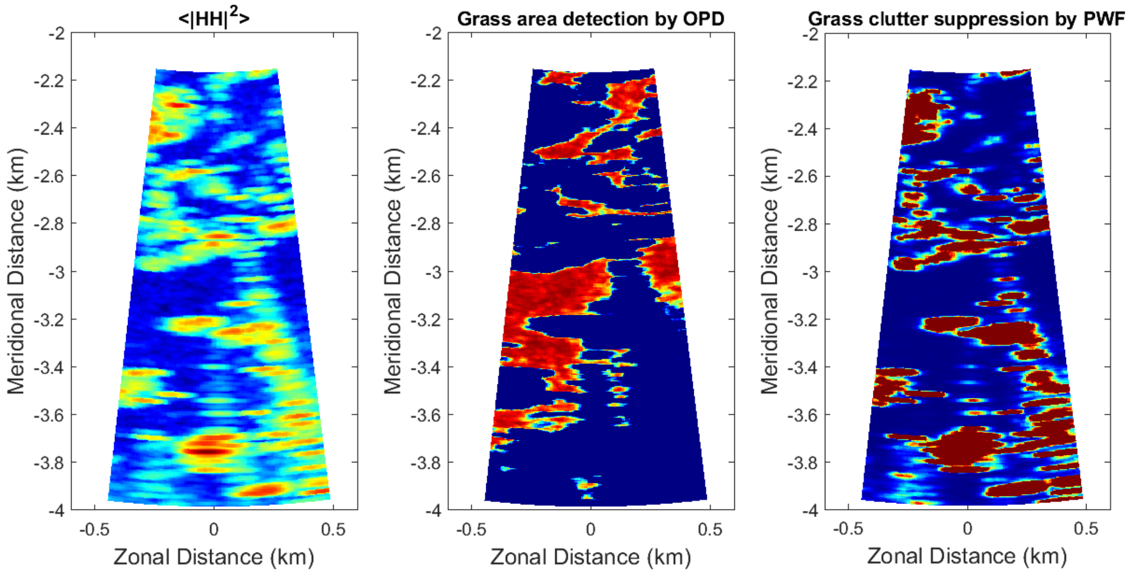


Figure 5.10: Grass area detection performance of OPD and grass clutter suppression of PWF

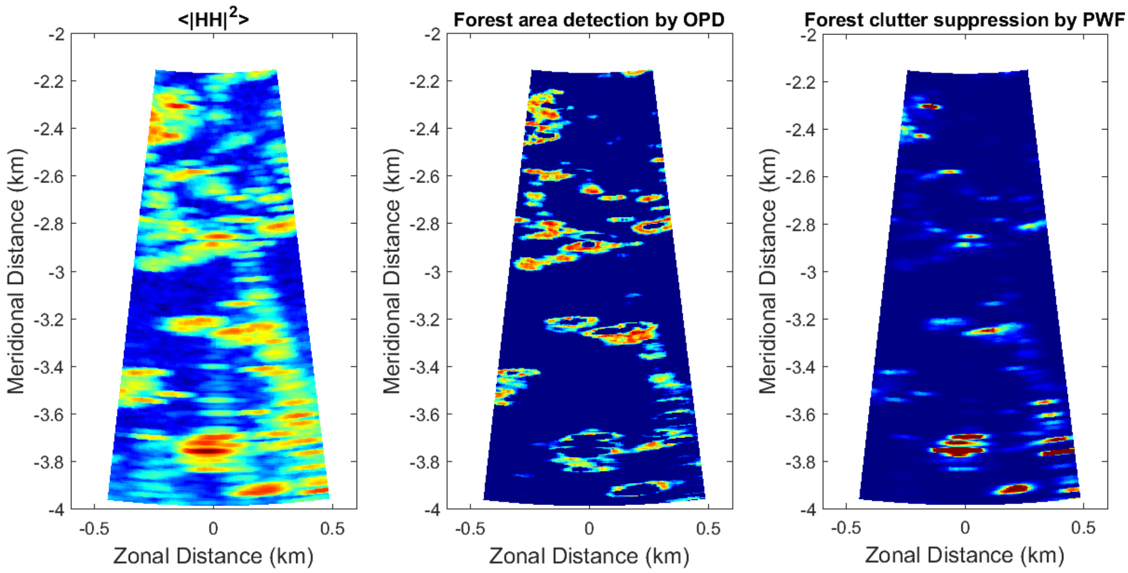


Figure 5.11: Forest area detection performance of OPD and forest clutter suppression of PWF

## 5.2 Conclusions

This chapter describes mainly the analysis and comparison of the polarimetric detection algorithms performances: three detectors based on physical approaches, which are the single channel $HH$ detector, the span detector, the Power Maximum Synthesis (PMS) detector, and two detectors based on statistical approaches, which are the Polarimetric Whitening Filter (PWF) and the Optimal Polarimetric Detector (OPD). The performances of each detector are shown using the 2D maps of the detector outputs, which can be clearly compared with the observed radar scenario seen from the geo-referenced

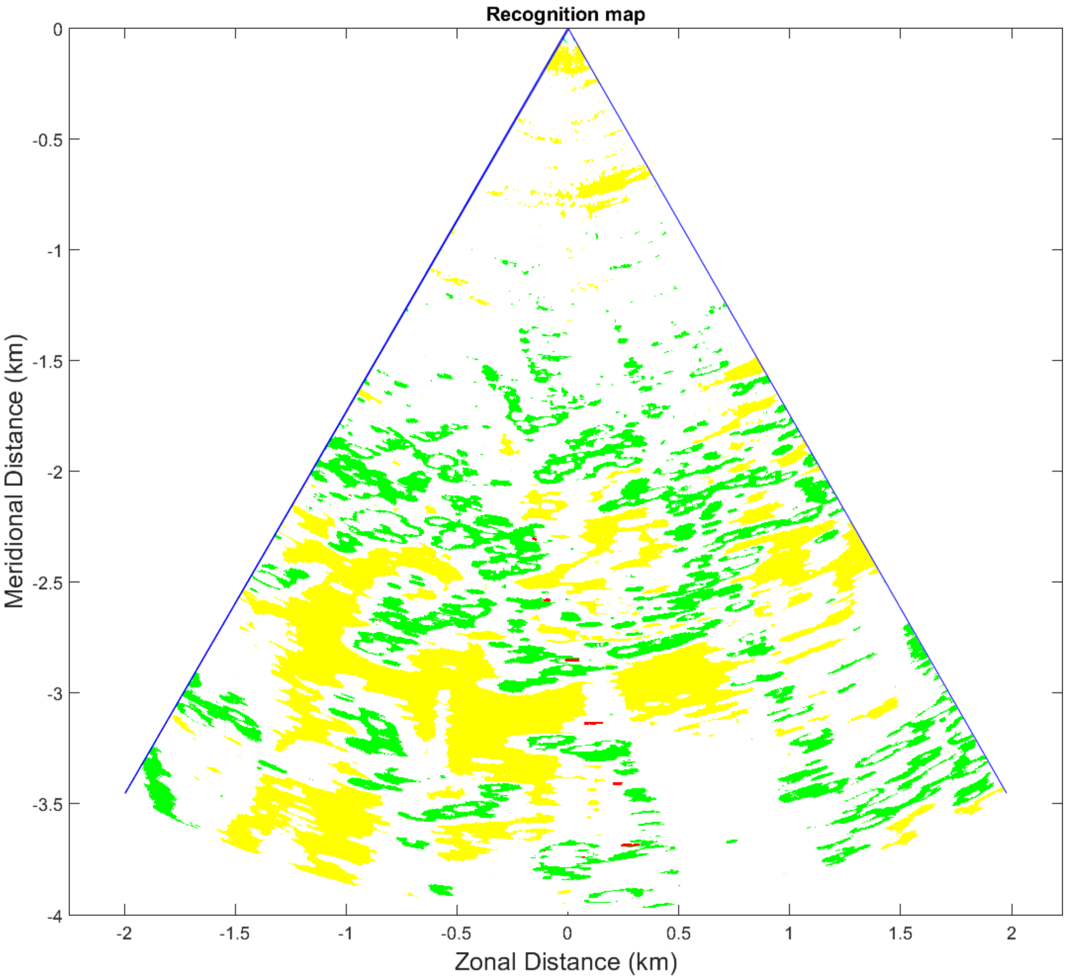


Figure 5.12: Recognition map of reference targets and ground-based clutter

geographical map.

For a complex measured scenario, polarimetric radar detectors, which are based only on physical approaches for maximization of the received from the target scattered signal, are not effective for the detection of the reference targets. In the studied cases, they are the power line masts arranged in a line. These poor performances of the physical-approches-based detectors applied to the really measured data are in good agreement with the simulation results.

For the two detectors based on statistical approaches that are performed with measurement data, they have a significant improvement in the abilities of target detection and clutter suppression compared with detectors that only consider physical information.

The Polarimetric Whitening Filter, which uses a priori information about the polarization covariance matrix of the clutter, demonstrates excellent results in the suppression of this specific type of clutter. It is not sensitive in terms of the similarity between the "reference" covariance matrix used in the filter and this matrix in the analyzed spatial location. With the covariance matrix previously estimated as the average for multiple locations of a specific type of clutter, it can impressively suppress this type of clutter.

In the case where both target and clutter characteristics are a priori known, the optimal polarimetric detector is the best choice for polarimetric contrast enhancement and reference target detection, which also confirms the theoretical expectation. With respect to the gain of detectability, compared with the single channel detector output map, the Polarimetric Whitening Filter and the Optimal Polarimetric Filter perform significant improvement, which are also displayed by the interpretation of geo-reference PPI representaion. In this chapter, experimental results are provided for the detection of power line masts, grasslands, and forests. The comparison of three different varieties of targets indicates that the OPD method is sensitive to the variability of the polarimetric characteristics of the reference target. Furthermore, one of the most important advantages of OPD is that it can be implemented in parallel for different clutter types within a simple real-time streaming signal processing algorithm. At the end of this chapter, a recognition map is created as an image of the mixture of 2D data of OPD output using RGB pallets for every variety of targets. The recognition map presents the detection results of power line masts, grasslands, and forests together and provides an explicit correspondence to the terrain features observed from the realistic scenario on the global map.

# 6 Conclusion And Future Work

## 6.1 Conclusion

The radar target detection in heavy clutter, when surrounding objects scatter comparable to the target amount of sensing signal energy, is still an acute problem for modern surveillance radars. One of the possible solutions is to improve the contrast between the target and the surrounding clutter using the difference in their polarization parameters. Quite a wide set of detection algorithms that use polarimetric information have been proposed in previous research. They can mainly be divided into two classes. The first set tries to detect the target using some physical approaches by maximizing the received signal from the target scattered. This set includes the single channel detector, the span detector, and the power maximization detector. The second class of polarimetric detectors uses *a priori* information about targets' and/or clutter's polarimetric characteristics to maximize the signal-to-clutter ratio. This set consists of two algorithms - the Polarimetric Whitening Filter and the Optimal Polarimetric Detector. The main disadvantages of previous studies of such algorithms are that they were developed and tested mostly for cases where the clutter has been assumed to be spatially homogeneous within reasonable intervals of radar ranges and azimuths. In real-world scenarios, such homogeneity cannot be observed in most cases of target detection in ground-based clutter, which is usually characterized by high spatial variability, following the variety of surface-based objects, terrain types, and features. This research aims to estimate the potential for the use of polarimetric information for target detection in the cases of spatially inhomogeneous clutter.

The research started with the study of the performance of the polarimetric detection algorithms mentioned above and with the estimation and analysis of their sensitivity to the difference in the polarimetric characteristics of the target and clutter. To achieve this goal, the polarimetric radar simulator that generates multi-channel polarimetric signals with specified signal-to-clutter ratios and a polarimetric covariance matrix has been developed. In this research, the gain of detectability is defined, which is the ratio of the probability of detection of other polarimetric detectors to that of a single channel detector (HH). The detectors' performances as a function of the relation between the target's and clutter's polarimetric characteristics were compared in the ROC curves and also in terms of gain of detectability using the simulated data. Then the analysis of simulation performances was used further as the background for the estimation of these algorithms' performances in the case of application to real experimentally measured polarimetric data with quite inhomogeneous clutter.

Based on S-band polarimetric Doppler FMCW PARSAX radar high-resolution range measurements ($\approx 3.3$ m) in azimuthal scanning mode, the spatial variability of the polarimetric characteristics of the rural / recreational area in the surroundings of the city of Delft was studied for the first time.

To improve the accuracy and reliability of the polarimetric information processing, the new noise-based method for the equalization/calibration of the polarimetric radar channels was proposed and tested. One of the important advantages of this method is that the amplitude of calibrated signals in every channel becomes equal to the square root of the signal-to-noise ratio. It opens the way for the absolute noise-based calibration of radar signals.

For further minimization of the influence of thermal noise on the polarization parameters, the estimation of the long ($\approx 0.5$ s) Doppler coherent integration of measured signals has been used with the following filtration of stationary signals with zero Doppler velocity. These signals were used to estimate the polarimetric covariance matrix with the moving spatial averaging window method. The size of such a window has been optimized based on the trade-off between the minimal degradation in the spatial resolution and the similarity of the pixels related to the same specific type of observed objects. For such interpretation of radar data, the geo-referenced plan position indicator (PPI) representation of the radar data was compared with Google Earth satellite images and maps.

Based on this interpretation, the reference target (the set of power-line mast constructions) and two types of ground-based clutter - the "forest" and the "grassland" were selected. The resulting polarimetric covariance matrices demonstrate the stable similarity of the polarimetric characteristics within the same class of clutter and the differences between different types of objects or terrain features. But in general, the analyzed radar scene has a high variability of polarimetric characteristics and can be defined as a case of heavy inhomogeneous clutter. In this thesis, an analysis of the spatial statistical characteristics of the reference target and different types of ground-based clutter is provided in terms of polarimetric covariance matrices.

The experimental validation of the set of polarimetric detection algorithms, which has been done using real PARSAX radar data, shows a few interesting results.

- The set of detection algorithms that use some physical approaches for maximization of the received from the target scattered signal, which in simulated cases of homogeneous clutter demonstrate quite reasonable detection performances and target-to-clutter contrasts, in the analyzed real-world scenario with a huge variety of clutter types and characteristics becomes completely non-effective. Application of the single channel detector, the span detector, and the power maximization detector to real data have quite similar results that did not show any improvements in "point target - to - distributed clutter" contrast.

- The Polarimetric Whitening Filter, which uses *a priori* information about the clutter polarimetric covariance matrix, shows excellent results in suppressing this specific type of clutter; it was also found within the simulation results. The filter shows not very high sensitivity in terms of the similarity between the "reference" covariance matrix used in the filter and this matrix in the analyzed spatial location. It allows the specific type of clutter to be suppressed using the covariance matrix, which was previously estimated as the average for multiple locations of this clutter, or has a predefined *a priori* form.

When the moving spatial averaging window is used to estimate the covariance matrix for the current location and use this matrix in the PWF for the next range or azimuth position, the filter is not efficient for the adaptive estimation of the polarimetric covariance matrix, due to the large variability of clutter types and their polarimetric characteristics. The resulting detection map will be very noisy, reflecting mostly not the detections of expected targets but the variability of clutter types and characteristics.

- The application of detection algorithms to real radar data confirms the theoretical expectation that the best target detection performances will be observed in the cases where both the target and the clutter characteristics are *a priori* known, and by algorithms that use both of these characteristics. In our case, it is the Optimal Polarimetric Detector. The Optimal Polarimetric Detector shows the best result for the detection of some "reference" target when it uses the polarimetric covariance matrix of this target and uses the spatial moving window to estimate the clutter's covariance matrix for every location. In this case, the maximum detector response will be in the location of objects with polarimetric characteristics that are similar to the "reference" target.

  Using this feature of the Optimal Polarimetric Detector, in this study we propose, test, and validate the new application of this detection algorithm - for the classification/mapping of inhomogeneous ground-based clutter. After defining a few observed types of clutter (this can be done by the comparison of geo-referenced radar signal's map with a satellite image or geographic map, e.g. in Google Earth), their polarimetric covariance matrix can be estimated and used in the detection algorithms as a matrix of "reference" target. The output signal of the detector will be proportional to the similarity of the observed radar signals with such signals for the selected clutter type. To our knowledge, this usage of detection algorithms for signal classification is novel. It also has an important advantage: it can be implemented in parallel for different clutter types within a simple real-time streaming signal processing algorithm.

The gain of detectability has been displayed by the interpretation of the geo-referenced plan position indicator (PPI) representation. Compared with the single channel detector output map, the Polarimetric Whitening Filter and the Optimal Polarimetric Filter have performed apparent improvement in terms of the gain of detectability.

The research performed in this thesis shows that the polarimetric detection algorithms that use *a priori* or directly estimated information about targets' and/or clutter's polarimetric characteristics to maximize the signal-to-clutter ratio - the Polarimetric Whitening Filter and the Optimal Polarimetric Detector - are promising and efficient technology for addressing target detection in strong inhomogeneous interferences from the ground-based clutter. They provide the best detection performance - the highest probability of detection and the smallest false alarm rate. The novelty of this study is defined not only by the novel analysis and validation of these algorithms' applicability to the real high-resolution polarimetric radar observations of the radar scene with highly inhomogeneous clutter, but also by the demonstration of the novel usage of these detection algorithms for targets and clutter classification, which can be done in real-time, within the signal streaming mode.

## 6.2 Limitations and Future Work

There are several recommendations for future research that could be addressed.

One of the limitations of this study is that the power line masts, which form the set of reference targets, show a lot of variability in their averaged covariance matrices. As a result, every power line mast can be detected using an optimal polarimetric detector with its own covariance matrix as the reference target. The question of how to average the individual covariance matrices of the set of similar reference targets (e.g. the set of power line masts) to achieve their detection within one run of the optional polarimetric detector can be a topic for further research.

According to the theory of the polarimetric whitening filter, this type of detector is supposed to reduce the specific type of clutter with *a priori* known covariance matrix. As follows from the filter's name, it is done with the whitening of the input multidimensional signal. In this report, excellent performance of such a whitening filter has been demonstrated, showing that PWF can work very well for the suppression of homogeneous clutter. One of the possible recommendations for further research could be related to the improvement of the effectiveness of this filtration algorithm in the case of non-homogeneous clutter, whose polarimetric characteristics vary unsteadily in space. It could also be beneficial to discover the possibility of using the PWF for several types of clutter at the same time.

In this study, the PARSAX polarimetric data has been used. After noise-based calibration and Doppler processing, the polarimetric data with zero Doppler velocity were filtered out and used for the estimation of the covariance matrix range-azimuth map. This map has been used for the statistical simulation of input polarimetric data for the detection algorithms. In fact, in this study, the experimentally measured data were used only for the estimation of the covariance matrix, but not for the signal. One of the possible future work could be a study of the efficiency of the detection algorithms implementations that use real measured radar returns as input feature vectors on a slow-time scale. These data can be the same as for covariance matrix estimation, or they can be measured independently, during another scan of the radar.

# Appendix A: Effect of the Size of the Moving Average Window

A

This Appendix illustrates the effects of the size of the moving average window on the value of averaged elements of the covariance matrix. Plots represent the azimuthal dependency of the elements, measured at the fixed range.

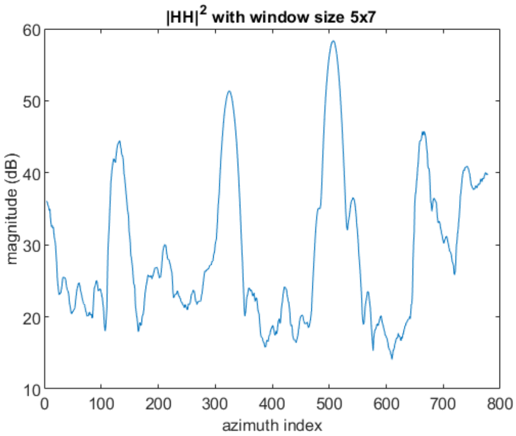


(a) $C_{11}$ (window size 5x7)

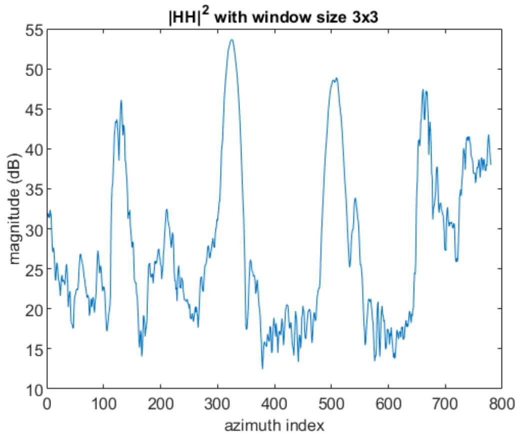


(b) $C_{11}$ (window size 3x3)

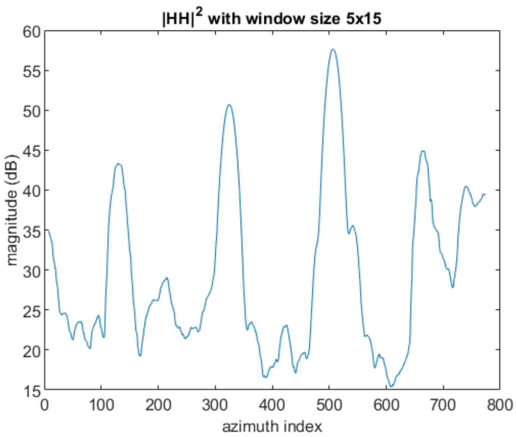


(c) $C_{11}$ (window size 5x15)

Figure A.1: Amplitude of the element $C_{11}$ along the azimuth index for the various sizes of moving average window

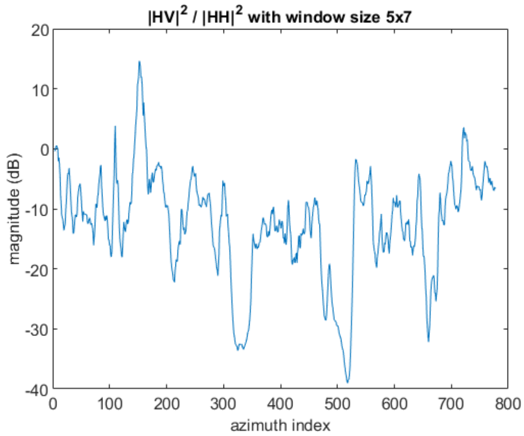


(a) $C_{22}$ window size 5x7

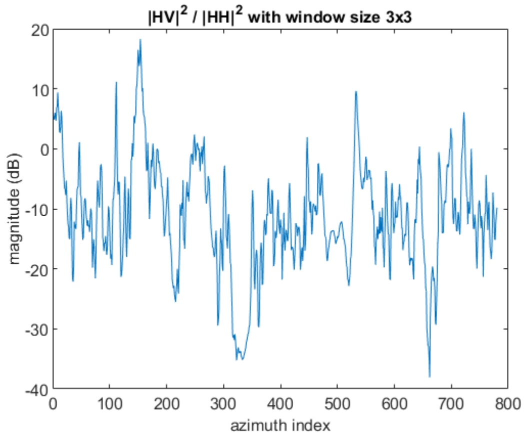


(b) $C_{22}$ window size 3x3

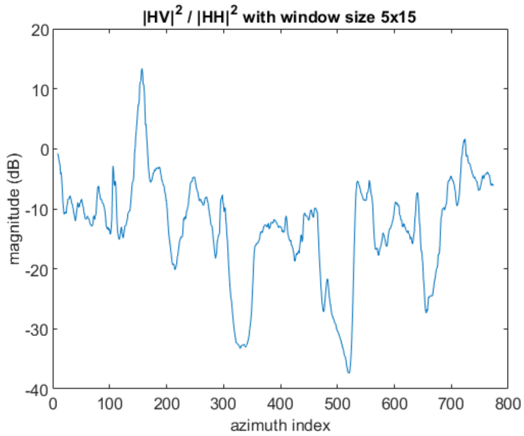


(c) $C_{22}$ window size 5x15

Figure A.2: Amplitude of the element $C_{22}$ along the azimuth index for the various sizes of moving average window

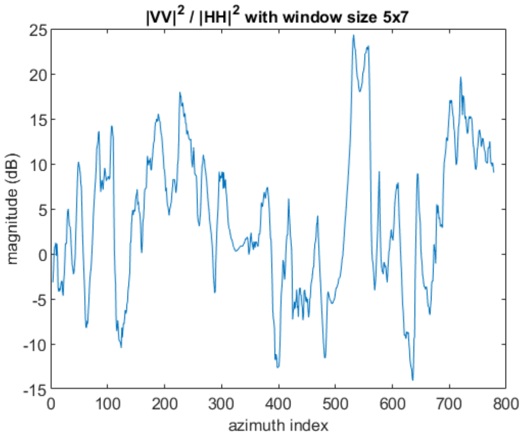


(a) $C_{33}$ window size 5x7

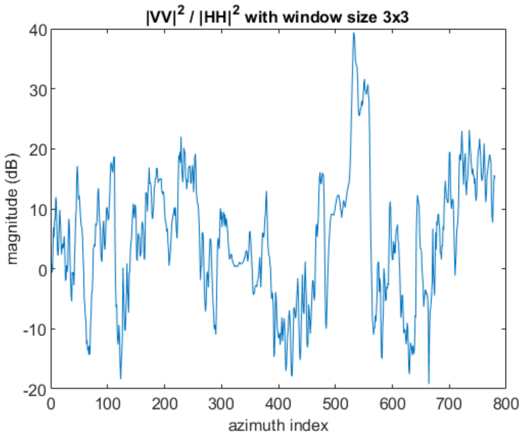


(b) $C_{33}$ window size 3x3

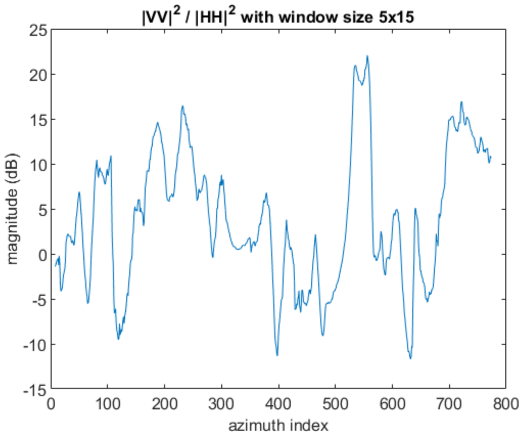


(c) $C_{33}$ window size 5x15

Figure A.3: Amplitude of the element $C_{33}$ along the azimuth index for the various sizes of moving average window

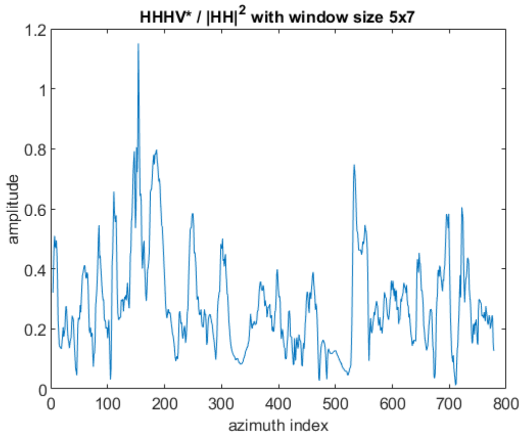


(a) $C_{12}$ window size 5x7

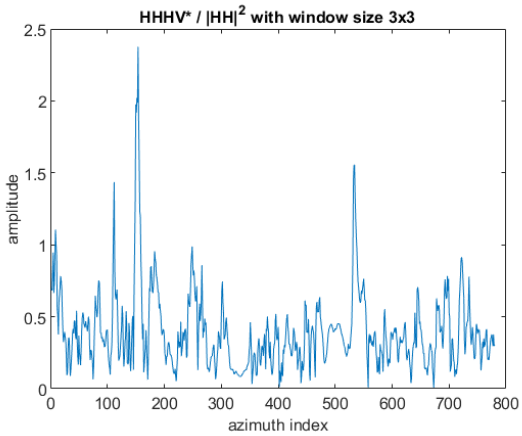


(b) $C_{12}$ window size 3x3

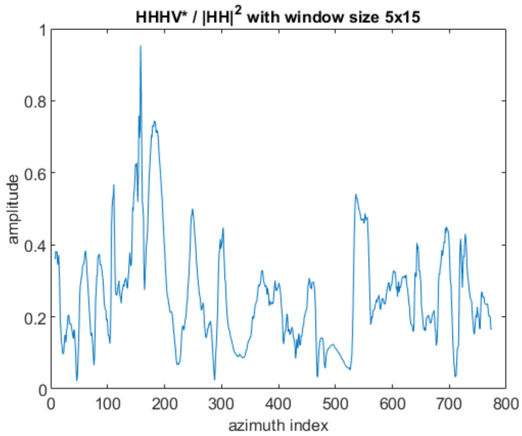


(c) $C_{12}$ window size 5x15

Figure A.4: Amplitude of the element $C_{12}$ along the azimuth index for the various sizes of moving average window

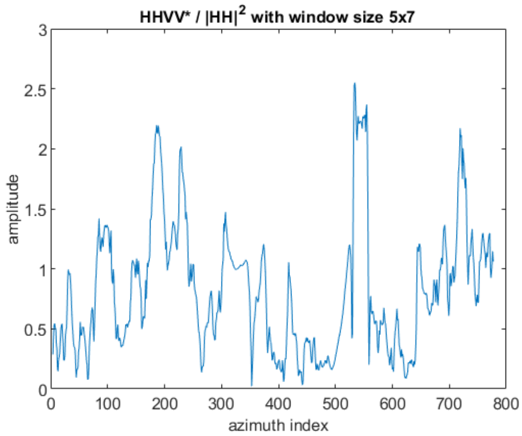


(a) $C_{13}$ window size 5x7

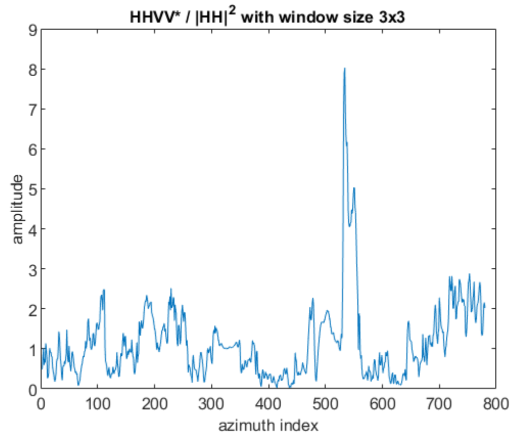


(b) $C_{13}$ window size 3x3

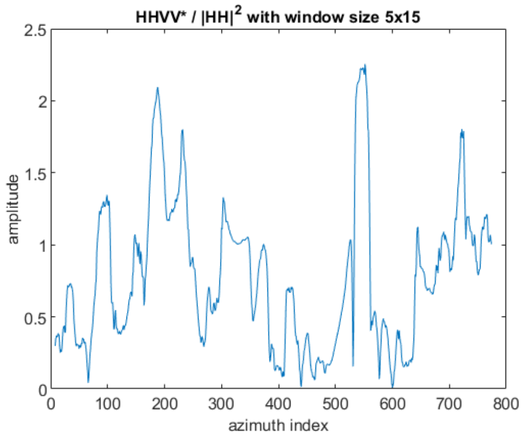


(c) $C_{13}$ window size 5x15

Figure A.5: Amplitude of the element $C_{13}$ along the azimuth index for the various sizes of moving average window

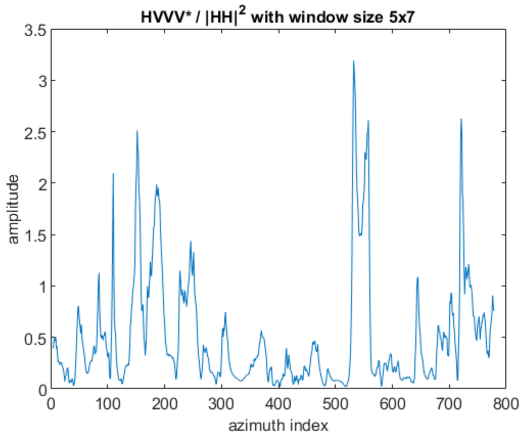


(a) $C_{23}$ window size 5x7

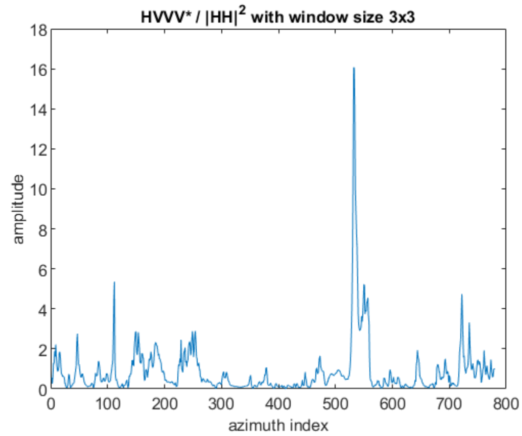


(b) $C_{23}$ window size 3x3

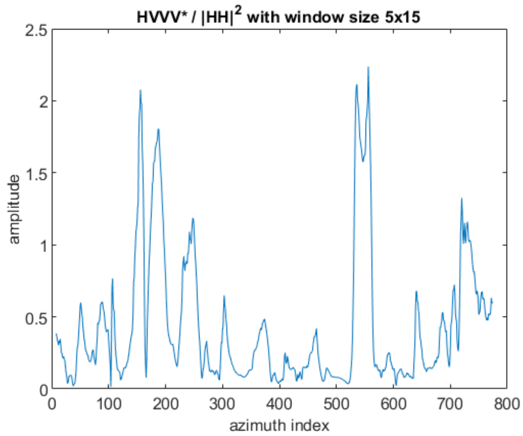


(c) $C_{23}$ window size 5x15

Figure A.6: Amplitude of the element $C_{23}$ along the azimuth index for the various sizes of moving average window

# Appendix B: Maps of the Covariance Matrix Elements

B

This Appendix presents the geo-located maps of the polarization covariance matrix elements that were estimated using the averaging within the spatial moving window.

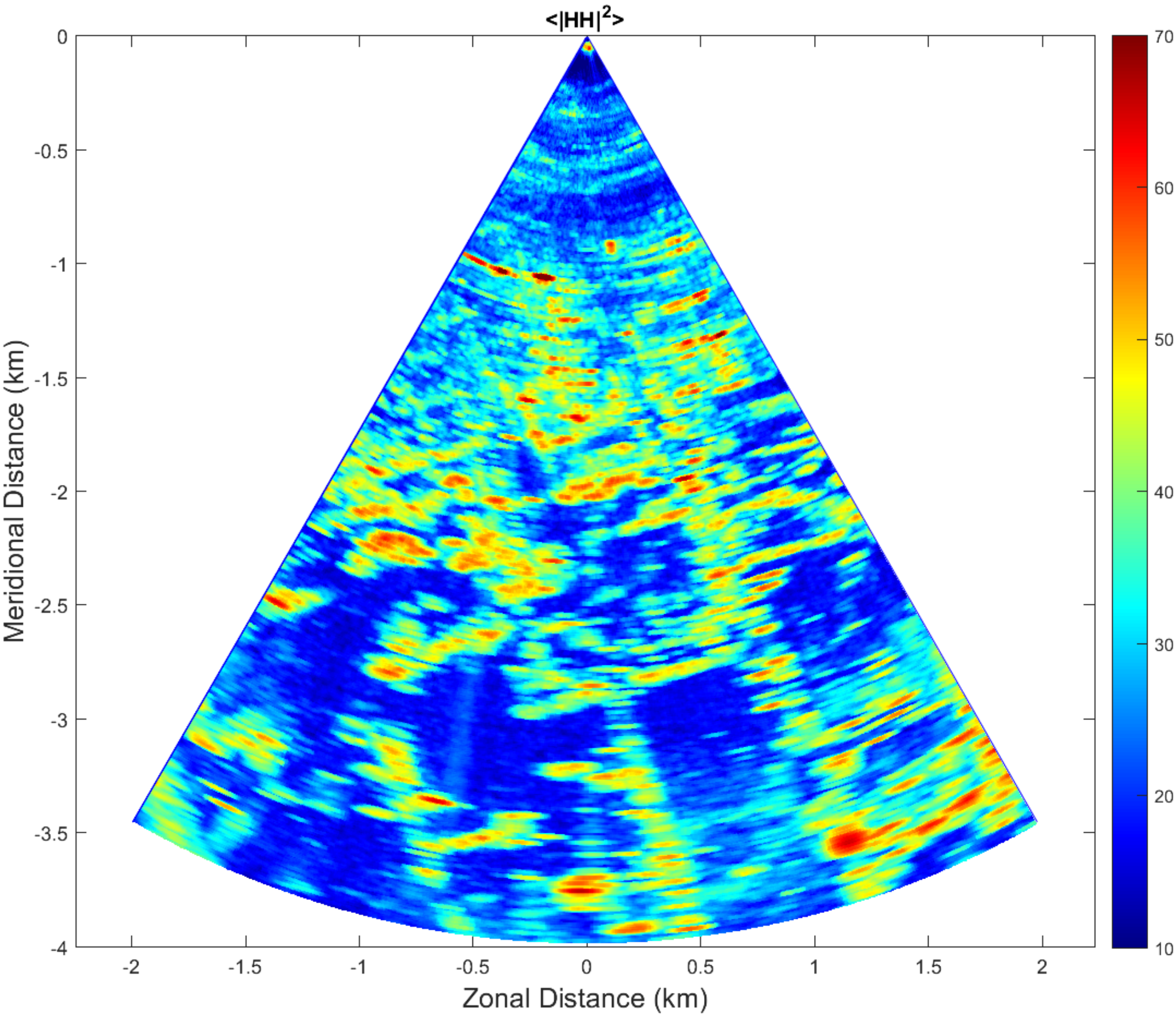


Figure B.1: Map of the covariance matrix element $C_{11}$ that was estimated using moving average window

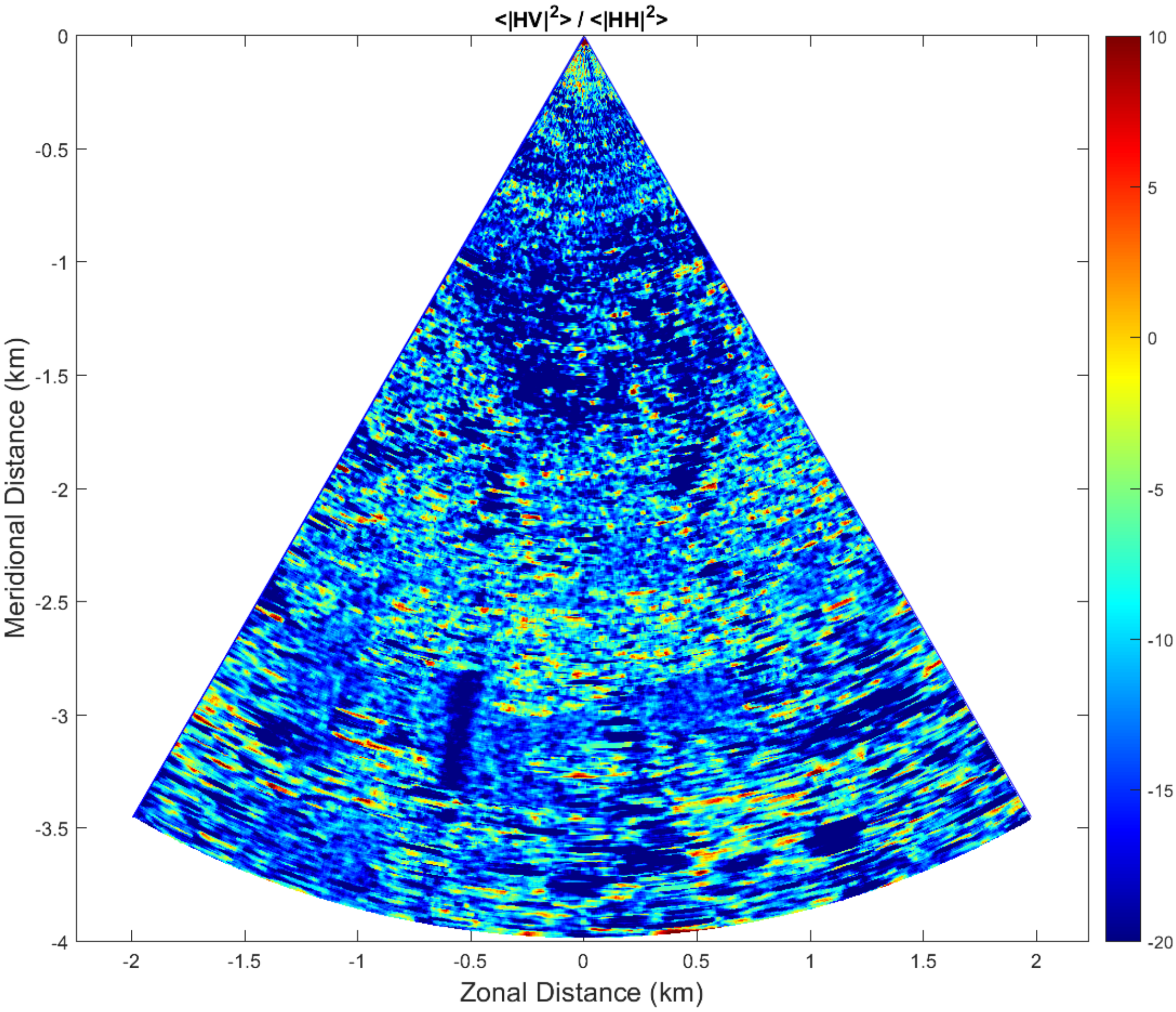


Figure B.2: Map of the covariance matrix element $C_{22}$ that was estimated using moving average window

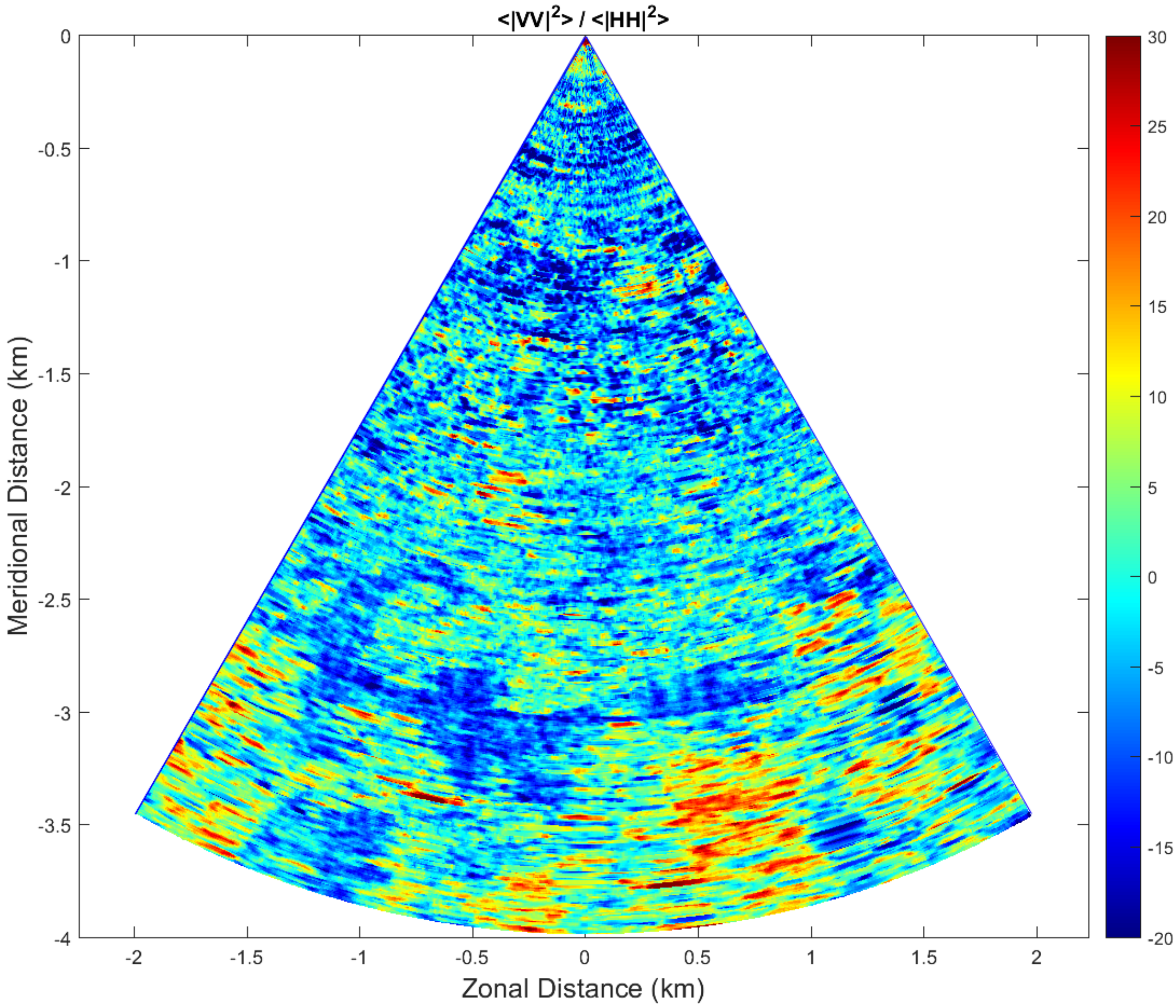


Figure B.3: Map of the covariance matrix element $C_{33}$ that was estimated using moving average window

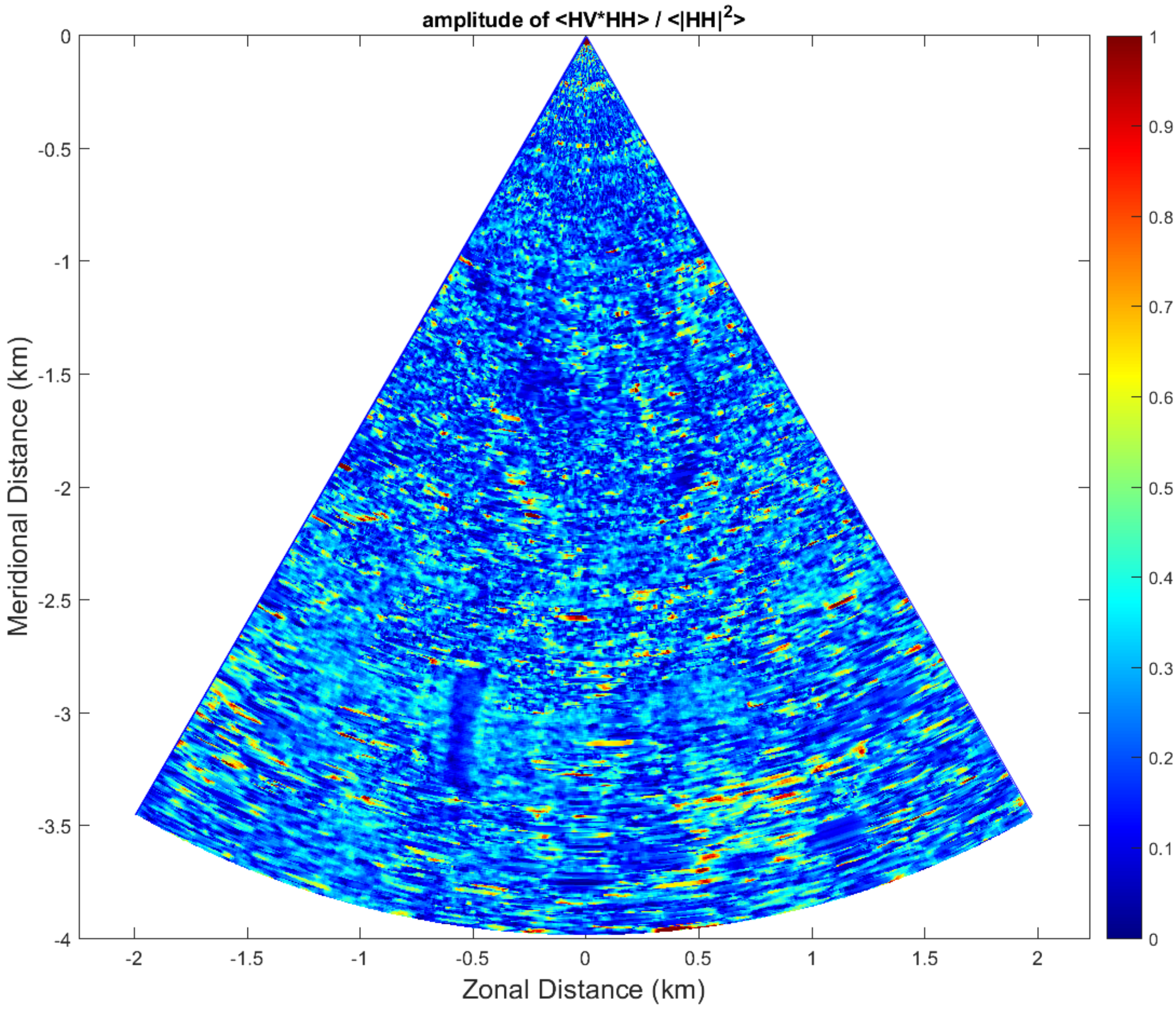


Figure B.4: Map of the covariance matrix element $C_{12}$ that was estimated using moving average window

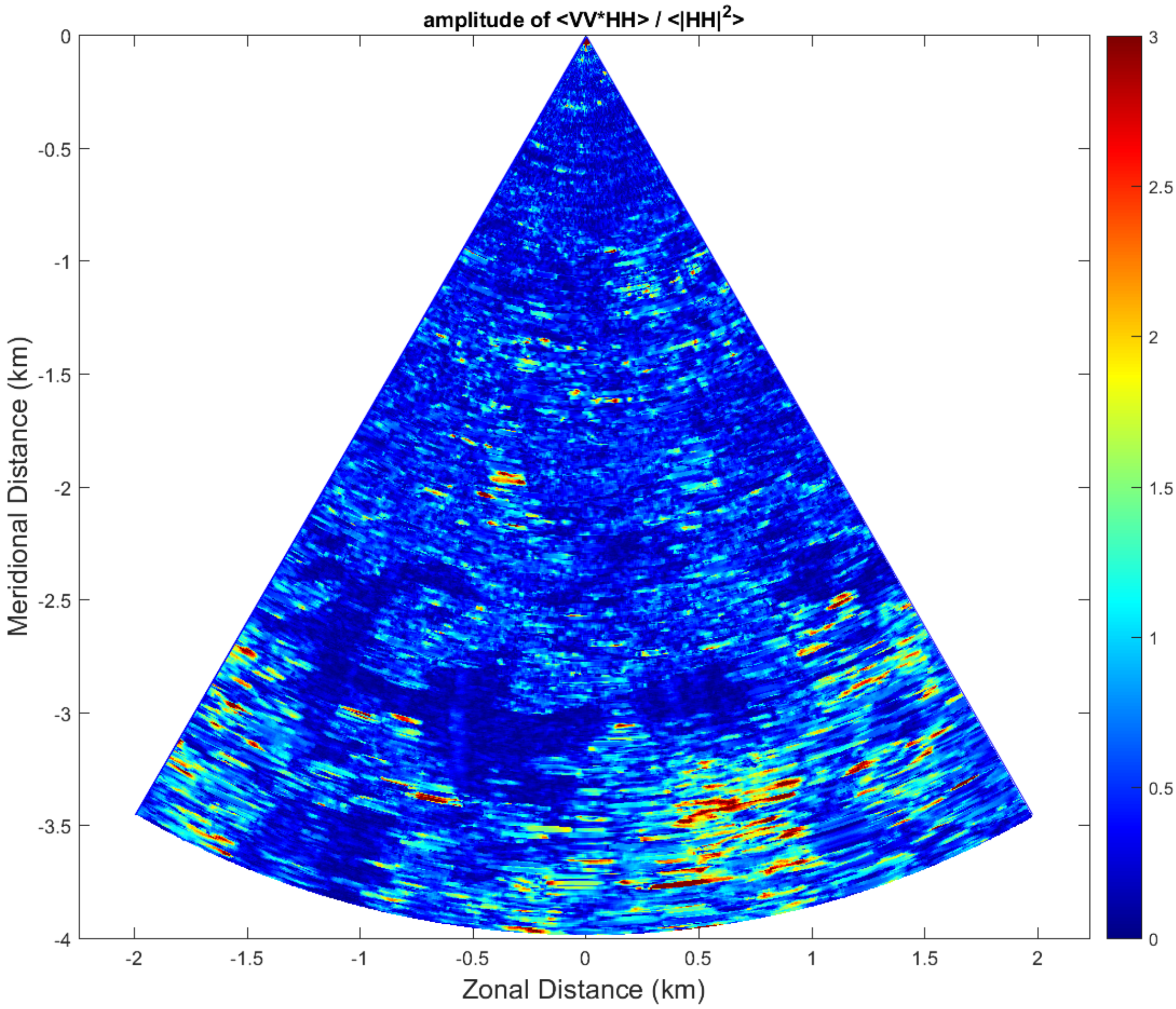


Figure B.5: Map of the covariance matrix element $C_{13}$ that was estimated using moving average window

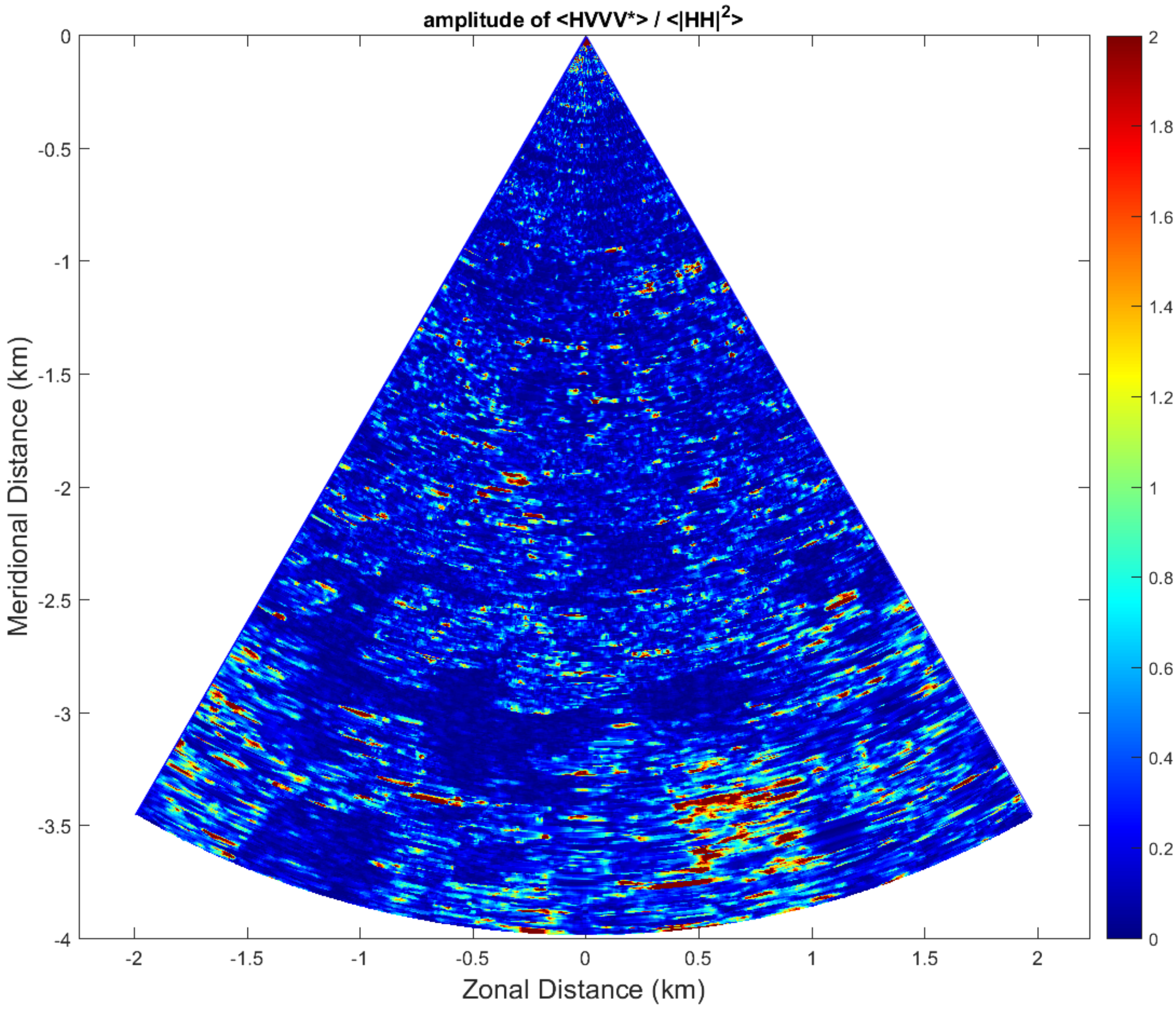


Figure B.6: Map of the covariance matrix element $C_{23}$ that was estimated using moving average window

# Appendix C: Efficiency of Noise-Based Calibration

C

This Appendix illustrates the the efficiency of noise-based calibration on the improvement of accuracy and reliability with using the span detector.

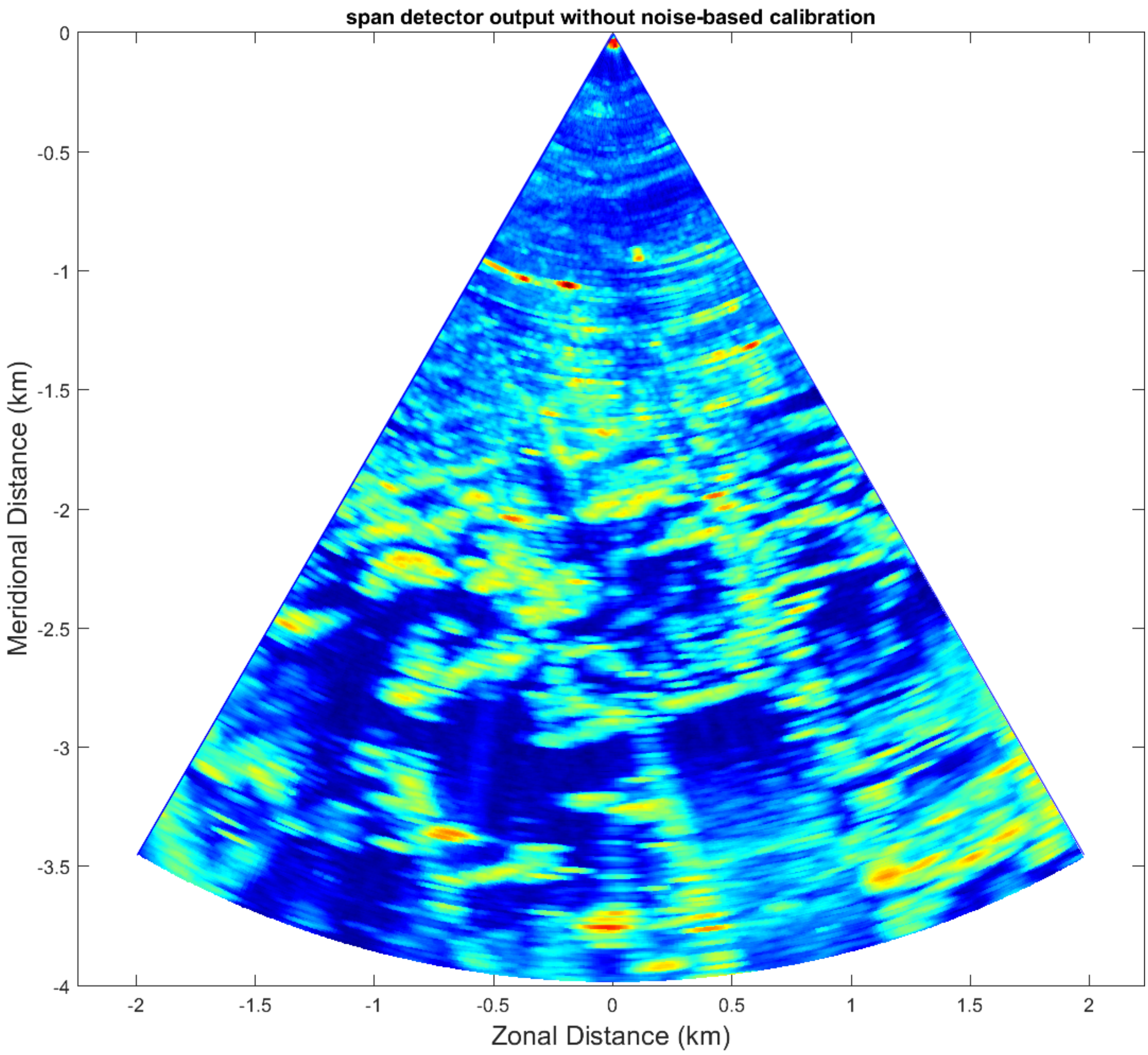


Figure C.1: Span detector without noise-based calibration

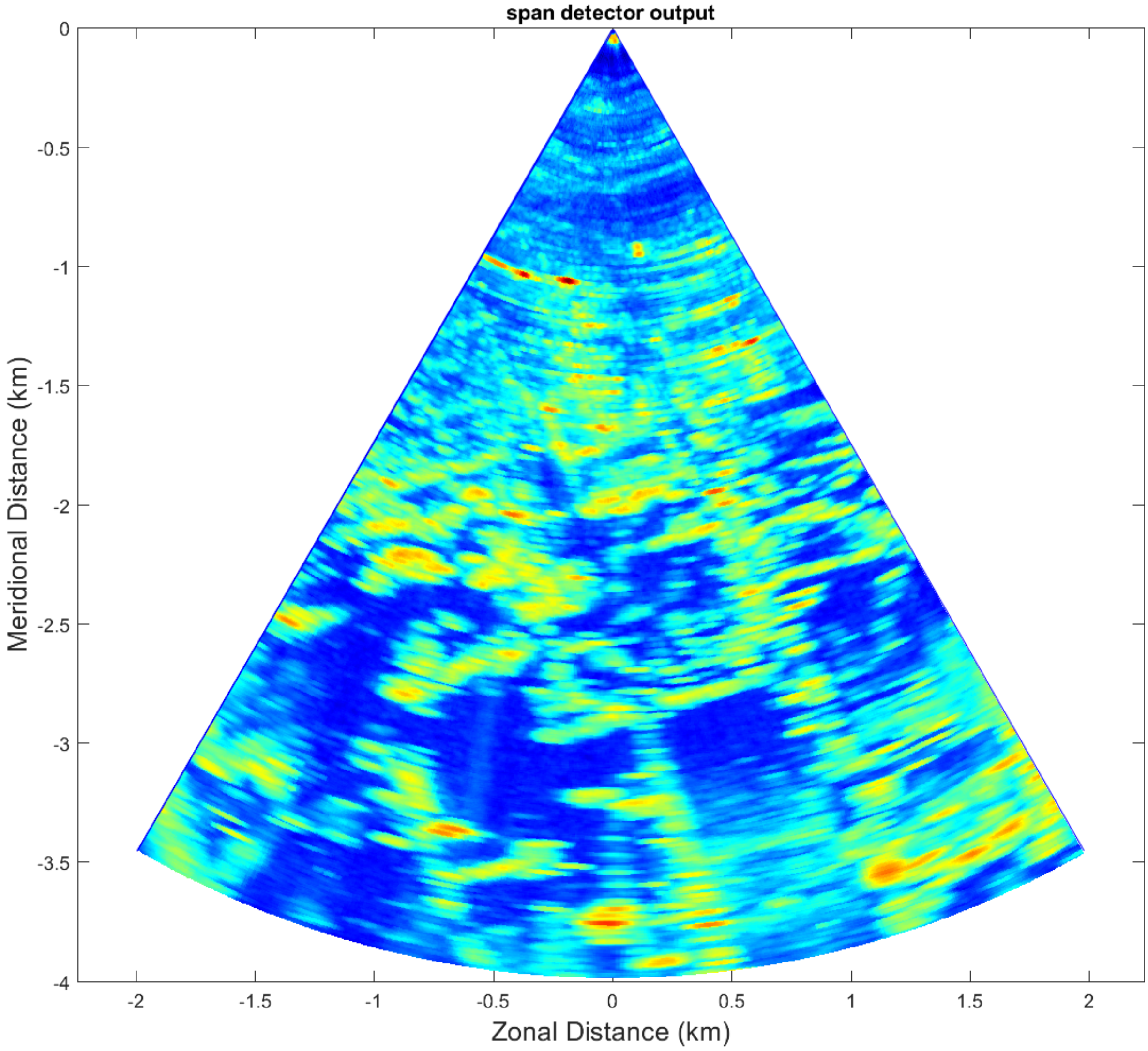


Figure C.2: Span detector with noise-based calibration

# List of Figures

# List of Tables

# Bibliography


[1] L. Du, L. Li, B. Wang, and J. Xiao, "Micro-doppler feature extraction based on time-frequency spectrogram for ground moving targets classification with low-resolution radar," *IEEE Sensors Journal*, vol. 16, 05 2016.

[2] L. M. Novak, M. B. Sechtin, and M. J. Cardullo, "Studies of target detection algorithms that use polarimetric radar data," *IEEE Transactions on Aerospace and Electronic Systems*, vol. 25, no. 2, pp. 150–165, 1989.

[3] L. M. Novak, M. C. Burl, and W. Irving, "Optimal polarimetric processing for enhanced target detection," *IEEE Transactions on Aerospace and Electronic Systems*, vol. 29, no. 1, pp. 234–244, 1993.

[4] C. Unal, "Spectral polarimetric radar clutter suppression to enhance atmospheric echoes," *Journal of Atmospheric and Oceanic Technology - J ATMOS OCEAN TECHNOL*, vol. 26, pp. 1781–1797, 09 2009.

[5] R. Chaney, M. Bud, and L. Novak, "On the performance of polarimetric target detection algorithms," *IEEE Aerospace and Electronic Systems Magazine*, vol. 5, no. 11, pp. 10–15, 1990.

[6] D. Giuli, "Polarization diversity in radars," *Proceedings of the IEEE*, vol. 74, no. 2, pp. 245–269, 1986.

[7] H. Mott, *Polarization in antennas and radar.* Wiley-Interscience, 1986.

[8] C. Zeng, D. Li, X. Luo, D. Song, H. Liu, and J. Su, "Ground maneuvering targets imaging for synthetic aperture radar based on second-order keystone transform and high-order motion parameter estimation," *IEEE Journal of Selected Topics in Applied Earth Observations and Remote Sensing*, vol. 12, no. 11, pp. 4486–4501, 2019.

[9] P. Iervolino, R. Guida, and P. Whittaker, "A new glrt-based ship detection technique in sar images," in *2015 IEEE International Geoscience and Remote Sensing Symposium (IGARSS).* IEEE, 2015, pp. 3131–3134.

[10] ——, "A novel ship-detection technique for sentinel-1 sar data," in *2015 IEEE 5th Asia-Pacific Conference on Synthetic Aperture Radar (APSAR).* IEEE, 2015, pp. 797–801.

[11] F. C. Robey, D. R. Fuhrmann, E. J. Kelly, and R. Nitzberg, "A cfar adaptive matched filter detector," *IEEE Transactions on aerospace and electronic systems*, vol. 28, no. 1, pp. 208–216, 1992.

[12] D. Pastina, P. Lombardo, and T. Bucciarelli, "Adaptive polarimetric target detection with coherent radar. i. detection against gaussian background," *IEEE Transactions on Aerospace and Electronic Systems*, vol. 37, no. 4, pp. 1194–1206, 2001.

[13] T. Liu, J. Zhang, G. Gao, J. Yang, and A. Marino, "Cfar ship detection in polarimetric synthetic aperture radar images based on whitening filter," *IEEE Transactions on Geoscience and Remote Sensing*, vol. 58, no. 1, pp. 58–81, 2020.

[14] T. Liu and G. Lampropoulos, "A new polarimetric cfar ship detection system," in *2006 IEEE International Symposium on Geoscience and Remote Sensing*. IEEE, 2006, pp. 137–140.

[15] S. R. Cloude and E. Pottier, "An entropy based classification scheme for land applications of polarimetric sar," *IEEE transactions on geoscience and remote sensing*, vol. 35, no. 1, pp. 68–78, 1997.

[16] F. Nunziata, M. Migliaccio, and C. E. Brown, "Reflection symmetry for polarimetric observation of man-made metallic targets at sea," *IEEE Journal of Oceanic Engineering*, vol. 37, no. 3, pp. 384–394, 2012.

[17] Q. Chen, Y. Jiang, L. Zhao, and G. Kuang, "Polarimetric scattering similarity between a random scatterer and a canonical scatterer," *IEEE Geoscience and Remote Sensing Letters*, vol. 7, no. 4, pp. 866–869, 2010.

[18] Y. Wang and H. Liu, "Polsar ship detection based on superpixel-level scattering mechanism distribution features," *IEEE Geoscience and Remote Sensing Letters*, vol. 12, no. 8, pp. 1780–1784, 2015.

[19] G. Gao, G. Shi, and S. Zhou, "Ship detection in high-resolution dual-polarization sar amplitude images," *International Journal of Antennas and Propagation*, vol. 2013, 2013.

[20] O. Krasnov, "Working materials: Polarimetric radar calibration and noise-based equalization of the measurement channels," Delft University of Technology, Tech. Rep., 2022.

[21] A. Kostinski and W. Boerner, "On foundations of radar polarimetry," *IEEE Transactions on Antennas and Propagation*, vol. 34, no. 12, pp. 1395–1404, 1986.

[22] J.-S. Lee and E. Pottier, *Polarimetric radar imaging: from basics to applications*. CRC press, 2009.

[23] D. Giuli, M. Fossi, and L. Facheris, "Radar target scattering matrix measurement through orthogonal signals," in *IEE Proceedings F (Radar and Signal Processing)*, vol. 140, no. 4. IET, 1993, pp. 233–242.

[24] O. A. Krasnov, L. P. Ligthart, Z. Li, P. Lys, and F. van der Zwan, "The parsax-full polarimetric fmcw radar with dual-orthogonal signals," in *2008 European Radar Conference*. IEEE, 2008, pp. 84–87.

[25] O. A. Krasnov and L. P. Ligthart, "Radar polarimetry using sounding signals with dual orthogonality-parsax approach," in *The 7th European Radar Conference*. IEEE, 2010, pp. 121–124.

[26] G. P. Babur, O. A. Krasnov, and L. P. Ligthart, "Quasi-simultaneous measurements of scattering matrix elements in polarimetric radar with continuous waveforms providing high-level isolation in radar channels," in *2009 European Radar Conference (EuRAD).* IEEE, 2009, pp. 1–4.

[27] J. Kong, A. Swartz, H. Yueh, L. Novak, and R. Shin, "Identification of terrain cover using the optimum polarimetric classifier," *Journal of Electromagnetic Waves and Applications*, vol. 2, no. 2, pp. 171–194, 1988.

[28] R. Fante, "Detection of multiscatter targets ink-distributed clutter," *IEEE Transactions on Antennas and Propagation*, vol. 32, no. 12, pp. 1358–1363, 1984.

[29] R. S. Raghavan, "Coherent airborne mimo detection of multiscatter targets," *IEEE Transactions on Aerospace and Electronic Systems*, vol. 54, no. 2, pp. 978–991, 2018.

[30] L. M. Novak, G. J. Owirka, and C. M. Netishen, "Performance of a high-resolution polarimetric sar automatic target recognition system," *Lincoln Laboratory Journal*, vol. 6, no. 1, 1993.

[31] M. Vespe, C. J. Baker, and H. D. Griffiths, "Radar target classification using multiple perspectives," *IET Radar, Sonar & Navigation*, vol. 1, no. 4, pp. 300–307, 2007.

[32] R. J. Burkholder, "Analytic solutions for the bistatic radar signature of a dihedral target of arbitrary angle," in *2018 International Applied Computational Electromagnetics Society Symposium (ACES).* IEEE, 2018, pp. 1–2.

[33] D. Perissin and A. Ferretti, "Urban-target recognition by means of repeated spaceborne sar images," *IEEE Transactions on Geoscience and Remote Sensing*, vol. 45, no. 12, pp. 4043–4058, 2007.

[34] J. J. Van Zyl, *Synthetic aperture radar polarimetry.* John Wiley & Sons, 2011.

[35] A. Marino, *A new target detector based on geometrical perturbation filters for Polarimetric Synthetic Aperture Radar (POL-SAR).* Springer Science & Business Media, 2012.

[36] P. Zhang, J. F. Zhang, D. Ma, and T. Liu, "Contrastive analysis of the performances of radar multi-look polarimetric detectors," in *2017 IEEE Radar Conference (RadarConf)*, 2017, pp. 1373–1378.

[37] G. Vasile, J.-P. Ovarlez, F. Pascal, and C. Tison, "Coherency matrix estimation of heterogeneous clutter in high-resolution polarimetric sar images," *IEEE Transactions on Geoscience and Remote Sensing*, vol. 48, no. 4, pp. 1809–1826, 2010.

[38] M. Pourahmadi, M. J. Daniels, and T. Park, "Simultaneous modelling of the cholesky decomposition of several covariance matrices," *Journal of Multivariate Analysis*, vol. 98, no. 3, pp. 568–587, 2007.

[39] A. Krishnamoorthy and D. Menon, “Matrix inversion using cholesky decomposition,” in *2013 Signal Processing: Algorithms, Architectures, Arrangements, and Applications (SPA)*, 2013, pp. 70–72.

[40] N. J. Higham, “Analysis of the cholesky decomposition of a semi-definite matrix,” *Reliable Numerical Computation*, 1990.

[41] S. Gogineni and A. Nehorai, “Polarimetric mimo radar with distributed antennas for target detection,” *IEEE Transactions on Signal Processing*, vol. 58, no. 3, pp. 1689–1697, 2009.

[42] J. R. Roman, M. Rangaswamy, D. W. Davis, Q. Zhang, B. Himed, and J. H. Michels, “Parametric adaptive matched filter for airborne radar applications,” *IEEE Transactions on Aerospace and Electronic Systems*, vol. 36, no. 2, pp. 677–692, 2000.

[43] X. Chen, Y. Cheng, H. Wu, and H. Wang, “Heterogeneous clutter suppression for airborne radar stap based on matrix manifolds,” *Remote Sensing*, vol. 13, no. 16, p. 3195, 2021.

[44] O. Green, L. David, A. Galperin, and Y. Birk, “Efficient parallel computation of the estimated covariance matrix,” *arXiv preprint arXiv:1303.2285*, 2013.

[45] L. David, A. Galperin, O. Green, and Y. Birk, “Efficient parallel computation of the estimated covariance matrix,” in *2010 IEEE 26-th Convention of Electrical and Electronics Engineers in Israel*. IEEE, 2010, pp. 977–981.